Design optimization of mechanical induced-draft counter-flow wet cooling towers

by

Amgad Abdullah Abdalshaikh Bahanan

A thesis submitted in partial fulfillment of the requirements for the degree of

Master of Science

Department of Mechanical Engineering

University of Alberta

Abstract

Cooling towers are utilized in a wide variety of industrial applications for dissipating waste heat into the atmosphere. The design of effective, economical, and environment-friendly cooling towers is paramount for industrial applications. In this thesis, a numerical optimization framework for cooling tower design is presented as an innovative alternative to the time consuming trial-and-error design process. The analysis component of the framework predicts the thermal and hydrodynamic performance of mechanical induced-draft counter-flow wet cooling towers through the solution of a one-dimensional zone-specific thermodynamic model and air draft equation. Furthermore, the analysis component of the framework evaluates the environmental impact of cooling tower operation in cold climatic conditions by predicting the visible plume length through the solution of an integral axisymmetric turbulent plume model. The optimization component of the framework embodies the iterative design procedure by applying numerical optimization. The numerical optimization framework is used to solve three design problems: (i) airflow selection; (ii) size optimization; and (iii) size optimization with visible plume constraint. The method of feasible directions (MFD) is the optimization algorithm to solve the first design problem, while the other two design problems are solved by a multi-objective genetic algorithm (MOGA). The presented investigation related to the size optimization problem is the first attempt in the literature to study quantitatively the best possible trade-offs between the capital and operating costs of the cooling tower. Additionally, visible plume constraint is introduced for the first time in the thermo-economical performance optimization of wet cooling towers.

The results obtained from the airflow selection show that increasing the fill height leads to smaller airflow requirements which decreases fan power consumption. There is a threshold

fill height beyond which fan power savings become small. This threshold is determined by the location in the fill where the air becomes saturated with vapor. The results obtained from the size optimization show that the design with the lowest capital cost delivers a desired cooling performance at peak operating conditions with 3.1% more air mass flow rate, 13.0% less fill height, and 37.9% less tower frontal area with respect to the design with the lowest operating cost. The design with the lowest capital cost has 39.2% less cooling tower volume on account of a 141.0% increase in fan power consumption. On the other hand, the design with the lowest operating cost delivers the desired cooling performance at the same operating conditions with 3.0% less air mass flow rate, 14.9% more fill height, and 61.0% more tower frontal area with respect to the design with lowest capital cost. The design with the lowest operating cost consumes 58.5% less fan power on account of a 64.5% increase in cooling tower volume. The results obtained from the size optimization with visible plume constraint show that the visible plume length is reduced by one order of magnitude with 26% more air mass flow rate, 48% less fill height, and 6% more tower frontal area with respect to an optimal cooling tower design with the same volume when the cooling tower operates at an ambient temperature of 12.5°C and relative humidity of 40%. Such an optimal design consumes 55% more fan power in order to provide an adequate entrainment of ambient air into the plume core, which helps in accelerating plume dilution. On the other hand, the same results show that, at the same relative humidity, the suggested design becomes insufficient in reducing the visible plume length as the ambient temperature drops below 10.0°C. In such ambient conditions, the effect of a high condensation rate overcomes the effect of high plume entrainment.

Keywords: cooling tower, evaporative cooling, numerical modelling, optimization, visible plume

Preface

This thesis is an original work by Amgad Bahanan. No part of this thesis has been previously published.

To my family

Acknowledgements

I would like to thank my supervisors, Professors Morris Flynn and Marc Secanell, for their support and guidance through this study. I am very grateful for the countless discussions we had concerning my research project in which I have gained valuable lessons about conducting research.

I would like to acknowledge Mr. Abdullah Bugshan for his generous sponsorship of my master's program from the travel costs to the tuition costs.

I would like to acknowledge International Cooling Tower (ICT) for their sponsorship of this project and valuable insights. I would like to acknowledge the financial support I received from the Natural Sciences and Engineering Research Council of Canada (NSERC) through a Collaborative Research and Development Grant.

Last but not least, I would like to express my sincere gratitude to my parents, Abdullah and Salma, my aunt, Fatima, my sisters, Sarah, Suad, and Sumiah, and my brothers, Ahmed, Osamah, and Mohammed for their unconditional love and support.

Contents

List of Tables

List of Figures

Chapter 1

Introduction

1.1 Motivation

A tremendous amount of heat is produced as a result of energy conversion at an industrial scale, e.g., in power generation, refrigeration, and oil refinery. This heat is treated as a waste byproduct that needs to be continually dissipated. Water is a good medium to dissipate waste heat because of its abundance and desirable physical properties such as a large heat capacity and a large heat of vaporization [2]. The option of using water on a once-through basis such that the water only circulates once through the cooling system, is under increasing regulatory scrutiny and is being phased out in some countries [2]. By discharging hot water directly into natural water-bodies, e.g., lakes and riverbeds, the ambient water temperature increases which reduces the saturation value of dissolved oxygen and thereby affects biological balances with the ecosystem [3]. Open recirculating cooling water systems should replace once-through systems to avoid the environmental damage from thermal shocks and pollution [2]. Cooling towers are used in the open recirculating cooling water systems to dissipate into the atmosphere the heat absorbed by water from process fluids. Thereby, cooling towers are utilized in a wide variety of industrial applications. Thermo-electric power plants use cooling towers for turbine condenser cooling or diesel engine cooling [4]. Chemical and petrochemical plants use cooling towers to cool the water integral to their operations. For example, oil refineries use cooling towers to achieve low operating temperatures for condensing the volatile vapors in atmospheric crude oil distillation unit [5]. Metallurgical plants use cooling towers extensively to dissipate the heat produced by protective atmosphere generators used to cool the whole interior of the furnace in order to prevent metal scaling [4]. Refrigeration and air conditioning plants use cooling towers to remove heat absorbed from a facility or building into the atmosphere.

There are some concerns that are associated with cooling towers despite the great benefits that they bring for the industrial world. These concerns are of an operational, economical,

and environmental nature [2, 6]. Operational concerns tend to be related to a specific locality, therefore their solutions usually result in non-transferrable and/or minor modifications in modern cooling towers [6]. For example, cooling towers that operate in freezing weather require some special considerations, e.g., the use of a basin immersion heater to prevent water freezing. The economical concerns of cooling towers are associated with moderate to high capital and operating costs. These costs are influenced by construction expenses and power consumption of the fans and pumps used in modern cooling towers. The major environmental concerns of cooling towers stem from their atmospheric emissions, particularly when these emissions take the form of visible plumes (or water droplets). Visible plumes are formed when the water vapor discharged from the cooling tower condensates into small droplets. Concerns arise when the visible plume becomes inconvenience, or even worse, hazardous for the surrounding community [7]. Wind can deflect the plumes causing them to make contact with the ground and thereby creating a localized foggy condition. Persistent fog reduces visibility on nearby roadways, which contributes to traffic safety issues. Also, when cooling towers are located in close proximity to an airport, a dense visible plume that remains aloft may interfere with airport operations and flight pathways [7]. In cold regions where the ambient temperature is below 5°C, icing of roadways, sidewalks, and electrical transmission lines can create hazardous conditions [8]. On an aesthetic level, the visual impact of a tall plume may be undesirable if located near commercial or residential areas, or areas designated for public recreational use [7]. Moreover, a bacteria named Legionella can be spread from contaminated cooling towers by the water droplets within the visible plume. Legionella emitted by contaminated cooling towers represent an environmental risk factor, in particular in the neighbourhood of prone individuals, as it can cause severe health problems and even mortality [9].

Cooling tower design has been under study for the purpose of improving overall efficiencies by boosting cooling performance while addressing the economical and environmental concerns related to the cooling tower. The design of effective, economical, and environment-friendly cooling towers is paramount for industrial applications; however, it is a complex endeavor due to the fact that it involves multiple physical processes and a large number of design parameters. This dissertation aims to study cooling tower design by leveraging recent advances in multi-phase flow modelling and numerical optimization tools. The development of an optimization framework in this thesis is essential for understanding the compatibility between performance, economical, and environmental considerations of an optimized cooling tower design.

1.2 Background

1.2.1 Cooling tower arrangement

Cooling towers are heat exchangers that are designed and manufactured in several types and arrangements. In wet cooling towers, the process water to be cooled is sprayed directly into the cooling tower and because of the direct contact between water and air, a portion of the water is evaporated. In this case, the water is cooled by both sensible and latent heat transfer where the latter component dominates the cooling process. In dry cooling towers, the water is passed through finned tubes and the air has no direct contact with water. In this case, the water is cooled by sensible heat transfer only. In hybrid cooling towers, a dry-cooling section is incorporated with a wet-cooling section.

Cooling towers are further categorized based on the air draft type. Mechanical-draft cooling towers utilize fans that force or draw air through the towers, usually referred to as forced draft and induced draft, respectively. Natural-draft cooling towers rely only on buoyancy to drive the airflow, thereby exploiting the density difference between the heated air inside the tower and the relatively cool ambient air outside to drive the airflow. Furthermore, cooling towers are categorized based on the flow orientation of air and water within the tower. In counter-flow cooling towers, the airflow is vertically upward in the opposite direction to the water flow that is downward. In cross-flow cooling towers, air flows horizontally and therefore perpendicular to the water, which again falls downward. The pros and cons of each cooling tower arrangement are discussed in [4–6, 10]. This thesis will focus particularly on the design of mechanical induced-draft counter-flow wet cooling towers.

A typical design of the cooling tower in question consists of seven basic components, i.e., fan, drift eliminator, water distribution system, fill, rain zone, air inlet, and basin – see Figure 1.1. The incoming hot water that was heated by an external process enters the water distribution system manifolds and is discharged through spray nozzles inside the tower. The spray nozzles form a part of the water distribution system and they are responsible for spraying the hot water evenly over the entire fill. The water is partially cooled while it passes downwards through the spray zone, however, most of the cooling occurs as the water travels through the fill. Water exits the fill medium as small droplets passing through the rain zone, where some additional, albeit typically modest (i.e. 10-20% of overall heat rejection), cooling occurs [11]. Finally, the cool water is collected in the basin that is located at the tower bottom and then it is drained and recirculated after adding makeup water lost to either evaporation or blowdown. On the other hand, ambient cool air is drawn into the cooling tower through the air inlet located at the tower base. The louvers form an arrangement of horizontal blades at the air inlet that prevent the escape of falling water while allowing free entry of ambient air. The air continues its path upwards through the rain, fill, and spray

zones all the while collecting heat and moisture from the falling water. Before reaching the fan, the air passes through the drift eliminator to recapture any small liquid water droplets that are entrained in the airflow. The drift eliminator consists of parallel blades arranged on the air discharge side of the tower and their shape requires the entrained water droplets to change direction several times prior to being discharged out of the tower. Air passes through the drift eliminator unhindered, but water droplets impinge upon the drift eliminator blades and then drip back down onto the fill and ultimately onto the basin. Finally, the air is discharged through the fan into the atmosphere. The fan is driven by an electric motor where a transmission unit of some sort is situated between the motor and the fan.

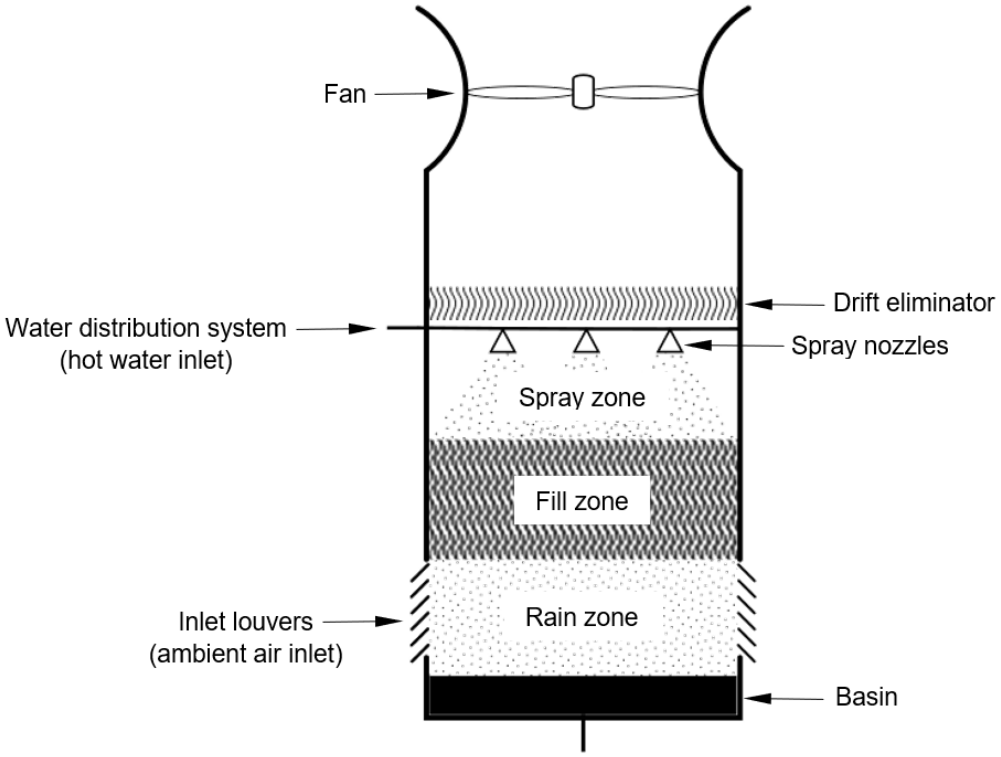

Figure 1.1 – Schematic of a mechanical induced-draft counter-flow wet cooling tower.

The fill is an essential wet cooling tower component that determines the tower effectiveness for heat rejection. The cooling tower effectiveness is influenced by the ability of the fill to promote maximum contact between the water and air and the maximum residence time of the former [6, 12]. An ideal fill is one that boosts air-water contact while imposing the least possible restriction to the airflow. The two basic fill classifications are splash type and film type. Splash-type fill consists of successive offset levels of horizontal and parallel bars that break up the descending water by causing it to cascade from one level to the next. This fill type is characterized by reduced static pressure losses and it is not conducive to fouling.

However, the disadvantage of the splash fill is its high sensitivity to inadequate support [6]. Long term performance reliability requires that the splash bars remain horizontal and be supported on close centers [6]. Film-type fill consists of a series of corrugated flutes bound together to form a lock. Each of these flutes in essence becomes a small cooling vessel specifically designed to accommodate a portion of the water loading and the remaining region is dedicated to the airflow. The advantage of a film-type fill is its higher cooling efficiency per unit of fill volume, but its cooling performance is extremely sensitive to poor distribution [6]. Modern cooling towers use film-type fills made of PVC sheets because this material has good strength characteristics, is light in weight, and easy to manufacture [4, 6]. In general, film-type fills have a denser configuration than the splash-type fills, thus less volume of a film-type fill is required for a given heat capacity. In contrast, more fan power consumption is associated with film-type fills than will splash-type fills [12].

1.2.2 Cooling tower analysis

Cooling tower performance analysis is an old practice that has been developed on the basis of zero-dimensional thermodynamic models. Since the earliest theoretical model for cooling tower operation was developed by Mosscrop in 1899, it was recognized that cooling results from the effect of evaporation combined with a transfer of sensible heat [13]. The challenge of studying the dual transfer of heat and mass was overcome in a more ingenuous and elegant manner by Merkel [14] who combined the two transfer processes into one using enthalpy potential. Merkel's theory is based on three critical assumptions to reduce the solution of heat and mass transfer to a tractable calculation. These assumptions are: (i) the Lewis factor relating heat and mass transfer coefficients [1] is equal to 1; (ii) the air exiting the tower is always saturated with water vapor; (iii) the amount of water evaporated is small and can therefore be neglected in the energy balance. Since Merkel's paper was discovered in the German technical literature and translated into English in 1941 by Nottage [15], the model has been widely adopted in the cooling towers industry. Analogously, Merkel's model has been integrated into rating tables and industry standards utilized for cooling tower design [13]. Other zero-dimensional thermodynamic models were proposed for describing the heat and mass transfer in cooling towers; however, these models are often based on the assumptions applied in the Merkel model [16]. Numerous attempts have been made to extend the scope and accuracy of the Merkel method. These are reviewed in comprehensive detail in section 1.3.2 below.

Cooling tower performance can be characterized by three parameters, i.e., cooling tower

[1] Formally, the Lewis factor is defined as the ratio of thermal diffusivity to mass diffusivity. The dimensionless number can be expressed as the ratio of the heat transfer Stanton number to the mass transfer Stanton number.

approach, cooling tower range, and Merkel number. The cooling tower approach is defined as the difference between the outlet water temperature and the ambient air wet-bulb temperature. The cooling tower range is defined as the difference between the inlet and outlet water temperatures. A dimensionless number commonly called the Merkel number or cooling tower characteristic can serve as a benchmark for overall performance. The Merkel number, Me, estimates the amount of effort needed to achieve a specified degree of mass transfer [5]. It is defined as follows

$$\mathrm{Me} = \frac{\beta a_f A_{\mathrm{ct}} H_{\mathrm{ct}}}{m_w} \tag{1.1}$$

where β is the average mass transfer coefficient in kg/(m^2.s), a_f is the specific interface area in m^2/m^3, the product $A_{\mathrm{ct}}H_{\mathrm{ct}}$ represents the active cooling volume in m^3, and m_w is the water mass flow rate in kg/s.

The atmosphere represents the ultimate heat sink for cooling towers. During wet cooling tower operation, there is a loss of water due to evaporation where water vapor is discharged into the atmosphere. At a relatively high humidity, the surrounding air is too laden with moisture to absorb the water vapor that is discharged from the cooling tower and, consequently, the air becomes supersaturated. Part of the water vapor condensates into small droplets, resulting in a visible plume formed above the cooling tower. The process of visible plume formation is illustrated by the psychrometric chart in Figure 1.2. At the saturation curve, air relative humidity is 100%. Above this curve, there is a supersaturated region where the visible plume exists. The sub-saturated region lies below the saturation curve where the plume is no longer visible. Point A represents the saturated cooling tower exhaust air, while point C represents a corresponding ambient condition. The mixture of cooling tower effluent and ambient air follows the line AC if the mixing process is adiabatic. As can be seen, most of the mixing process occurs in the supersaturated region. The visible plume exists along the line AB. The line CB is located within the sub-saturated region where water droplets have evaporated and the plume is no longer visible. The area between the line AB and the saturation curve is called the visible plume potential. The area in question quantifies the visible plume intensity and it is computed as follows [17]

$$\text{Visible plume potential} = 2\int_{\omega_B}^{\omega_A} \sqrt{\omega}\, \mathrm{d}\omega \tag{1.2}$$

where ω is the air humidity ratio in $\mathrm{g}_w/\mathrm{kg}_{da}$ in which the subscripts w and da indicate water and dry air, respectively.

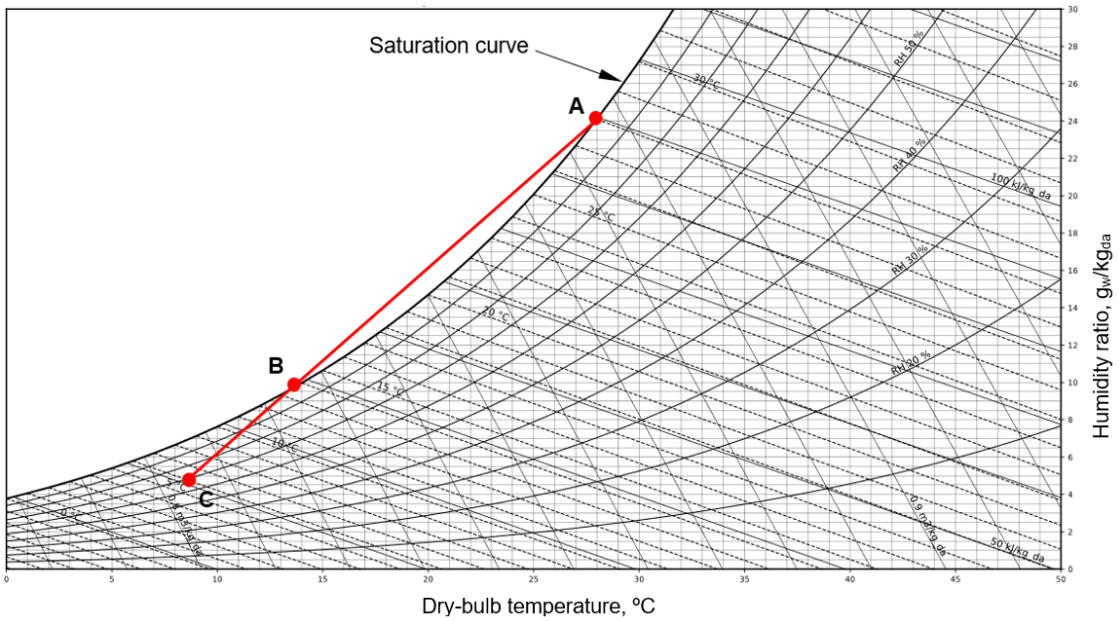

Figure 1.2 – Psychrometric chart illustrating visible plume formation.

1.2.3 Design and optimization

Cooling tower design problems can be formulated as optimization problems. The optimization problem is formulated through the standard design optimization problem. Such a mathematical model is defined as the minimization of a cost function while satisfying all equality and inequality constraints with respect to a number of design variables [18]. The standard design optimization problem is stated as follows

$$\begin{aligned} &\text{minimize} && f(\mathbf{x}) && \\ &\text{w.r.t.:} && x_k && \text{for } k = 1, 2, ..., n \\ &\text{subject to:} && h_i(\mathbf{x}) = 0 && \text{for } i = 1, 2, ..., p \\ & && g_j(\mathbf{x}) \leq 0 && \text{for } j = 1, 2, ..., q \end{aligned} \tag{1.3}$$

where $f(\mathbf{x})$ is the objective function, $\mathbf{x}$ is a vector of length n consisting of design variables, $h_i(\mathbf{x})$ are the equality constraints (i constraints total), and $g_j(\mathbf{x})$ are the inequality constraints (j constraints total). Note that the standard design optimization model treats only minimization problems. This is no restriction, as maximization of a function $F(\mathbf{x})$ is the same as minimization of a transformed function $f(\mathbf{x}) = -F(\mathbf{x})$. Once the optimization problem been formulated, an optimization algorithm is applied to find its solution with the help of a computer. There is a collection of optimization algorithms, each of which is tailored to a particular type of optimization problem [19]. Optimization algorithm selection determines whether the problem is solved rapidly or slowly and, indeed, whether the solution is found at all [19].

1.3 Literature review

There are numerous works in the literature that address cooling towers from different aspects, namely the design procedure, modelling of the thermal performance, modelling of cooling tower atmospheric plumes, and optimization.

1.3.1 Practical approaches to cooling tower design

The cooling tower design process has been discussed in many reference texts [4, 5, 10, 13, 20] and industry standards [21, 22]. Cheremisinoff and Cheremisinoff [5] suggested a procedure for obtaining a preliminary estimate of cooling tower size. The procedure leverages the Merkel method and estimates the required fill geometry and airflow using an empirical approach that does not account for the air pressure losses. Baker [13] explained the procedure for developing rating charts used for cross-flow cooling tower selection. The rating charts are widely used by cooling tower manufacturers as they make the tedious process of selecting an appropriate design more convenient. Jaber and Webb [23] proposed a basic approach to design counter-flow or cross-flow cooling towers using the standard e-NTU method. Hill et al. [4] refereed to the possibility of making an economic choice between a cooling tower design with either high capital cost and low operating cost or a low capital cost and higher operating cost. The authors revealed that the former design is capable of delivering the required cooling performance with large fill and low fan power, while the latter design can deliver the same cooling performance with small fill and greater fan power. Erens [20] presented an iterative method for solving the Merkel equation together with the air draft equation in order to find the required air velocity for meeting specific operating conditions. Mohiuddin and Kant [24, 25] presented a methodology for cooling tower selection.

Based on the above review, the optimization framework in this thesis should incorporate both hydrodynamic and thermal analysis in order to estimate not only cooling performance but also the total pressure losses that air experiences when moving through each component of the cooling tower. With this information in hand, fan power consumption can be estimated for a given cooling performance. Moreover, the optimization framework in question should be able to account for capital and operating costs, and be able to provide designs with different trade-offs between both costs.

1.3.2 Thermal performance modelling

Cooling tower thermal performance analysis is often based on zero-dimensional thermodynamic models. The validity and accuracy of these models have been the subject of many research studies. Sutherland [26] investigated the effect of ignoring water evaporation on the

accuracy of the Merkel model. The author concluded that cooling towers can be undersized by 5-15% when the Merkel model is employed for the performance analysis. Webb [27] found that the error in assuming that the Lewis factor is unity is minor. This result was reinforced by Kloppers and Kröger [28], who determined that Lewis factor variations become especially small when the ambient air temperature is high. Poppe and Roğenger [29] proposed a complete and more accurate zero-dimensional thermodynamic model that more properly accounts for water evaporation and that does not require the Lewis factor to be unity. Poppe's model has not been as widely adopted in the cooling tower industry as compared to the Merkel model because of its greater complexity, i.e., Poppe's model requires simultaneous numerical integration of three differential equations. Kloppers and Kröger [30, 31] conducted a comprehensive comparison of the Merkel, Poppe, and e-NTU models for the prediction of both cross-flow and counter-flow wet cooling tower performance under a range of ambient conditions. The authors found that the Poppe model predictions are more accurate than the other two models particularly when hot and dry ambient conditions are applied. Furthermore, the authors suggested that if only the outlet water temperature is of interest, then use of the Merkel model or the e-NTU model is acceptable.

The solution of the Merkel, Poppe, and e-NTU models does not estimate the local flow parameters inside the tower. This is because the models in question are zero-dimensional and use the water temperature (not the vertical coordinate) as the key independent variable. Correspondingly, Klimanek and Białecki [32] re-arranged the mass and heat balance equations applied for a counter-flow fill into a system of ordinary differential equations. This system presents a two point boundary value problem where the independent variable is the vertical position in the fill and the solution variables are water mass flow rate, air humidity ratio, air temperature, and water temperature. Klimanek and Białecki's model predictions achieved good agreement with Poppe's model results, however, the new solution methodology was able to provide a spatial distribution of the flow parameters in the vertical direction inside the fill. A limitation of Klimanek and Białecki's model is that it takes a tower-centric approach and assigns a single overall Merkel number when modelling the disparate transfer process in the rain, spray and fill zones. This shortcoming was overcome in the recent study by Zargar et al. [1] who applied a Klimanek-type analysis but defined distinct Merkel numbers for the different cooling tower zones. The augmented model developed by Zargar et al. [1] was validated against selected field data of an actual cooling tower.

Cooling tower performance has also been studied using multi-dimensional models. In this respect, Majumdar et al. [33, 34] presented one of the first two-dimensional computational fluid dynamics (CFD) models in literature. They solved the Reynolds averaged Navier–Stokes (RANS) equations with an algebraic model, together with mass conservation equations for air, water vapor, and liquid water, and an energy equation for the liquid and

gas phases. The source terms of the mass and energy conservation equations were represented based on the use of the Merkel model applied for the fill zone. On the other hand, their numerical CFD model neglects heat and mass transfer in the spray and rain zones. Hawlader and Liu [35] adopted the same model presented by Majumdar et al. [33, 34] to analyze inlet-fill interactions in a natural draft wet cooling tower. However, instead of ignoring the rain zone, Hawlader and Liu [35] modelled droplet flow in the rain zone using a one-dimensional Lagrangian particle tracking model. Klimanek et al. [36–38] developed two-dimensional and three-dimensional numerical CFD models for a natural-draft wet cooling tower utilizing the standard $k-\epsilon$ as the turbulence closure model within FLUENT [39]. The authors modelled the fill as a porous medium using the solution methodology proposed by Klimanek and Białecki [32]. Similar to Klimanek et al. [36, 37], Al-Waked and Behnia [40–42] developed a three-dimensional numerical CFD model but paid particular attention to the effect of droplet diameter, inlet water temperature, number of nozzles, water flow rate, number of tracks per nozzle, and windbreak walls on the thermal performance of a natural draft cooling tower. Williamson et al. [43, 44] concluded that the cooling performance predictions of zero-dimensional thermodynamic models appear to agree well with the predictions of the comprehensive CFD models.

Cooling tower models of varying fidelity have been developed over the years to predict the thermal performance of different cooling tower types. In this thesis, the one-dimensional zone-specific thermodynamic model by Zargar et al. [1] is used in the optimization framework for the following three reasons: (i) the model analyzes the zone-specific performance more accurately in a variety of ambient air conditions including those classified as hot and dry; (ii) the model accurately estimates the quality of the exhaust air at the tower exit compared to the Merkel or e-NTU models because both of them always assume the exiting humid air to be saturated (relaxing this assumption provides a more accurate evaluation of the thermal performance and the plume source conditions); and (iii) the use of a one-dimensional model can significantly reduce the required CPU time for the computations compared to CFD multi-dimensional models.

1.3.3 Atmospheric plume modelling

An extensive theoretical work has been undertaken to study the formation and dispersion of cooling tower plumes. The developed theoretical models of moist plumes aims to predict the visible plume length and trajectory in the atmosphere by applying time-averaged equations representing the conservation of mass, momentum, heat, and water vapor. These models are based on some assumptions that simplify the physics associated with the turbulent entrainment of ambient air into the plume, the thermodynamic aspects of water vapor,

the deflection of the plume by the wind, and atmospheric stratification. The earliest moist plume model in literature, called MTT model, was proposed by Morton [45] and it is based on Taylor's entrainment hypothesis, i.e., the entrainment rate at the plume edge is proportional to the mean vertical velocity at plume core. Csanady [46] considered the effect of ambient wind in the derivation of the moist plume model in a homogeneous ambient and in a stratified ambient. Wigley and Slawson [47] expanded the work of Csanady [46] and illustrated in detail the difference between dry and moist plume behavior under various atmospheric stratification conditions. Briggs [48, 49] conducted a comprehensive review of plume modelling and suggested the use of "two-thirds law" for the prediction of bent-over buoyant plumes. In turns, Briggs's two-thirds law is widely supported by field observations and by some laboratory experiments.

Attempts have continued to improve the plume modelling accuracy. Carhart et al. [50] reviewed the performance accuracy of 16 popular moist plume models by comparing their predictions with field data and single-phase laboratory data. The authors suggested that improvements should take place in the following five areas in order to reflect physically correct assumptions: (i) the balance between momentum transfer and dilution mechanisms; (ii) the nature of correct moisture thermodynamics; (iii) the effect of the tower wake on the plume trajectory and dilution; (iv) the atmospheric turbulent diffusion formulations; and (v) the representation of the plume merging process. Schatzmann and Policastro [51] developed an integral moist plume model that addresses (i)-(iii). Carhart and Policastro [52] developed an advanced integral single-source moist plume model called the Argonne National Laboratory and University of Illinois (ANL/UI) model that addresses (i)-(iv). Janicke and Janicke [53] proposed another advanced integral model called PLURIS that accounts for a three-dimensional wind profile and arbitrary source conditions for both dry and moist plumes.

Predictions of the likelihood of visible plume formation from cooling towers have been analyzed most recently using MTT-type theoretical models. Li et al. [54] developed an integral model for uniform and coaxial plumes [2] The authors introduced a term called the resistance factor for describing the likelihood of visible plume formation and/or a recirculation of moist air back into the cooling tower inlet louvers. Zargar et al. [1] adopted an integral moist plume model coupled with one-dimensional zone-specific counter-flow wet cooling model. Their plume model does not consider the impact of wind forcing nor the ambient stratification, which confines its predictions more accurately within short elevation above the cooling tower only. Furthermore, their model was validated against the results presented by Li et al. [54]. Zargar et al. [1] revealed that coupling the plume model with

[2]Coaxial plumes consist of an inner core of wet air enveloped by an outer stream of drier (through still buoyant) air.

their proposed augmented model can assess visible plume severity more accurately.

The prediction accuracy of the integral moist plume model included in Zargar et al. [1] accommodates the nature of a cooling tower design problem. The plume visibility as a design requirement demands a short visible plume, or , in critical instances, a total elimination of fog formation. Therefore, the required plume model for assessing visible plume severity used for cooling tower design does not necessarily incorporate the impact of wind forcing nor the ambient stratification. The latter two phenomena appear more significantly at high elevations. The integral moist plume model included in Zargar et al. [1] is used in the optimization framework in this thesis.

1.3.4 Cooling tower optimization

Cooling towers optimization has been explored from three different perspectives, i.e., the design of cooling tower in isolation, the design of cooling tower within a cooling cycle, and the control of cooling tower performance. The cooling system in question consists of a condenser, cooling tower, circulating water pump, and associated piping and accessories. The aim of optimizing a cooling system is to obtain the operating conditions of each component in such manner that the combination will result in a minimum evaluated cost. A number of optimization studies are found in the literature related to different cooling tower types as a part of heat exchanger networks [55–57], vapor compression refrigeration systems [58, 59], hybrid-ground heat pump systems [60], mine cooling systems [61], geothermal power plants [62], and auxiliary cooling systems of a combined-cycle power plant [63]. Moreover, the optimal control of cooling towers, from the point of view of tower operation, has been discussed in [64, 65]. This thesis is concerned with the design optimization of a cooling tower in isolation.

Table 1.1 summarizes the available optimization studies of cooling towers in isolation. Only a part of the optimization studies in the table has considered cooling tower economics. Söylemez [66] studied the thermo-hydraulic performance optimization of mechanical forced-draft counter-flow wet cooling towers by adapting the e-NTU model to predict the cooling tower performance. Singh and Das [67] studied the thermal performance optimization of the same cooling tower type using a multi-objective formulation. The authors developed empirical correlations for the objective functions, i.e., cooling tower range, Merkel number, effectiveness, and evaporation rate with respect to the design variables, i.e., air mass flow rate and water mass flow rate. All objectives were simultaneously optimized for maximizing the cooling tower performance using an elitist non-dominated sorting genetic algorithm. The authors concluded that there are different optimal operating points for each fill type. Singla et al. [68] solved a single-objective optimization problem for estimating the air mass flow

rate and water mass flow rate in order to satisfy a given Merkel number using differential evolution. The authors concluded that there are different combinations of the air mass flow rate and water mass flow rate to satisfy a given value of the Merkel number. Williamson et al. [69] studied the thermal performance optimization of a natural draft wet-cooling tower at specific operating conditions. The authors employed the extended Merkel model, which accounts for the heat and mass transfer in the spray, fill, and rain zones, in conjunction with a genetic optimization algorithm in order to optimize the fill shape and water distribution profile across the tower. To account for varying water distributions in different regions of the fill, the authors divided the fill into four zones in parallel, each with an independent fill depth and water flow rate. The results showed that the optimal layout is with both the water flow rate and the fill height decreasing towards the centre of the tower. However, the authors reported that the potential improvement in cooling performance is very marginal when measured against a design where the water is distributed uniformly.

The optimization studies outlined in Table 1.1 that considered cooling tower economics are discussed next. Söylemez [70] studied the thermo-economical performance optimization of mechanical forced-draft counter-flow wet cooling towers. The e-NTU model was employed to predict the cooling tower performance at fixed ambient air conditions and inlet water flow rate. Kloppers and Kröger [71] studied the thermo-economical performance optimization of a natural draft wet-cooling tower at fixed design ambient air conditions, inlet water flow rate, and outlet water temperature. Both authors employed the extended Merkel model in conjunction with a gradient-based optimization algorithm to optimize three geometrical dimensions of the cooling tower. It was found that the air inlet height is the most critical parameter influencing the combined capital and operating costs compounded over the economic life of the cooling tower. Ataei et al. [72] studied the thermo-economical performance optimization of a mechanical induced-draft counter-flow wet cooling tower at fixed design ambient air conditions, inlet water flow rate, and outlet water temperature. The authors concluded that there is a trade-off between the capital and operating costs with respect to the heat and mass transfer area. Serna-González et al. [73] studied the thermo-economical performance optimization of a mechanical draft counter-flow wet cooling tower at fixed cooling load and different ambient conditions. The authors employed the Merkel model in conjunction with a mixed-integer nonlinear programming. Their proposed methodology was capable of finding the optimum operational parameters and fill dimensions, as well as the optimum fill type and draft type. The optimization problem was constrained at specific range for the cooling tower approach, inlet water temperature, outlet water temperature, and water-to-air mass ratio. The authors concluded that, not surprisingly, the cooling tower approach is a critical constraint when assessing the total annual cost of the cooling tower, which increases significantly at low cooling tower approach. Rao and Patel [74] studied the

thermo-economical performance optimization of a mechanical forced-draft counter-flow wet cooling tower at fixed cooling load and different ambient conditions. The authors adopted the same thermal analysis, economical model, and performance constraints used by Serna-González et al. [73], however, Rao and Patel [74] used an artificial bee colony optimization algorithm. Furthermore, Rao and Patel [74] minimized the total annual cost with respect to only three design variables, i.e., air mass velocity, water mass velocity, and water-to-air mass ratio. Rao and Patel [74] found that using a low air mass flow rate reduces the total annual cost by particularly reducing the fan power consumption, even though in such case a longer fill height is required to meet the cooling load. Rao and More [75] reproduced the results by Rao and Patel [74] by employing a proposed self-adaptive Jaya algorithm. The authors found that their algorithm is more computationally efficient than the ABC algorithm in finding the optimal cooling tower design because the self-adaptive Jaya algorithm requires less population size. Rubio-Castro et al. [76] employed a similar methodology to Serna-González et al. [73] to study thermo-economical performance optimization of the same cooling tower type. Thoroughly, the authors applied the same economical model and performance constraints, however, Rubio-Castro et al. [76] adopted the Poppe model for cooling tower performance prediction instead of the Merkel model. Their results showed that the optimal design was significantly different when using the Poppe model instead of Merkel model particularly in terms of the evaporated water mass flow rates, fan power consumption, and fill height. The authors attributed this difference in the optimal designs to the fact that the Merkel model neglects the effect of the water loss by evaporation on the enthalpy change of the water stream. Moreover, the Merkel model assumes the outlet air is always saturated with water vapor. Rubio-Castro et al. [76] stated that the use of the Poppe model in the thermo-economical performance optimization leads to more reliable optimal designs of wet cooling towers.

Based on the above review, there are some missing points that were not addressed in the thermo-economical performance optimization of cooling towers. The use of multiple objectives is not explored; a multi-objective formulation was employed in only one thermal performance optimization study by Singh and Das [67] where the objective functions are the Merkel number, cooling tower effectiveness, and evaporation rate. The solution of multi-objective optimization presents the best possible trade-offs between capital and operating costs for given design specifications. This variety in the optimal designs helps the user decide on the most appropriate cooling tower design for a given application (and scheme for financing). Another venue that was not explored previously is including plume visibility as a design requirement. No optimization study has introduced the visible plume length as an additional constraint along with the performance constraints. However, there are approaches from the previous optimization studies that could be adopted in the present study. Characterizing the performance constraint by restricting the outlet water temperature

is applied when the inlet water mass flow rate and temperature are fixed design operating conditions. Also, considering a specific range for the water-to-air mass ratio (later refereed to as the liquid-to-gas ratio) for film-type fills should be applied in the present study [73–76]. This is to ensure that the cooling tower performance is not degraded when the fill is too dry nor flooded with water. Introducing the air mass flow rate and fill geometry as design variables is another aspect that is adopted in the present study.

Table 1.1 – Chronological summary of the literature on cooling tower design optimization.

Reference	**Cooling tower type**	**Thermodynamic model**	**Optimization parameters**	**Optimization method**
Söylemez [70], 2001	Mechanical forced-draft counter-flow wet cooling tower	e-NTU model	Minimize the total cost of the cooling tower throughout its life cycle with respect to the mass and heat transfer area	One-dimensional line search
Söylemez [66], 2004	Mechanical forced-draft counter-flow wet cooling tower	e-NTU model	Minimize the water-to-air mass ratio with respect to mean temperature of water and ambient pressure	One-dimensional line search
Kloppers and Kröger [71], 2004	Natural draft counter-flow wet cooling tower	Extended Merkel model	Minimize the total cost of the cooling tower throughout its life cycle with respect to the cooling tower height, air inlet height, and diameter at the bottom of the cooling tower	LFOPC optimization algorithm
Williamson et al. [69], 2008	Natural draft counter-flow wet cooling tower	Extended Merkel model	Maximize cooling tower range with respect to the fill height and water mass flow rate for each of the four parallel fill sections	Genetic algorithm

Ataei et al. [72], 2009	Mechanical induced-draft counter-flow wet cooling tower	Extended Merkel model	Minimize the total cost of the cooling tower throughout its life cycle with respect to the geometrical dimensions	One-dimensional line search
Serna-González et al. [73], 2010	Mechanical draft counter-flow wet cooling tower	Merkel model	Minimize the total cost of the cooling tower throughout its life cycle with respect to the operational parameters, fill dimensions, fill type, and draft type, subjected to constrained cooling tower approach, constrained inlet water temperature, constrained outlet water temperature, and constraint water-to-air mass ratio	Mixed-integer nonlinear programming
Rao and Patel [74], 2011	Mechanical forced-draft counter-flow wet cooling tower	Merkel model	Minimize the total cost of the cooling tower throughout its life cycle with respect to air mass velocity, water mass velocity, and water-to-air mass ratio, subjected to constrained cooling tower approach, constrained inlet water temperature, constrained outlet water temperature, and constraint water-to-air mass ratio	Artificial bee colony algorithm

Rubio-Castro et al. [76], 2011	Mechanical forced-draft counter-flow wet cooling tower	Poppe model	Minimize the total cost of the cooling tower throughout its life cycle with respect to the operational parameters, fill dimensions, and fill type, subjected to constrained cooling tower approach, constrained inlet water temperature, constrained outlet water temperature, and constraint water-to-air mass ratio	Mixed-integer nonlinear programming
Singh and Das [67], 2016	Mechanical forced-draft counter-flow wet cooling tower	Empirical correlations for the performance parameters developed using collected experimental data	Optimize cooling tower range, Merkel number, effectiveness, and evaporation rate with respect to air mass flow rate and water mass flow rate for different fill types	Elitist non-dominated sorting genetic algorithm
Singla et al. [68], 2016	Mechanical forced-draft counter-flow wet cooling tower	Empirical correlations for the performance parameters developed using collected experimental data	Satisfy a given value of the Merkel number by estimating air mass flow rate and water mass flow rate	Differential evolution

Roa and More [75], 2017	Mechanical forced-draft counter-flow wet cooling tower	Merkel model	Minimize the total cost of the cooling tower throughout its life cycle with respect to air mass velocity, water mass velocity, and water-to-air mass ratio, subjected to constrained cooling tower approach, constrained inlet water temperature, constrained outlet water temperature, and constraint water-to-air mass ratio	Self-adaptive Jaya algorithm

1.4 Objectives

As the preceding literature review makes clear, there has been no optimization study that considers thermal performance and plume visibility as design requirements. Most optimization studies focused on thermo-economical performance optimization, but they did not introduce the visible plume length as an additional constraint to the optimization problem. Furthermore, the trade-off between capital and operating costs was not explored quantitatively due to the combination of the two cost types into a single objective function in the optimization problem. Finally, researchers have employed only zero-dimensional thermodynamic models in various works related to the optimization of different types of cooling towers. Particularly, the use of the Merkel or e-NTU model does not accurately estimate quality of the exhaust air at the tower exit because these two models always assume the exiting humid air to be saturated. Relaxing this assumption, as it was done by Rubio-Castro et al. [76] using Poppe model, could provide a more accurate evaluation of the thermal performance and the plume source conditions. Even using Poppe model, the use of a lumped heat transfer approach does not comprehensively assess the cooling performance of each tower zone. The shortcomings in thermal analysis mentioned previously could be avoided when the one-dimensional zone-specific thermodynamic model by Zargar et al. [1]. Another useful feature of the model is that it is coupled with an integral plume model.

This study aims to address the limitations outlined above. More specifically the goals can be stated as:

1. Develop a numerical optimization framework that can account for thermal performance

and plume visibility simultaneously.

2. Study the trade-offs between capital and operating costs in the design of a mechanical induced-draft counter-flow wet cooling tower with and without including visible plume constraint.

1.5 Thesis layout

Chapter 1

Chapter 1 presents an introduction to the thesis and the motivation for studying cooling tower design. A literature review is presented that summarizes past and present research efforts in: practical approaches to cooling tower design, modelling the thermal performance of cooling towers, atmospheric plume modelling, and cooling tower optimization. The first chapter ends by stating the objectives of the present work and by summarizing the thesis layout.

Chapter 2

Chapter 2 outlines the analysis methodology to be pursued when modelling mechanical induced-draft counter-flow wet cooling towers. In this chapter, the governing equations for the wet cooling tower and its plume are presented. The derivation of the air draft equation for the cooling tower in question is discussed. Then, the implementation of cooling tower analysis within the software package CoolIT is described.

Chapter 3

Chapter 3 presents the cooling towers design methodology as this is influenced by the principles of optimization. Three design problems are presented along with the corresponding optimization formulations and solution methods to be applied. Thus a numerical optimization framework is presented to solve the three optimization problems.

Chapter 4

Chapter 4 presents the results of the three design problems discussed in Chapter 3 supported with discussion, post-optimality analysis, and verification.

Chapter 5

Chapter 5 summarizes the conclusions of the present study and presents the possible avenues for future research.

Chapter 2

Cooling tower modeling

2.1 Thermal analysis

The thermal analysis of a wet cooling tower is based on the modelling of heat and mass transfer processes by simplifying complex air/water flow interaction to a simple volumetric heat and mass balance applied for a control volume. Zargar et al. [1] adopted a numerical model that is capable of evaluating the main thermodynamic properties of water and air inside a counter-flow wet cooling tower as well as the main properties of the associated atmospheric plume above the cooling tower. This numerical model is a result of coupling a one-dimensional zone-specific thermodynamic model with turbulent plume model. The use of this model is ideal for the thermal analysis needed for cooling tower design optimization for the following three reasons: (i) the model analyzes the zone-specific performance more accurately in a variety of ambient air conditions including the hot and dry conditions; (ii) the model enables the addition of a plume visibility constraint to the design optimization problem; (iii) the use of one-dimensional model can significantly reduce the required CPU time for the computations compared to CFD multi-dimensional models.

2.1.1 1D zone-specific counter-flow wet cooling tower thermodynamic model

In a counter-flow wet cooling tower, water falls vertically down through the three critical zones of the cooling tower where airflow is opposite to the direction of water flow as shown in Figure 2.1. Heat and mass are exchanged between water and air at the interface. The water is eventually cooled to the final temperature at the basin because of latent and sensible heat transfer between the water and air. The thermodynamic model is derived by following the solution methodology proposed by Klimanek and Bialecki [32] and later expanded by Zargar et al. [1]. The model is limited by the following assumptions:

1. A thin film of saturated air at the water temperature is assumed to exist at the

air–water interface. The humidity ratio difference between the local air at any height and the interfacial region drives a flow of water vapor to the local air.

2. The water temperature is taken as the bulk average value at each vertical location.

3. The local air temperature and humidity ratio at any height are assumed to be at their bulk average values.

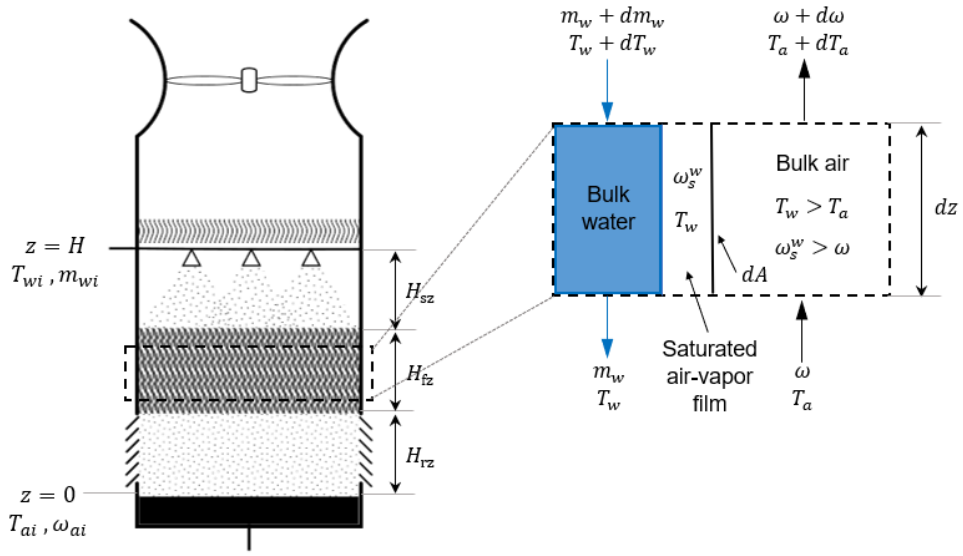

Figure 2.1 – Differential control volume for a segment of the wet cooling tower, reproduced from reference [1].

Assuming the outlet air is not supersaturated, by applying energy and mass balances on a differential control volume for a segment of the wet cooling tower shown in Figure 2.1, the governing equations for the water mass flow rate, m_w, humidity ratio of unsaturated air, ω, unsaturated air temperature, T_a, and water temperature, T_w, are obtained. The result is a system of four ordinary differential equations, i.e., (2.1-2.4) [1]. The derivation is presented in detail in [1, 77].

$$\frac{\mathrm{d}m_w}{\mathrm{d}z} = \beta\, a_f\, A_{\mathrm{ct}}(\omega_s^w - \omega) \tag{2.1}$$

$$\frac{\mathrm{d}\omega}{\mathrm{d}z} = \frac{\beta a_f A_{\mathrm{ct}}(\omega_s^w - \omega)}{m_a} \tag{2.2}$$

$$\frac{\mathrm{d}T_a}{\mathrm{d}z} = \frac{\beta a_f A_{\mathrm{ct}}[\mathrm{Le_f}(T_w - T_a)(c_{pa}^a + \omega c_{pv}^a) + (c_{pv}^w T_w - c_{pv}^a T_a)(\omega_s - \omega)]}{m_a(c_{pa}^a + c_{pv}^a \omega)} \tag{2.3}$$

$$\frac{\mathrm{d}T_w}{\mathrm{d}z} = \frac{\beta a_f A_{\mathrm{ct}}\left[\mathrm{Le_f}(T_w - T_a)(c_{pa}^a + \omega c_{pv}^a) + (r_0 + c_{pv}^w T_w - c_{pw}^w T_w)(\omega_s - \omega)\right]}{m_w c_{pw}^w} \tag{2.4}$$

where $\mathrm{d}z$ is the small vertical distance of the differential control volume, β is the average mass transfer coefficient in kg/(m^2.s), a_f is the specific interface area in m^2/m^3 (also called area density) being the ratio of the air-water interface area and the volume of the fill, A_{ct} is the tower cross-sectional area, ω_s is the humidity ratio of the saturated air at the air-water interface, m_a is the mass flow rate of air, $\mathrm{Le_f}$ is the Lewis factor which connects the mass transfer coefficient and the heat transfer coefficient, r_0 is the latent heat of vaporization evaluated at a reference temperature of 0°C, c_{pv} is the average specific heat capacity measured at constant pressure for wet air, c_{pa} is the average specific heat capacity measured at constant pressure for dry air, and c_{pw} is the average specific heat capacity of water. The superscript 'a' indicates that the material property is evaluated at the bulk air temperature, T_a, while the superscript 'w' indicates that the material property is evaluated at the bulk water temperature, T_w.

If the upflowing air becomes supersaturated with vapor, the governing equations must then be modified to capture the physics of supersaturated air. Such a condition occurs for a high rate of evaporation and it is characterized by the formation of fine water droplets or mist [1]. A new system of four ODEs for supersaturated air then applies, i.e., (2.5-2.8) [1]. The derivation is presented in detail in [1, 77].

$$\frac{\mathrm{d}m_w}{\mathrm{d}z} = \beta a_f A_{\mathrm{ct}}(\omega_s^w - \omega_s^a) \tag{2.5}$$

$$\frac{\mathrm{d}\omega}{\mathrm{d}z} = \frac{\beta a_f A_{\mathrm{ct}}(\omega_s^w - \omega_s^a)}{m_a} \tag{2.6}$$

$$\begin{aligned}\frac{\mathrm{d}T_a}{\mathrm{d}z} = \frac{-\beta a_f A_{\mathrm{ct}}}{m_a}\Big[&\mathrm{Le_f} c_{pa}^a (T_a - T_w) - \omega_s^w (r_0 + c_{pv}^w T_w) \\ &+ c_{pw}^a (\mathrm{Le_f}(T_a - T_w)(\omega - \omega_s^a) + T_a(\omega_s^w - \omega_s^a)) \\ &+ \omega_s^a (r_0 + c_{pv}^a \mathrm{Le_f}(T_a - T_w)) + c_{pv}^w T_w\Big] \\ &/ \left[c_{pa}^a + c_{pw}^a \omega + \frac{\mathrm{d}\omega_s^a}{\mathrm{d}T_a}(r_0 + c_{pv}^a T_a - c_{pw}^a T_a) + \omega_s^a (c_{pv}^a - c_{pw}^a)\right]\end{aligned} \tag{2.7}$$

$$\frac{\mathrm{d}T_w}{\mathrm{d}z} = \frac{\beta a_f A_{\mathrm{ct}}[(r_0 + c_{pv}^w T_w - c_{pw}^w T_w)(\omega_s^w - \omega_s^a) + \mathrm{Le_f}(T_w - T_a)(c_{pa}^a + c_{pw}^a(\omega - \omega_s^a) + c_{pv}^a \omega_s^a)]}{m_w c_{pw}^w} \tag{2.8}$$

In solving the governing equations for unsaturated or supersaturated air, the triple product of $\beta a_f A_{\mathrm{ct}}$ appears. The relationship between $\beta a_f A_{\mathrm{ct}}$ and a Merkel number, Me, is given by

$$\beta a_f A_{\mathrm{ct}} = \frac{\mathrm{Me}\, m_w}{H_i} \tag{2.9}$$

where m_w is the water mass flow rate and H_i is the height of the cooling tower zone in question. The correlations that compute each of $\mathrm{Me_{rz}}$, $\mathrm{Me_{fz}}$, $\mathrm{Me_{sz}}$, and $\mathrm{Le_f}$ are found in Appendix B. The thermophyical properties of water and air, i.e., c_{pa}, c_{pv}, c_{pw}, and ω_s are computed using the equations presented in Appendix A.

In order to solve the above systems of ODEs, four boundary conditions are required. The inlet air temperature, T_{ai}, and humidity ratio, ω_{ai}, are specified at the bottom of the rain zone ($z = 0$). Meanwhile, the inlet water temperature, T_{wi}, and mass flow rate, m_{wi}, are specified at the top of the spray zone ($z = H$). Thus, we write

$$T_a(z = 0) = T_{ai};\ \omega_a(z = 0) = \omega_{ai} \tag{2.10}$$

$$T_w(z = H) = T_{wi};\ m_w(z = H) = m_{wi} \tag{2.11}$$

The total rate of heat transfer for each zone in the cooling tower could be estimated by calculating the rates of latent and sensible heat transfer in the zone in question. For the region of a cooling tower zone where the air remains sub-saturated, the rates of latent and sensible heat transfer are estimated by [1]

$$Q_l = \int_0^h a_f \beta A_{\mathrm{ct}} (r_0 + c_{pv}^w T_w)(\omega_s^w - \omega)\, dz \tag{2.12}$$

$$Q_s = \int_0^h a_f \beta A_{\mathrm{ct}} \mathrm{Le_f}\, (c_{pa}^a + \omega\, c_{pv}^a)(T_w - T_a)\, dz \tag{2.13}$$

where h is the region height where the air is sub-saturated. Conversely, the rates of latent and sensible heat transfer are estimated for the region of a cooling tower zone where the air becomes supersaturated by [1]

$$Q_l^{(s)} = \int_0^{h_s} a_f \beta A_{\mathrm{ct}} \left[r_0 + c_{pv}^w T_w (\omega_s^w - \omega_s^a)\right]\, dz \tag{2.14}$$

$$Q_s^{(s)} = \int_0^{h_s} a_f \beta A_{\mathrm{ct}} \mathrm{Le_f} \left[c_{pa}^a + \omega_s^a\, c_{pv}^a + c_w^a\, (\omega - \omega_s^a)\right] (T_w - T_a)\, dz \tag{2.15}$$

where h_s is the region height where the air is supersaturated. For a cooling tower zone with the height, H_i, where the air enters sup-saturated and leaves supersaturated, the rates of latent and sensible heat transfer for this zone are $\left(Q_l + Q_l^{(s)}\right)$ and $\left(Q_s + Q_s^{(s)}\right)$, respectively, providing that $H_i = h + h_s$.

2.1.2 Atmospheric plume model

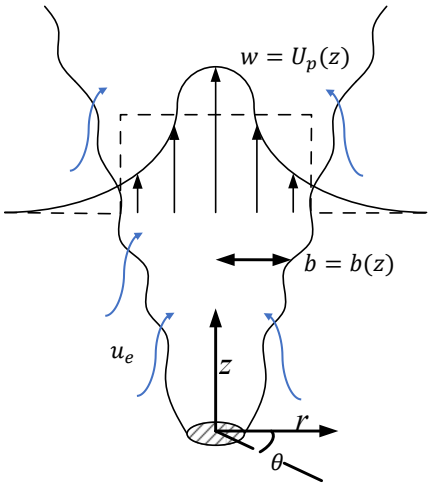

Figure 2.2 – Schematic of an axisymmetric plume in a homogeneous ambient with no wind where $b = b(z)$ is the plume radius, $w = U_p(z)$ is the top-hat vertical velocity denoted by the dashed lines, and u_e is the entrainment velocity expressed as $u_e = \gamma w$.

The air leaving from a wet cooling tower is loaded with moisture and warmer than outside ambient air. At a relatively high humidity, the surrounding air is too moisture laden to absorb the water vapor that is discharged from the cooling tower and it becomes supersaturated. Part of the ascended water vapor condensates into small droplets, resulting in a visible plume formed above the cooling tower. The interaction between the plume and the atmospheric air can be studied by theoretical models. The atmospheric plume model presented by Zargar et al. [1] is adapted from the work of Wu and Koh [78]. According to the assumptions used in Wu and Koh's plume model, the model applies when the flow satisfies the following conditions: (i) Boussinesq approximation is valid. This implies that the variations of plume density throughout the flow field are small, i.e., less than 10%; (ii) the plume pressure is hydrostatic throughout the flow field since the pressure variation in the radial direction is too small compared to the pressure variation in the vertical direction; (iii) the molecular transport is neglected in comparison with the turbulent transport, i.e., a large Peclet number for the plume is applied; (iv) the ambient stratification is neglected. This implies that the ambient temperature and humidity are assumed independent of elevation; (v) the impact of wind forcing is not considered; (vi) the cross-plume profiles exhibit a top-hat profile that is self-similar in nature. This modeling approach is used for mathematical convenience; (vii) axisymmetric and statistically steady approximations are applied. The governing equations for the atmospheric plume model describe the conservation of mass, momentum, energy, and

moisture as follows [1]

$$\frac{\mathrm{d}Q}{\mathrm{d}z} = 2\gamma\sqrt{\pi M} \tag{2.16}$$

$$\frac{\mathrm{d}M}{\mathrm{d}z} = g\,\frac{Q}{M}\left(\frac{\Theta}{T_a} - W\right) \tag{2.17}$$

$$\frac{\mathrm{d}}{\mathrm{d}z}\left(\Theta - \frac{r_o}{c_{pa}}W\right) = 0 \tag{2.18}$$

$$\frac{\mathrm{d}}{\mathrm{d}z}(H + W) = 0 \tag{2.19}$$

where $\gamma \simeq 0.117$ for the plume entrainment coefficient, Q is the volume flux, M is momentum flux, Θ is the temperature deficiency flux, W is the specific liquid moisture deficiency flux, and H is the specific humidity flux. The derivation of the plume model in question is presented in detail in [77]. Each flux term is defined by the following integrals

$$Q = \int_A U_p \,\mathrm{d}A \tag{2.20}$$

$$M = \int_A U_p^2 \,\mathrm{d}A \tag{2.21}$$

$$\Theta = \int_A (T_p - T_a)\, U_p \,\mathrm{d}A \tag{2.22}$$

$$W = \int_A (\sigma_p - \sigma_a)\, U_p \,\mathrm{d}A \tag{2.23}$$

$$H = \int_A (\omega_p - \omega_a)\, U_p \,\mathrm{d}A \tag{2.24}$$

where U, T, σ, ω, and A are, respectively, the vertical velocity, temperature, specific liquid moisture, humidity ratio, and plume cross-sectional area. The superscript 'p' indicates that the property is for the plume, while the superscript 'a' indicates that the property is for ambient air. Along with (2.16)-(2.19), the atmospheric plume model is completed by requiring [1]

$$\begin{aligned} \sigma_p &= 0; \quad \text{for} \quad \omega_p < \omega_{sat} \quad \text{(dry plume)} \\ \sigma_p &= \omega_{sat}(T_p, p); \quad \text{for} \quad \omega_p \geq \omega_{sat} \quad \text{(wet plume)} \end{aligned} \tag{2.25}$$

where p is the total pressure, and ω_{sat} is the saturation specific humidity evaluated at the plume temperature and the total pressure. The details for calculating ω_{sat} are given in Appendix A. Solving the model leads to the prediction of plume properties such as temperature,

humidity, vertical velocity, and where saturation is achieved and exceeded. In order to solve the plume model, the source conditions are required and they are evaluated at the cooling tower exist, i.e., at $z = 0$ which is referred to the fan shroud location in this case. The plume source conditions are defined by four physical quantities, i.e., volume flux, Q_o, momentum flux, M_o, total sensible heat flux, $\left(\Theta_o - \frac{r_o}{c_{pa}} W_o\right)$, and total moisture flux, $(H_o + W_o)$.

$$Q_o = U_o A_o \tag{2.26}$$

$$M_o = U_o^2 A_o \tag{2.27}$$

$$\Theta_o - \frac{r_o}{c_{pa}} W_o = U_o A_o \left(T_o - T_a\right) \tag{2.28}$$

$$H_o + W_o = U_o A_o \left(\omega_o - \omega_a\right) \tag{2.29}$$

The plume source velocity, U_o, is calculated from $U_o = \frac{m_a}{\rho A_o}$, where ρ is the plume source density which is estimated using equation (A.16) and A_o is the plume area at the source which is estimated from the inner diameter of the fan cylinder.

2.2 Air draft equation

The air draft equation helps in estimating the total pressure that the fan must overcome in order to move the air through the cooling tower. The equation is derived by applying the conservation of energy between the inlet (point 1) and discharge (point 2) in Figure 2.3 such that

$$\left(p_2 + \alpha_2 \frac{\rho_2 v_2^2}{2} + \rho_2 g z_2\right) - \left(p_1 + \alpha_1 \frac{\rho_1 v_1^2}{2} + \rho_1 g z_1\right) = \Delta p_{\text{fan}} - \Delta p_{\text{loss}} + \Delta p_{\text{buoy}} \tag{2.30}$$

In this case, p_1 and p_2 are equal to the atmospheric pressure. The atmospheric pressure differentials due to the pressure gradient in a gravity field can be ignored for mechanical draft cooling towers [16], so $p_1 = p_2$. Air near the cooling tower inlet is assumed stationary, i.e., $v_1 = 0$. For incompressible and uniform flow, the kinetic energy coefficient, α, is equal to 1. Furthermore, the hydrostatic pressure at point 2, i.e., $\rho_2 g z_2$, is neglected by considering that it is nearly the same as Δp_{buoy}. Then, equation (2.30) becomes

$$\Delta p_{\text{fan}} = \Delta p_{\text{loss}} + \frac{\rho_2 v_2^2}{2} \tag{2.31}$$

The fan performs work by overcoming the total static pressure loss, Δp_{loss}, and imparting the dynamic pressure $\frac{\rho_2 v_2^2}{2}$ to the air. The total static pressure loss, Δp_{loss}, is because of the

resistance that air experiences when moving through each component of the cooling tower, i.e., the inlet section, rain zone, fill zone, spray zone, drift eliminator, and fan cylinder. Summing all pressure losses, the total static pressure loss can be obtained as

$$\Delta p_{\text{loss}} = \Delta p_{\text{in}} + \Delta p_{\text{rz}} + \Delta p_{\text{fz}} + \Delta p_{\text{sz}} + \Delta p_{\text{de}} + \Delta p_{\text{fc}} \tag{2.32}$$

The pressure drop across a component of the cooling tower varies with the dynamic pressure in the flow and it can be estimated by [11]

$$\Delta p = K \frac{\rho v^2}{2} \tag{2.33}$$

Both the density ρ and velocity v are for moist air. The latter variable can be written as $\frac{m_a(\omega+1)}{\rho A}$.

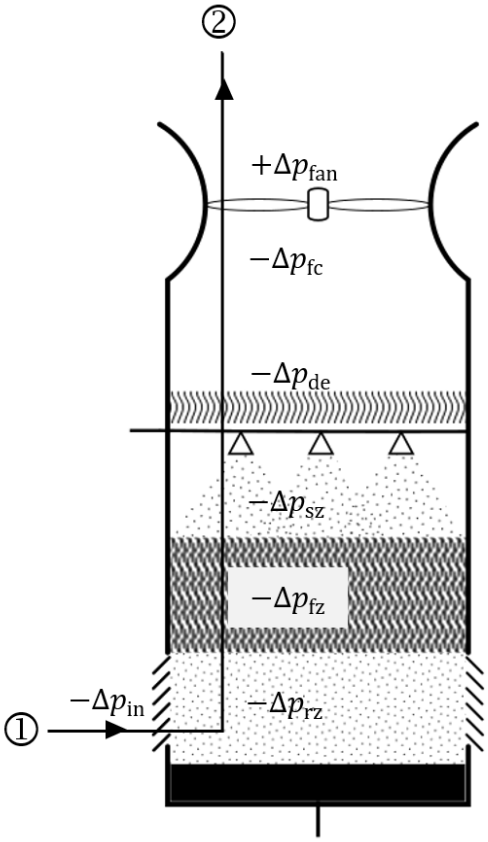

Figure 2.3 – Locations of pressure changes that the air stream experiences in the cooling tower.

The inlet louvers offer a flow resistance that depends on the inclination angle of the louvers. Changing the airflow direction from horizontal to vertical causes flow separation at the edges which adds to the pressure drop across the inlet section.

$$\Delta p_{\text{in}} = \left(\frac{K_{\text{il}}}{A_{\text{ai}}^2} + \frac{K_{\text{in}}}{A_{\text{ct}}^2} \right) \frac{m_a^2(\omega_1 + 1)^2}{2\rho_1} \tag{2.34}$$

The pressure loss coefficient for the louvers, K_{il}, and for the inlet, K_{in}, are respectively divided by the square of air inlet area, A_{ai}^2, and the square of tower frontal area, A_{ct}^2. Kröger [11] reported that $K_{\text{il}} = 2.5$ is valid for a 30° louver with 80% or more open area for a mechanical induced-draft counter-flow cooling tower. Kröger [11] reported a formula for K_{in} that depends on the ratio $A_{\text{ct}}/A_{\text{ai}}$ for isotropically packed induced draft rectangular towers.

The pressure drop across the rain zone is caused by the drag of the falling water and the fill supports including pillars and crossbeams.

$$\Delta p_{\text{rz}} = (K_{\text{rz}} + K_{\text{fs}}) \frac{m_a^2(\omega_1 + 1)^2}{2\rho_1 A_{\text{ct}}^2} \tag{2.35}$$

The pressure loss coefficient for the rain zone, K_{rz}, is estimated using an empirical relation presented in Appendix C. Kröger [11] and Kloppers [16] reported that the pressure loss coefficient for fill support system, K_{fs}, can be taken as 0.5. The air humidity is increasing through the rain zone, however, this rise is small relative to the ambient humidity ratio. Therefore, using moist air properties at point 1 can be justified for evaluating Δp_{rz}.

The pressure drop across the fill can be estimated using an empirical equation for the applicable fill. It accounts for the form drag and viscous drag effects. Furthermore, this empirical equation accounts for the effect of the fill height as well as the effects that are dependent on the water mass flow rate and the configuration of the fill [16].

$$\Delta p_{\text{fz}} = \left(F_1 \bar{v}^{F_2} + v_w^{F_3} F_4 \bar{v}^{F_5}\right)(F_6 + F_7 H_{\text{fz}}) + \frac{1}{2}\left[\frac{m_a^2(\omega_2 + 1)^2}{\rho_2 A_{\text{ct}}^2} - \frac{m_a^2(\omega_1 + 1)^2}{\rho_1 A_{\text{ct}}^2} -\right] \tag{2.36}$$

The second term of the equation accounts for a change of air momentum owing to buoyancy effects. The constants F_1 to F_7 are the fitting parameters and they are unique for each fill type, i.e., they depend on the fill type and configuration. Meanwhile, $\bar{v}$ is the average velocity of moist air before and after the fill and it can be approximated by using moist air properties at points 1 and 2. In a wet cooling tower, there is no mixing with any external air stream in the plenum chamber which justifies using the the properties of air at point 2 for calculating Δp_{fz}.

$$\bar{v} = \frac{m_a(\omega_1 + \omega_2 + 2)}{2\bar{\rho} A_{\text{ct}}} \tag{2.37}$$

$$\bar{\rho} = \frac{2}{\frac{1}{\rho_1} + \frac{1}{\rho_2}} \tag{2.38}$$

The pressure drop across the spray zone is caused by the drag of the sprayed water and the water distribution system including pipes and spray nozzles.

$$\Delta p_{\text{sz}} = (K_{\text{sz}} + K_{\text{wd}}) \frac{m_a^2(\omega_2 + 1)^2}{2\rho_2 A_{\text{ct}}^2} \tag{2.39}$$

The pressure loss coefficient for the spray zone, K_{sz}, is estimated using an empirical relation presented in Appendix C. Kröger [11] and Kloppers [16] reported that the pressure loss coefficient for water distribution system, K_{wd}, can be taken as 0.5.

The drift eliminator is located above the spray zone where the bottom of the drift eliminator defines the top boundary of the spray zone. The pressure drop across the drift eliminator is calculated based on an empirical correlation applying the same moist air properties used for calculating Δp_{sz}.

$$\Delta p_{\text{de}} = E_1 \left[\frac{m_a(\omega_2 + 2)}{\rho_2 A_{\text{ct}}} \right]^{E_2} \tag{2.40}$$

The constants E_1 and E_2 are the fitting parameters and they are unique for each drift eliminator type.

The pressure drop across the fan system is to account the fan upstream loss. The airflow experiences a resistance by obstacles located on the upstream of the fan, i.e, fan casing and fan hub.

$$\Delta p_{\text{fc}} = K_{\text{up}} \frac{m_a^2(\omega_2 + 1)^2}{8\rho_2\pi^2 \left(d_{\text{fan}}^2 - d_{\text{hub}}^2\right)^2} \tag{2.41}$$

The pressure loss coefficient for the upstream obstacles, K_{up}, depends on the casing inlet length, inlet type, and the fan hub diameter, d_{hub} [11]. The shroud inlet can have a cylindrical, conical, or bell-mouth shape [11].

The pressure rise required by the fan, Δp_{fan}, can then be determined from equation (2.31) where the dynamic pressure term is given by

$$\frac{\rho_2 v_2^2}{2} = \frac{m_a^2(\omega_2 + 1)^2}{8\rho_2\pi^2 \left(d_{\text{fan}}^2 - d_{\text{hub}}^2\right)^2} \tag{2.42}$$

Installing a diffuser downstream of the fan is recommended because it can reduce the work done for the pressure rise [11]. The rate of work done by the electrical motor that drives the fan is called the fan input power, W_{fan}, where

$$W_{\text{fan}} = \frac{\dot{V}\Delta p_{\text{fan}}}{\eta_{\text{fan}}\,\eta_{\text{tu}}} \tag{2.43}$$

where η_{fan} and η_{tu} are the efficiencies of fan and transmission unit, respectively. $\dot{V}$ is the volumetric flow rate of the moist air discharged by the fan and it is estimated by

$$\dot{V} = \frac{m_a(\omega_2 + 1)}{\rho_2} \tag{2.44}$$

2.3 Cooling tower simulation package (CoolIT)

A computer program, CoolIT, is developed by Energy Systems Design Laboratory (ESD-Lab) at the University of Alberta to analyze the performance of mechanical-draft induced counter-flow wet/hybrid cooling towers. The program is developed in Python programming language with using object-oriented programming (OOP). The program offers users the ability to apply the one-dimensional augmented model by Zargar et al.[1] for the thermal analysis of the wet cooling tower and its plume. All the model equations presented in Chapter 2, correlations for the loss and transfer coefficients presented in Appendices B and C, and thermophysical property relations presented in Appendix A are included in the program. The program has a graphical user interface (GUI) that has a number of tabs related to cooling tower components where the relevant input parameters are specified.

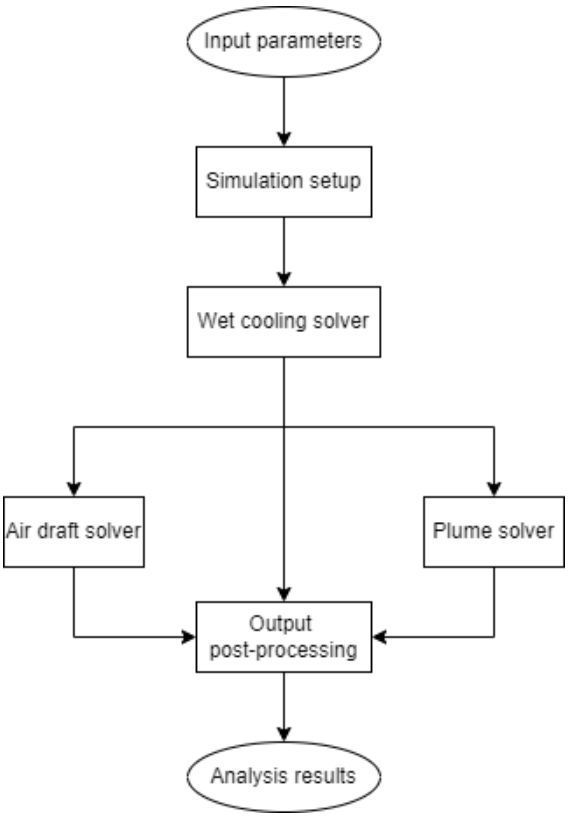

Figure 2.4 – Implementation of the analysis routine for a wet cooling tower in CoolIT.

Figure 2.4 is a schematic that illustrates graphically the implementation of the analysis routine in CoolIT for evaluating the performance of a wet cooling tower. The routine starts with reading the input parameters including ambient conditions, the tower's geometrical dimensions, the inlet temperature of water and air, the mass flow rate of water and air, and

other constants associated with some of the cooling tower components. For setting up the simulation, other parameters are computed based on the configuration of the cooling tower, e.g., the air inlet velocity is computed from the inlet area for air. The simulation begins with the wet cooling solver where the governing equations of the thermodynamic model are solved by considering the zone-specific Merkel numbers for each of the rain, fill, and spray zones. The plume solver carries out the integration of the plume equations which finds the plume properties with respect to height above the cooling tower. In a separate series of calculations, the air draft solver evaluates the pressure drop through each component of the cooling tower in order to find the total pressure drop. By extension, the air draft solver estimates the fan input power. The results from each solver are processed later to be presented in the form of figures and tables. These figures, for example, show the vertical distributions of water temperature, air temperature, humidity ratio, and mass flow rate of water inside the wet cooling tower as well as the variation of plume temperature and relative humidity with respect to height. The tables summarize key information such as the pressure drop, Merkel number, and rate of heat rejection for each cooling tower zone. Finally, a detailed report containing all of the key input and output variables relevant to the calculations is generated; thereby, the analysis routine in CoolIT is completed.

In the wet cooling solver, the governing equations of the thermodynamic model are categorized into two sets of ordinary differential equations, i.e., (2.1-2.4) for sub-saturated air and (2.5-2.8) for supersaturated air. If the solver recognizes that the air becomes saturated somewhere within one of the rain, fill or spray zones, it switches from numerically solving equations (2.1-2.4) to numerically solving equations (2.5-2.8). The wet cooling solver uses the Python boundary value problem (BVP) solver "solve_bvp" [79]. The solver in question uses a fourth-order collocation algorithm based on residual and adaptive step size control [79]. A one-dimensional mesh is generated with the total number of nodes is 1000, large enough to ensure that the computed results are mesh independent. The governing equations are solved with a relative tolerance of 10^{-5}. The initial guess required by the solver is obtained by applying the following approximations, developed by Kloppers [16], for the water and air outlet temperatures:

$$T_{wo} \approx \frac{T_{wi} + 2\,T_{wbai} + T_{ai}}{4} \tag{2.45}$$

$$T_{ao} \approx \frac{T_{ai} + T_{wi}}{2} \tag{2.46}$$

where T_{wi} is the inlet water temperature, and T_{ai} and T_{wbai} are the ambient dry-bulb and wet-bulb temperatures, respectively. Note that the humidity ratio of the exiting air can be approximated based on T_{ao} where

$$\omega_{ao} \approx \omega_s(T_{ao}) \tag{2.47}$$

In turn, the outlet water flowrate can be estimated from

$$m_{wo} \approx m_{wi} - m_a(\omega_{ao} - \omega_{ai}) \tag{2.48}$$

where m_{wi} is the inlet water mass flow rate, m_a is the air mass flow rate, and ω_{ai} is the ambient humidity ratio.

In the plume solver, the governing equations of the plume model, i.e., (2.16-2.19), are integrated numerically in z from the plume source up to some prescribed elevation using Python's "odeint" function. This function uses LSODE (Livermore Solver for Ordinary Differential Equations) of the FORTRAN77 package ODEPACK [80]. The solver in question deals with stiff and nonstiff systems in that it uses an Adams-Moulton method in the nonstiff case then automatically switches to using a Backward Differentiation Formula (BDF) method in the stiff case. The plume solution is achieved with a default tolerance of 1.5×10^{-8}.

Chapter 3

Cooling tower design methodology

A numerical optimization framework for cooling tower design is presented as an innovative alternative to the time consuming trial-and-error design process that is widely adopted in cooling tower industry. The procedure followed through the cooling tower design is summarized below:

1. Specify cooling tower design elements.
2. Formulate the optimization problem that characterizes the required cooling tower design.
3. Carry out the numerical simulations to express the objective functions and constraints in terms of the design variables.
4. Carry out the optimization process by finding the optimal values of the selected design variables.

3.1 Design problem elements

To formulate a proper optimization problem, four elements need to be defined: (i) design input parameters, e.g. operating conditions; (ii) design objectives; (iii) design constraints; and (iv) design variables. Each element consists of a set of parameters related to the cooling tower, as shown in Table 3.1. These elements are reviewed in comprehensive detail in sections 3.1.1-3.1.4 below.

3.1.1 Design operating conditions

Design operating conditions are the thermal parameters on which cooling tower design is performed. These conditions consist of ambient air wet-bulb temperature, inlet water flow rate, and inlet water temperature.

Table 3.1 – Elements of wet cooling tower design problem.

Design operating conditions	Design objectives	Design constraints	Design variables
Ambient air dry-bulb and wet-bulb temperatures	Capital cost	Cooling performance	Air mass flow rate
Inlet water flow rate	Operating cost	Fill functioning	Tower frontal area
Inlet water temperature	Total cost	Noise generation	Fill height
		Visible plume	Rain zone height
			Spray zone height

Ambient air dry-bulb and wet-bulb temperatures

The ambient air dry-bulb and wet-bulb temperatures are essential factors in the design and selection of cooling towers. The dry-bulb temperature, T_{ai}, is defined as the external outdoor temperature measured by a dry-bulb thermometer. The wet-bulb temperature, T_{wbai}, is defined as the temperature that ambient air would reach if saturated adiabatically by the addition of water vapor. It is the lowest temperature the water can be cooled to by evaporative cooling. Both temperatures follow daily and seasonal cycles that depend on prevailing weather patterns. From a design perspective, selection of temperatures that are not exceeded by more than 5% during a normal summer yields satisfactory performance for most industrial installations [5]. On this basis, a common rule is to select design dry-bulb and wet-bulb temperatures that will not be exceeded 3 to 5% of the time in an average year [13]. Erens [20] recommended that the use of published weather data for selecting the design ambient air temperatures should be taken with caution because it can often lead to under-design in long periods.

Inlet water flow rate

The inlet water flow rate, m_{wi}, is the total mass flow rate of water supplied to the cooling tower. A low water flow leads to poor water distribution over the fill, whereas too high water flow rate causes fill flooding and obstructs the airflow. For a given heat load, the cooling tower range is determined by the inlet water flow rate and it can be reduced by increasing the latter. In such a scenario, the cooling tower is too small to deliver the required cooling performance.

Inlet water temperature

The inlet water temperature, T_{wi}, is the temperature of the hot water entering the cooling tower via the distribution system. Ideally, it should be significantly greater than the design wet-bulb temperature to ensure that there is sufficient cooling potential available, even during the most challenging ambient conditions in the year. The cooling potential is defined as the temperature difference between inlet water temperature and ambient air wet-bulb temperature.

3.1.2 Design objectives

Design objectives represent the criteria for designating a cooling tower design as better than another. The general attitude throughout cooling tower industry is that the most efficient cooling tower is the most economical [5]. On this basis, cooling tower design objectives should describe the cooling tower economics. Cooling tower cost breaks down into four general categories, namely, capital cost, annual fixed expenses, operating cost, and capability penalties [5]. Annual fixed expenses are related to interest, amortization of the capital cost, interim replacement, maintenance, insurance, and taxes [5]. Capability penalties are the amount paid for each kilowatt of additional capacity when the cooling tower is unable to produce the required performance and it is measured at the maximum ambient air dry-bulb and wet-bulb temperatures and peak demand periods [5]. The latter two cost categories are out of the thesis scope. Thus, cooling tower design objectives are characterized by the capital and operating costs separately or by combining the latter two costs as in the total cost.

Capital cost

Capital cost is the fixed, one-time expenses undertaken for bringing a cooling tower project to a commercially operable status. This type of cost covers, but is not limited to, the expenses of cooling tower components such as structural materials, basin, air inlet louvers, fill, water distribution system (including pipes, nozzles, and laterals), drift eliminator, and fan (including motor, drive shaft, gearbox, supports, and fan stack). These expenses are not limited to purchase only, but it should also consider the expenses for transportation and installation. A variety of other aggregate costs can be expected in conjunction with cooling tower installation and some of these include costs for starting-up and commissioning, engineering, and permitting [7]. From a general perspective, the capital cost of a cooling tower, C_{capital}, is proportional to its size quantified by cooling tower total volume, V_{tower}, mathematically expressed as

$$C_{\text{capital}} \propto V_{\text{tower}} \tag{3.1}$$

$$V_{\text{tower}} = A_{\text{ct}} \ (H_{\text{rz}} + H_{\text{fz}} + H_{\text{sz}}) \tag{3.2}$$

where A_{ct} is the cooling tower frontal area, H_{rz} is the rain zone height, H_{fz} is the fill height, and H_{sz} is the spray zone height. A large cooling tower will cost more than a smaller one considering the differences between their main components. For example, a large cooling tower may come with more fill material than in the small cooling tower and thus the capital cost of the former would be higher.

Operating cost

Operating costs are the ongoing expenses incurred from the normal day-to-day running of a cooling tower. In the operation of mechanical-draft cooling tower, auxiliary energy is consumed for driving the fan and for pumping the water. The expenses related to the consumed energy is a major component of the operating cost. Since pumping power is relatively small compared to fan power, the operating cost, $C_{\text{operating}}$, can be considered to be proportional to the fan motor power consumption, W_{fan}, mathematically expressed as

$$C_{\text{operating}} \propto W_{\text{fan}} \tag{3.3}$$

In situations where the cooling tower is not located near a water source that is available for industrial usage, i.e., large ponds or canals, the expenses of accessing a municipal water supply for makeup water are incorporated in the operating cost. The latter case is not considered in the current study.

Total cost

Total cost is the combined capital and operating costs, $C_{\text{capital}} + C_{\text{operating}}$, compounded over the economic life-cycle of the cooling tower. The total cost is the economic factor that normally decides the final cooling tower design [5].

3.1.3 Design constraints

The proposed cooling tower design is accepted once it meets all design requirements. These requirements are collectively called design constraints and they define the feasible alternatives of a given cooling tower design problem. The design constraints in question are related to cooling performance, fill functioning, noise generation, and visible plume abatement.

Cooling performance constraint

The performance constraint is defined by restricting the cooling tower to deliver a desired outlet water temperature, T_{desired}, at design ambient air dry-bulb and wet-bulb temperatures, T_{ai} and T_{wbai}, respectively. In other words, the desired cooling performance is indicated by dissipating a known amount of heat from a stream of hot process water to ambient air that enters the cooling tower so eventually the water exits the cooling tower at the desired temperature. The determination of the heat to be dissipated by a cooling tower is an essential factor that affects the tower size. The cooling performance constraint can be expressed as an inequality constraint as follows:

$$T_{wbai} + 2.8\,\text{K} \leq T_{wo}\left(T_{ai}, T_{wbai}\right) \leq T_{\text{desired}} \tag{3.4}$$

where the lower limit ensures that the cooling tower delivers a performance that is guaranteed in the cooling tower industry. The cooling performance was found unstable when the tower operates at an approach less than 2.8 K [6, 22].

Fill functioning constraint

The fill functioning constraint is defined by restricting the liquid-to-gas ratio, L/G, to fall in the range 0.5 - 2.5 for film-type fills [81]. This is to ensure that the film-type fill is neither too dry nor flooded with water. In either case, the cooling tower performance is significantly degraded. The fill operation constraint can be expressed as an inequality constraint as follows:

$$0.5 \leq L/G \leq 2.5 \tag{3.5}$$

where the lower limit indicates the situation where more air is accommodated in the cooling tower, whereas the upper limit indicates the situation where more water is accommodated in the cooling tower.

Noise generation constraint

Constraints over noise generation are met by restricting the air velocity, v_a, to be less than a threshold at which the noise generated by air movement falls within an acceptable range, e.g., as dictated by Occupational Health and Safety and/or the proximity of the tower to residences, hospitals, etc. Other than the air movement inside the cooling tower, there are potential sources of cooling tower noise such as falling water, fans, and pumps, however, the noise generation constraint in this thesis is related only to the air movement. The air velocity threshold of the noise generation constraint is set to be 5 m/s for two reasons: (i) this is the maximum air velocity for which the use of pressure loss coefficient correlation for the rain zone (C.2) is valid; and (ii) this is the maximum air velocity for which the noise

generation is accepted according to the 25 dB noise criteria rating for a rectangular duct located in occupied space [82]. In the latter case, the cooling tower is approximately treated as a rectangular air duct. The noise generation constraint can be expressed as an inequality constraint as follows:

$$1.0\,\mathrm{m/s} \leq v_a \leq 5.0\,\mathrm{m/s} \tag{3.6}$$

$$v_a = \frac{m_a}{\rho_{ai}\, A_{\mathrm{ct}}} \tag{3.7}$$

Visible plume constraint

The visible plume constraint is met by restricting the length, h_{vp}, of the visible plume that forms above a wet cooling tower operating in cold ambient conditions to be less than a maximum allowable length, $h_{\max}$. The cold ambient conditions are characterized by the dry-bulb temperature, T_{cold}, and wet-bulb temperature, $T_{\mathrm{cold,wb}}$. The maximum allowable length for the visible plume is determined based on the limitations posed by the tower's location. For example, for a wet cooling tower that is located in close proximity to a highway, $h_{\max}$ is small in order to avoid any localized foggy condition resulted from deflecting the visible plume to ground level by the wind. The visible plume constraint can be expressed as an inequality constraint as follows:

$$h_{\mathrm{vp}}\left(T_{\mathrm{cold}}, T_{\mathrm{cold,wb}}\right) \leq h_{\max} \tag{3.8}$$

where $h_{\mathrm{vp}}\left(T_{\mathrm{cold}}, T_{\mathrm{cold,wb}}\right)$ is specified once the plume relative humidity falls below 100%. The plume properties are predicted by solving the atmospheric plume model presented in section 2.1.2 at the cold ambient conditions, T_{cold} and $T_{\mathrm{cold,wb}}$.

3.1.4 Design variables

Design variables are numerical inputs that are allowed to change during the design process. They are a set of variables that describe one possible cooling tower design. The design variables should be independent of each other. The number of independent design variables gives the degrees of freedom for the design problem. Also, it is important to choose the design variables that affect the performance and cost effectiveness of the cooling tower. The design variables considered in the wet cooling tower design have two categories:

1. **Airflow into the cooling tower**
   The amount of ambient air induced to flow into the cooling tower by the fan is quantified by air mass flow rate, m_a.

2. **Geometrical dimensions of the cooling tower**

   The geometrical dimensions of the cooling tower are shown schematically in Figure 3.1. The key dimensions are:

   - Cooling tower frontal area, A_{ct}
     For a rectangular cooling tower, $A_{\mathrm{ct}} = W_{\mathrm{ct}}\, L_{\mathrm{ct}}$, where W_{ct} and L_{ct} are the cooling tower width and length in meters, respectively. It is assumed that the fan diameter is 85% of the cooling tower width, i.e., $d_{\mathrm{f}} = 0.85\, W_{\mathrm{ct}}$.
   - Rain zone height, H_{rz}
     Note that the air inlet height, H_{ai}, is related to the rain zone height. It is assumed that the former is 20 cm less than H_{rz}, i.e., $H_{\mathrm{ai}} = H_{\mathrm{rz}} - 0.20\,\mathrm{m}$.
   - Fill height, H_{fz}
   - Spray zone height, H_{sz}

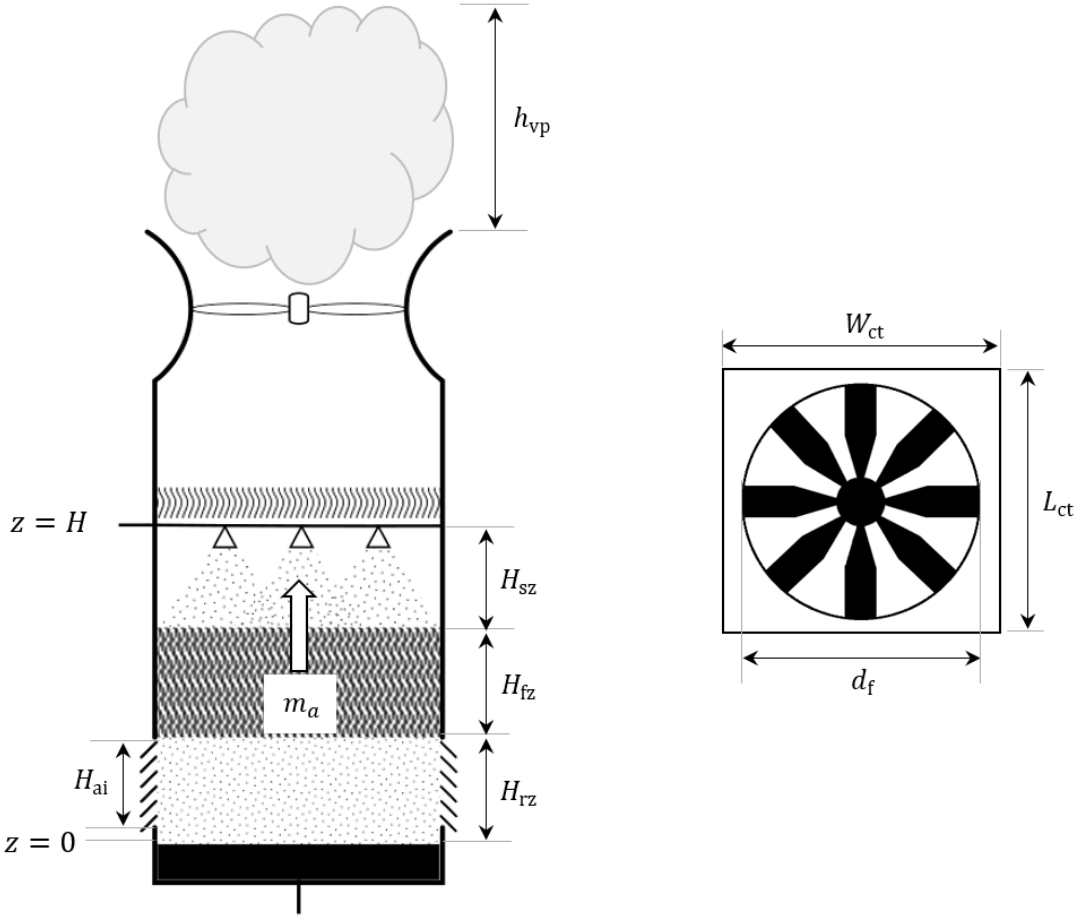

Figure 3.1 – Dimensions relevant to the design of a mechanical induced-draft counter-flow wet cooling tower.

3.2 Numerical optimization framework for cooling tower design

The numerical simulations and the optimization process are performed by means of a numerical optimization framework. The optimization framework in question consists of two components, i.e., an analysis component (CoolIT) and an optimization component (DAKOTA). The former component estimates the cooling tower performance and its impact on the environment by solving a one-dimensional zone-specific thermodynamic model, air draft equation, and integral atmospheric plume model. Section 2.3 discusses in detail the numerical simulation procedure. The latter component of the framework, i.e., DAKOTA, performs numerical optimization.

The design analysis kit for optimization and terascale applications, known as DAKOTA, is an open-source package developed by U.S. Sandia National Laboratories mainly to provide engineers and scientists with a systematic and rapid means for obtaining optimal designs using simulation-based models [83]. This is achieved through a flexible problem-solving environment that the DAKOTA package provides for the user. The user provides a set of DAKOTA commands in an input file and launches DAKOTA. In turn, DAKOTA invokes the computational models, collects their results, and implements the optimization algorithm. The output files from DAKOTA report the numerical results in a concise form presenting the iterations and function evaluations performed by the optimization algorithm.

With all the capabilities and features that are available within DAKOTA, the package is appropriate for the optimization component of the numerical framework developed for cooling towers design. First, DAKOTA has a generic interface to any computational model code including a Python interface. Therefore, CoolIT can be integrated with DAKOTA through a single and relatively simple Python interface. Second, DAKOTA offers standard methods to solve single-objective or multi-objective optimization problems. Third, DAKOTA has a parallel computing capability that uses the concept of multilevel parallelism. The parallel computing capability allows concurrent execution of independent design evaluations within an iterator [83]. This approach can be used when solving a multi-objective optimization problem in order to reduce the total computational time by performing the independent design evaluations in parallel.

DAKOTA can operate on any operating systems, e.g., Linux, Mac OS, and Windows. Once DAKOTA is installed, it uses a single input file to orchestrate the optimization algorithm. The DAKOTA input file specifies the necessary information about the optimization problem. Figure 3.2 illustrates the DAKOTA input file used to solve the size optimization problem for a wet cooling tower presented in section 3.5. There are six specification blocks that appear in the DAKOTA input file. These blocks are identified using the following key-

words: environment, model, method, variables, interface, and responses. In the environment block, the data type of DAKOTA output is specified by setting the keyword "tabular_data" for getting the output in a tabular format. In the model block, the logical unit for determining how a set of variables is mapped through the interface with the simulation is specified by setting the keyword "single" for a single set of variables, interface, and responses that is managed by DAKOTA. In the method block, selection of the optimization algorithm is specified with its settings. The number, type, and characteristics of the design variables are specified in the variables block. The interface block specifies the analysis driver file that manages the communication between DAKOTA and CoolIT. In the responses block, information about the objective functions, constraints and their derivative information is specified.

```
environment,
  tabular_data
  tabular_data_file = "size_opt_plume_abatement.dat"

model,
  single

method
  moga
    seed = 20000
    max_function_evaluations = 2500
    initialization_type     unique_random
    fitness_type     domination_count
    replacement_type below_limit = 5
      shrinkage_fraction = 0.8
    niching_type radial = 0.05 0.05
    crossover_type     shuffle_random
      num_offspring = 4 num_parents = 4
      crossover_rate = 0.7
    mutation_type     replace_uniform
      mutation_rate = 0.2
    convergence_type     metric_tracker
      percent_change = 0.05 num_generations = 100

variables,
  continuous_design = 3
    lower_bounds   390.988      0.3             25
    upper_bounds   1954.94      3.0             214
    scales         1.0          1.0             1.0
    scale_types    'auto'       'auto'          'auto'
    descriptors    'm_a'        'H_fi'          'A_fr'

interface,
  fork,
    parameters_file = 'params_moga.in'
    results_file    = 'results_moga.out'
    analysis_driver = 'dakota_analysis_wrapper.py'

responses,
  descriptors = 'fan_power'     'tower_volume'     'T_wo'     'air_velocity'     'plume_height'
  num_objective_functions = 2

  num_nonlinear_inequality_constraints = 3
    nonlinear_inequality_upper_bounds = 298.80    5.0     8.0
    nonlinear_inequality_lower_bounds = 293.43    1.0     0.0

  no_gradients
  no_hessians
```

Figure 3.2 – The DAKOTA input file for the size optimization problem with visible plume constraint.

A typical loosely-coupled interface is used for integrating DAKOTA with CoolIT. For this interface type, DAKOTA has no awareness of the internal details of the computational model [83]. DAKOTA and CoolIT exchange data by reading and writing short data files. The invocation of CoolIT is performed using system forks linkage where a separate process is created for the simulation. The communication between DAKOTA and CoolIT occurs through parameter and response files and it is managed by the analysis driver file. The system forks linkage has the potential to be more robust when performing function evaluations asynchronously [83]. Figure 3.3 shows the components of the interface between CoolIT with DAKOTA. The `read_parameters_file` function from the Python module `dakota.interfacing` is used to construct two objects that define the design variables and responses of the optimization problem. Once DAKOTA is executed, the data exchange between DAKOTA and CoolIT occurs in five steps described below.

1. **Generation of a parameters file**
   The DAKOTA optimizer creates a temporary parameters file containing the names of design variables with their initial values and the names of responses, i.e., objective functions and constraints, that DAKOTA requests from CoolIT. Then, a function parses this file in order to store the design variables and the response descriptors within two objects.

2. **Simulation pre-processing**
   A function parses the CoolIT input file containing information about the cooling tower being analysed. The CoolIT input file specifies the analysis method, geometrical dimensions, water inlet conditions, air inlet conditions, and constants relevant to the components inside the cooling tower. These components consist of the inlet, rain zone, fill zone, spray zone, drift eliminator, dry-cooling section, and fan. This function stores the initial parameters for the simulation within an object. A second function is then used to update the initial parameters with the values of design variables provided by DAKOTA.

3. **Simulation execution**
   The analysis routine for the cooling tower presented in Figure 2.4 is executed here using the updated simulation parameters. Once the simulation is completed, the results are stored within an object.

4. **Simulation post-processing**
   A function is used to store values of the required responses identified by their descriptors that were known from step 1. Some response variables are given in the simulation results and there are other variables computed individually. If the visible plume height

is a response, then step 3 is repeated again using the simulation parameters with cold ambient conditions, this to assess the severity of fog formation during winter months. By contrast, if fog formation is not an important consideration, the simulation is restricted to summertime operation where ambient temperatures are high and design considerations are dictated solely by the ability of the cooling tower to reject heat.

5. **Generation of a results file**
   A function is used to write a results file containing the response values in the order that DAKOTA expects. This file is parsed by DAKOTA later in order to complete the optimization algorithm.

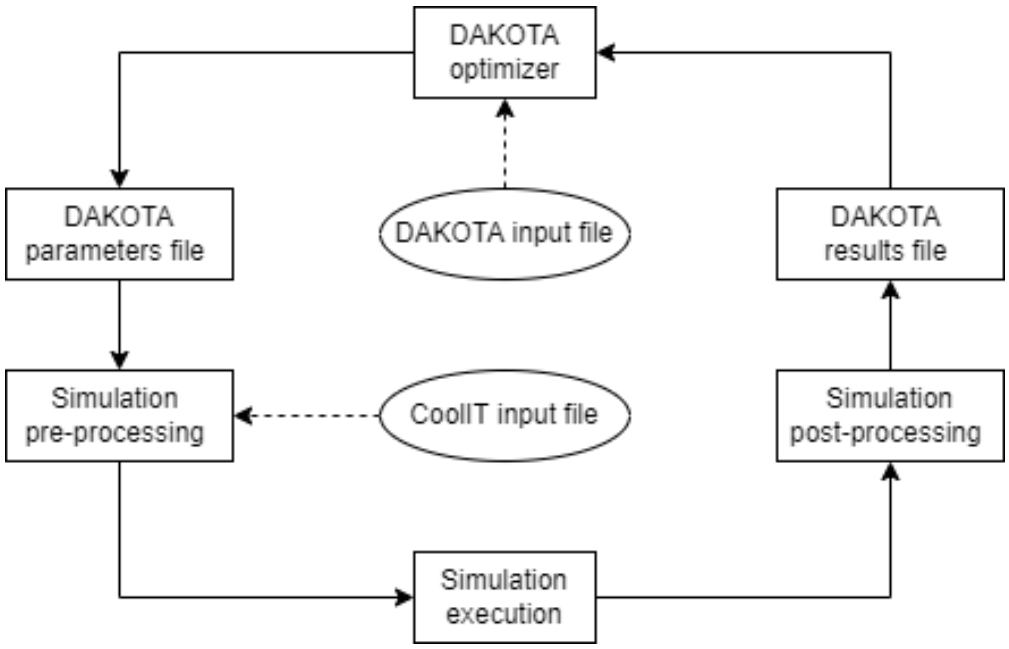

Figure 3.3 – Components of the interface between DAKOTA and CoolIT.

The above loop is terminated by the DAKOTA optimizer once the convergence criteria of the optimization algorithm is met. The numerical optimization framework is used to solve three cooling tower design problems concerning (i) airflow selection; (ii) size optimization; and (iii) size optimization with visible plume constraint. These design problems are discussed in the following sections.

3.3 Design problem 1: Airflow selection

3.3.1 Problem definition

Fan selection for mechanical-draft cooling towers is implemented based on knowledge of the fan operating point, which is given by the combination of the total airflow and the requisite static pressure. The target of this design problem is to determine the air mass flow rate, m_a, required for delivering a desired cooling performance at the design operating conditions. The desired cooling performance is characterized by the outlet water temperature, T_{wo}. In design problem 1, the cooling tower geometrical dimensions are known and they do not change during the design process. The specifications of the cooling tower in question are given in Table 3.2 and they correspond to data of a rectangular mechanical-draft counter-flow wet cooling tower presented in [1].

To determine the airflow requirement for the desired cooling performance, the cooling tower thermal analysis must eventually obtain the following result

$$T_{wo}(m_a) = T_{\text{desired}} \tag{3.9}$$

The residual of outlet water temperature, r_{wo}, measures the difference in cooling performance at a given m_a from the desired performance. For this purpose, it is necessary to minimize r_{wo} with respect to m_a in order to obtain a final cooling tower design that meets the specified requirements. On this basis, a single-objective constrained optimization problem can be formulated for the airflow selection design problem of a wet cooling tower as follows

$$\begin{aligned} &\text{minimize} && r_{wo} = \left(T_{wo} - T_{\text{desired}}\right)^2 \\ &\text{w.r.t.:} && m_a \\ &\text{subject to:} && 1.0\ \text{m/s} \leq v_a \leq 5.0\ \text{m/s} \\ & && 390.99\ \text{kg/s} \leq m_a \leq 1954.94\ \text{kg/s} \end{aligned} \tag{3.10}$$

The optimization problem consists of a single nonlinear objective function, one inequality constraint, and one design variable that is bounded between two limits. The objective function represents the residual of outlet water temperature that should be minimized. The noise generation constraint is applied since air velocity is related directly to the airflow inside the cooling tower. The only design variable in the optimization problem is air mass flow rate and it is limited within two bounds. Lower and upper bounds for m_a are chosen based on fulfilling the fill functioning constraint, i.e., $L/G = 2.5$ at the lower bound and $L/G = 0.5$ at the upper bound.

Figure 3.4 shows the sensitivity of outlet water temperature to variations in fill height with $0.3\text{m} \leq H_{\text{fz}} \leq 3.0\text{m}$ and air mass flow rate with $390.99\text{kg/s} \leq m_a \leq 1954.94\text{kg/s}$. Note,

Table 3.2 – Input parameters for design problem 1 [1]. Units for the constants C_1-C_4, F_1-F_6, and E_1-E_2 are resembled in the SI system.

Parameter	**Value**	**Unit**
Cooling tower length, L_{ct}	14.63	m
Cooling tower width, W_{ct}	14.63	m
Rain zone height, H_{rz}	4.26	m
Spray zone height, H_{sz}	0.76	m
Inlet water mass flow rate, m_{wi}	977.47	kg/s
Inlet water temperature, T_{wi}	308.61	K
Desired outlet water temperature, T_{desired}	298.80	K
Inlet air dry-bulb temperature, T_{ai}	302.47	K
Inlet air wet-bulb temperature, T_{wbai}	290.63	K
Inlet air pressure, p_{ai}	84185	Pa
Air inlet		
K_{in}	5.2	
Rain zone		
Average droplet diameter, $\bar{d}_d$	0.0035	m
Fill		
C_1	0.566	
C_2	0.822	
C_3	-0.774	
C_4	0.774	
F_1	0.062	
F_2	1.950	
F_3	1.000	
F_4	6.911	
F_5	16.060	
F_6	82.701	
Drift eliminator		
E_1	3.220	
E_2	1.858	
Fan		
K_{up}	0.52	

however, that in design problem 1, H_{fz} is fixed and therefore the objective function would be represented only by a vertical line in Figure 3.4 with a simple optimal location. The behavior of T_{wo} with respect to m_a is nonlinear, thus the objective function r_{wo} is nonlinear. On the other hand, the constraint v_a is linear with respect to m_a as presented in (3.7). As shown in Figure 3.4, the cooling tower is able to deliver the desired outlet water temperature, i.e., $T_{wo} = 298.80\,\text{K}$, at different combinations for H_{fz} and m_a. The orange curve separates the

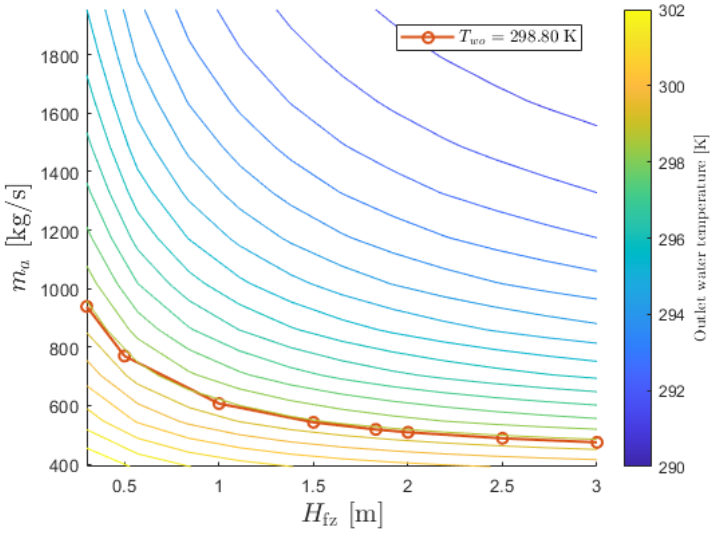

Figure 3.4 – Sensitivity of outlet water temperature with respect to fill height and air mass flow rate for design problem 1

.

domain into two regions, i.e., an insufficient cooling region where $T_{wo} < 298.80$ K and an excess cooling region where $T_{wo} > 298.80$ K.

3.3.2 Solution method

Definition 1 (Local Minimum [18]) *m_a^* is a **local minimum** in the feasible domain, Ω, of the optimization problem (3.10) if $r_{wo}(m_a^*) \leq r_{wo}(m_a) \;\; \forall\, m_a \in \Omega$ with $||m_a^* - m_a|| < \delta$.*

Definition 2 (Global Minimum [18]) *m_a^* is a **global minimum** in the feasible domain, Ω, of the optimization problem (3.10) if $r_{wo}(m_a^*) \leq r_{wo}(m_a) \;\; \forall\, m_a \in \Omega$.*

Methods used to solve single-objective constrained nonlinear optimization problems can be broadly classified into two groups: local methods and global methods. Local constrained optimization methods aim to obtain a local minimum and they are usually gradient-based methods, i.e., they require gradients computation of the objective function and constraints. There are two further classifications for the local constrained methods: sequential methods and local transformation-based methods. The most popular local sequential methods are: the method of feasible directions (MFD), sequential linear programming (SLP), and sequential quadratic programming (SQP) [84]. The main solution approach followed by the sequential methods is transforming the constrained optimization problem into a simpler constrained optimization problem [84]. On the other hand, the most popular local transformation-based methods are penalty methods and augmented Lagrangian methods [84]. The main

solution approach followed by the local transformation-based methods is transforming the constrained optimization problem into an unconstrained optimization problem by adding a penalty function to the objective function [84].

Global constrained methods aim to obtain a global minimum and they are usually gradient-free methods, i.e., they do not need any information about the gradients of the objective function or constraints. Instead, they are mostly based on stochastic procedures. There are two further classifications for the global constrained methods: direct methods and global transformation-based methods [84]. As the name suggests, the direct global methods solve the optimization problem without any transformation. In contrast, global transformation-based methods transforms the constraint optimization problem into an unconstrained optimization problem by adding a penalty function to the objective function. The most popular global transformation-based methods are genetic algorithms, evolutionary algorithms, and simulated annealing [84].

The method of feasible directions (MFD) is chosen to solve the optimization problem (3.10). The reasons for selecting MFD are as follows: (i) the MFD is relatively simple compared to other sequential methods; (ii) the MFD always produces a feasible design, which helps in reducing the computational time for obtaining the optimal design; and (iii) the MFD is offered by DAKOTA [83] through the keyword `conmin_mfd`.

3.3.2.1 Method of Feasible Directions (MFD)

The basic steps in the MFD involve first obtaining the search direction, S, in the design domain and the step size along this direction, δ [85]. Starting from a feasible initial design point, $m_a^{(0)}$, the search direction in question should minimize the objective function r_{wo} and guarantee that the constraint v_a is satisfied. The step size is found by performing a constrained one-dimensional line search. Then, the design variable is updated for the subsequent iteration by requiring

$$m_a^{(k+1)} = m_a^{(k)} + \delta^{(k)}\, S^{(k)} \tag{3.11}$$

The process of finding $\delta^{(k)}$ and $S^{(k)}$ is repeated until the convergence tolerance is met. Convergence is achieved when the relative change in the objective function is less than ϵ for two consecutive iterations, mathematically represented as follows

$$\left| \frac{r_{wo}^{(k)} - r_{wo}^{(k-1)}}{r_{wo}^{(k-1)}} \right| \leq \epsilon \tag{3.12}$$

The desired search direction minimizes the objective function while preserving a feasible design. This is achieved when the search direction makes an angle between 90° and 270°

with the tangent to the objective function [85]. The condition in question is referred to as the usability requirement [85], mathematically expressed as follows

$$\frac{dr_{wo}}{dm_a}\, S \leq 0 \tag{3.13}$$

If the constraint is active, i.e., $v_a = 5\,\mathrm{m/s}$, then moving along the search direction should remain in the feasible domain. This is achieved when the search direction makes an angle between 90° and 270° with the tangent to the constraint [85]. The condition in question is referred to as the feasibility requirement [85], mathematically expressed as follows

$$\frac{dv_a}{dm_a}\, S \leq 0 \tag{3.14}$$

Therefore, the desired search direction must be usable and feasible. In other words, the desired search direction must satisfy both equations (3.13-3.14). In this case, the desired search direction in question can be found by solving an optimization sub-problem to obtain the maximum possible reduction of r_{wo}

$$\begin{aligned} &\text{minimize} && \frac{dr_{wo}}{dm_a}\, S \\ &\text{w.r.t.:} && S \\ &\text{subject to:} && \frac{dv_a}{dm_a}\, S \leq 0 \\ & && S^2 \leq 1 \end{aligned} \tag{3.15}$$

To solve the above problem, the Karush-Kuhn-Tucker (KKT) conditions should be considered for equation (3.15). Thus,

$$\frac{dv_a}{dm_a}\, S^* \leq 0 \tag{3.16a}$$

$$S^{*2} \leq 1 \tag{3.16b}$$

$$\frac{\partial L}{\partial S} = \frac{dr_{wo}}{dm_a} S^* + \lambda_1 \left(\frac{dv_a}{dm_a} S^* + a^2 \right) + 2\lambda_2 \ \left(S^{*2} + b^2 \right) = 0 \tag{3.16c}$$

$$\frac{dv_a}{dm_a} S^* + a^2 = 0 \tag{3.16d}$$

$$S^{*2} + b^2 = 0 \tag{3.16e}$$

$$\lambda_1\, a = 0 \tag{3.16f}$$

$$\lambda_2\, b = 0 \tag{3.16g}$$

$$\lambda_1 \geq 0 \tag{3.16h}$$

$$\lambda_2 \geq 0 \tag{3.16i}$$

where S^* is the optimal search direction, L is the Lagrange function, λ_1 and λ_2 are the Lagrange multipliers, and a and b are the slack variables. The five unknown variables S^*, λ_1, λ_2, a, and b are obtained by solving a nonlinear system consisting of five equations (3.16c-3.16g).

When the constraint is inactive, i.e., $v_a \neq 5\,\mathrm{m/s}$, then the feasibility condition is no longer considered. Thus, the desired search direction in this case can be found by solving another optimization sub-problem, i.e.,

$$\begin{aligned} &\text{minimize} && \frac{dr_{wo}}{dm_a}\, S \\ &\text{w.r.t.:} && S \\ &\text{subject to:} && S^2 \leq 1 \end{aligned} \tag{3.17}$$

To solve the above problem, the Karush-Kuhn-Tucker (KKT) conditions should be considered for equation (3.17). Thus,

$$S^{*2} \leq 1 \tag{3.18a}$$

$$\frac{\partial L}{\partial S} = \frac{dr_{wo}}{dm_a} S^* + 2\lambda_1 \ \left(S^{*2} + c^2\right) = 0 \tag{3.18b}$$

$$S^{*2} + c^2 = 0 \tag{3.18c}$$

$$\lambda_1\, c = 0 \tag{3.18d}$$

$$\lambda_1 \geq 0 \tag{3.18e}$$

where S^* is the optimal search direction, L is the Lagrange function, λ_1 is the Lagrange multiplier, and c is the slack variable. The three unknown variables S^*, λ_1, and c are obtained by solving a nonlinear system consisting of three equations (3.18b-3.18d).

The next step is to determine the step size parameter, δ. The design variable for the next iteration, $m_a^{(k+1)}$, should meet two conditions as follows: (i) $r_{wo}\left(m_a^{(k+1)}\right) < r_{wo}\left(m_a^{(k)}\right)$; and

(ii) $m_a^{(k+1)}$ is feasible. If the search direction is not tangent to the constraint at iteration k, mathematically expressed as

$$\frac{dv_a}{dm_a}\, S^{(k)} \neq 0 \ , \tag{3.19}$$

then performing a one-dimensional search in parameter δ is straightforward. In this case, upper and lower bounds for δ are needed. The lower bound for δ must be zero so that the search direction is usable, i.e., (3.13) is satisfied. For the upper bound, suppose that the objective function is reduced by 10% at iteration $k+1$. Then, the following linear approximation of r_{wo} is valid [84]

$$r_{wo}\left(m_a^{(k+1)}\right) = 0.9\, r_{wo}\left(m_a^{(k)}\right) = r_{wo}\left(m_a^{(k)}\right) + \delta\, \frac{dr_{wo}}{dm_a}\, S^{(k)} \tag{3.20}$$

$$\delta = -\,\frac{0.1\, \left| r_{wo}\left(m_a^{(k)}\right)\right|}{\dfrac{dr_{wo}}{dm_a}\, S^{(k)}} \tag{3.21}$$

where the absolute value is to ensure that δ is positive. Furthermore, the value of δ should make the constraint active at iteration $k+1$. Using a linear approximation of v_a,

$$v_a\left(m_a^{(k+1)}\right) = v_a\left(m_a^{(k)}\right) + \delta\, \frac{dv_a}{dm_a}\, S^{(k)} = 0 \tag{3.22}$$

$$\delta = -\,\frac{v_a\left(m_a^{(k)}\right)}{\dfrac{dv_a}{dm_a}\, S^{(k)}} \tag{3.23}$$

To guarantee that the objective function is reduced by 10% simultaneously with remaining in the feasible domain, the upper bound for δ is obtained by

$$\delta_u = \min\left(\frac{-0.1\, \left| r_{wo}\left(m_a^{(k)}\right)\right|}{\dfrac{dr_{wo}}{dm_a}\, S^{(k)}} \,,\ \frac{-v_a\left(m_a^{(k)}\right)}{\dfrac{dv_a}{dm_a}\, S^{(k)}} \right) \tag{3.24}$$

After obtaining the upper and lower bounds for δ, a quadratic polynomial interpolation is applied to approximate both the objective function and constraint inside the bounds [84]. A set of values for δ is obtained and the smallest value is chosen to be the step size parameter for updating the design variable for the next iteration using (3.11) [84].

At each iteration, information of the gradients for the objective function and constraint is required. Since no analytical expression is available for r_{wo}, its derivative is approximated

using a finite difference method. By applying the central difference method, the derivative of r_{wo} is approximated by

$$\frac{dr_{wo}}{dm_a} = \frac{r_{wo}\left(m_a^{(i+1)}\right) - r_{wo}\left(m_a^{(i-1)}\right)}{2\,h} + \mathcal{O}(h^2) \tag{3.25}$$

Although the derivative of v_a can be expressed analytically, it is, for consistency's sake, approximated numerically using the same method

$$\frac{dv_a}{dm_a} = \frac{v_a\left(m_a^{(i+1)}\right) - v_a\left(m_a^{(i-1)}\right)}{2\,h} + \mathcal{O}(h^2) \tag{3.26}$$

Figure 3.5 illustrates the overall algorithm for the MFD to solve the optimization problem (3.10). Table 3.3 presents the input parameters required by DAKOTA when using `conmin_mfd` optimization algorithm.

Table 3.3 – DAKOTA input parameters for the MFD.

Parameter	**Value**
Convergence tolerance, ϵ	10^{-6}
Numerical gradients interval type	central
Finite difference step size, h	10^{-6}

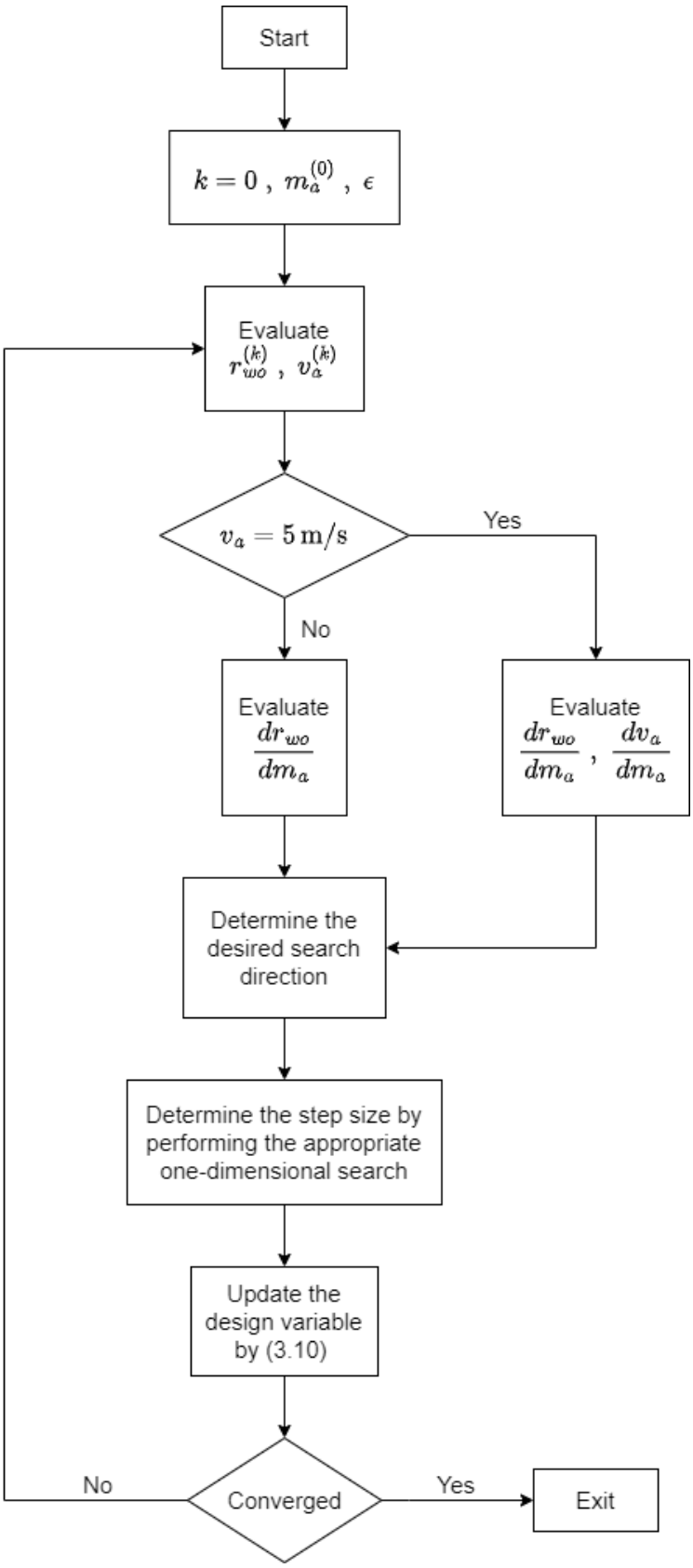

Figure 3.5 – Flowchart of the method of feasible directions (MFD) for solving the optimization problem (3.10).

3.4 Design problem 2: Size optimization

3.4.1 Problem definition

The target of this design problem is to determine the air mass flow rate, m_a, and geometrical dimensions of the wet cooling tower, i.e., the tower frontal area A_{ct}, and the heights of the rain zone H_{rz}, fill zone H_{fz}, and spray zone H_{sz}, necessary to achieve the best trade-off between the capital and operating costs while meeting all the design constraints for cooling performance, noise generation, and fill operation. The specifications of the cooling tower in question are given in Table 3.2. Four multi-objective constrained optimization problems can be formulated for design problem 2 based on the number of design variables as follows

$$\begin{aligned}
&\text{minimize} && W_{\text{fan}}\,, V_{\text{tower}} \\
&\text{w.r.t.:} && m_a\,, H_{\text{fz}} \\
&\text{subject to:} && 293.43\,\text{K} \leq T_{wo}\,(T_{ai}, T_{wbai}) \leq 298.80\,\text{K} \\
& && 1.0\,\text{m/s} \leq v_a \leq 5.0\,\text{m/s} \\
& && 390.99\,\text{kg/s} \leq m_a \leq 1954.94\,\text{kg/s} \\
& && 0.3\,\text{m} \leq H_{\text{fz}} \leq 3.0\,\text{m}
\end{aligned} \tag{3.27}$$

$$\begin{aligned}
&\text{minimize} && W_{\text{fan}}\,, V_{\text{tower}} \\
&\text{w.r.t.:} && m_a\,, H_{\text{fz}}\,, A_{\text{ct}} \\
&\text{subject to:} && 293.43\,\text{K} \leq T_{wo}\,(T_{ai}, T_{wbai}) \leq 298.80\,\text{K} \\
& && 1.0\,\text{m/s} \leq v_a \leq 5.0\,\text{m/s} \\
& && 390.99\,\text{kg/s} \leq m_a \leq 1954.94\,\text{kg/s} \\
& && 0.3\,\text{m} \leq H_{\text{fz}} \leq 3.0\,\text{m} \\
& && 25\,\text{m}^2 \leq A_{\text{ct}} \leq 214\,\text{m}^2
\end{aligned} \tag{3.28}$$

$$\begin{aligned}
&\text{minimize} && W_{\text{fan}}\,, V_{\text{tower}} \\
&\text{w.r.t.:} && m_a\,, H_{\text{fz}}\,, A_{\text{ct}}\,, H_{\text{rz}} \\
&\text{subject to:} && 293.43\,\text{K} \leq T_{wo}\,(T_{ai}, T_{wbai}) \leq 298.80\,\text{K} \\
& && 1.0\,\text{m/s} \leq v_a \leq 5.0\,\text{m/s} \\
& && 390.99\,\text{kg/s} \leq m_a \leq 1954.94\,\text{kg/s} \\
& && 0.3\,\text{m} \leq H_{\text{fz}} \leq 3.0\,\text{m} \\
& && 25\,\text{m}^2 \leq A_{\text{ct}} \leq 214\,\text{m}^2 \\
& && 4.0\,\text{m} \leq H_{\text{rz}} \leq 8.0\,\text{m}
\end{aligned} \tag{3.29}$$

$$
\begin{aligned}
&\text{minimize} && W_{\text{fan}}\,,\, V_{\text{tower}} \\
&\text{w.r.t.:} && m_a\,,\, H_{\text{fz}}\,,\, A_{\text{ct}}\,,\, H_{\text{rz}}\,,\, H_{\text{sz}} \\
&\text{subject to:} && 293.43\ \text{K} \leq T_{wo}\,(T_{ai}, T_{wbai}) \leq 298.80\ \text{K} \\
& && 1.0\ \text{m/s} \leq v_a \leq 5.0\ \text{m/s} \\
& && 390.99\ \text{kg/s} \leq m_a \leq 1954.94\ \text{kg/s} \\
& && 0.3\ \text{m} \leq H_{\text{fz}} \leq 3.0\ \text{m} \\
& && 25\ \text{m}^2 \leq A_{\text{ct}} \leq 214\ \text{m}^2 \\
& && 4.0\ \text{m} \leq H_{\text{rz}} \leq 8.0\ \text{m} \\
& && 0.5\ \text{m} \leq H_{\text{sz}} \leq 2.0\ \text{m}
\end{aligned}
\tag{3.30}
$$

The optimization problems (3.27-3.30) differ in the design variables vector, $\mathbf{x}$. The goal of each problem, however, is the same: minimize the objective functions, W_{fan} and V_{tower}, simultaneously while satisfying all constraints. The reason for solving four size optimization problems is to investigate the effect of adding a new design variable on the diversity of the optimal designs. Ultimately, the results will reveal the most influential design variables for the size optimization of wet cooling towers.

3.4.2 Solution method

The solution of each multi-objective constrained optimization problem represents the best compromises (or "trade-offs") of the objectives rather than one unique optimal design. On that basis, the solution consists of a set of optimal designs called a Pareto optimal set while each optimal design is called a Pareto optimum [86]. When the Pareto optimal set is plotted in objective space, the non-dominated vectors are collectively called the Pareto front [86].

Definition 3 (Pareto Optimality [86]) *A design* $\mathbf{x}^* \in \Omega$ *is said to be Pareto optimum with respect to the feasible region,* Ω*, if and only if there is no other design* $\mathbf{x} \in \Omega$ *for which* $\mathbf{v} = (W_{\text{fan}}(\mathbf{x})\,,\, V_{\text{tower}}(\mathbf{x}))$ *dominates* $\mathbf{u} = (W_{\text{fan}}(\mathbf{x}^*)\,,\, V_{\text{tower}}(\mathbf{x}^*))$*. The phrase* ***Pareto optimum*** *is taken to mean with respect to the entire decision variable space unless otherwise specified.*

Definition 4 (Pareto Dominance [86]) *A vector* $\mathbf{u}$ *is said to* ***dominate*** *another vector* $\mathbf{v}$ *(donated by* $\mathbf{u} \preceq \mathbf{v}$*) if and only if* $\mathbf{u}$ *is partially less than* $\mathbf{v}$*, i.e.,* $W_{\text{fan}}^{(\mathbf{u})} \leq W_{\text{fan}}^{(\mathbf{v})}$ *and* $V_{\text{tower}}^{(\mathbf{u})} \leq V_{\text{tower}}^{(\mathbf{v})}$.

Definition 5 (Pareto Optimal Set [86]) *For a given multi-objective constrained optimization problem, $F(\mathbf{x})$, the* ***Pareto optimal set****, $\mathcal{P}^*$, is defined as:*

$$\mathcal{P}^* := \{\mathbf{x}^* \in \Omega \,|\, \exists\, \mathbf{x} \in \Omega \; F(\mathbf{x}^*) \preceq F(\mathbf{x})\}$$

Definition 6 (Pareto Front [86]) *For a given multi-objective constrained optimization problem, $F(\mathbf{x})$, and Pareto optimal set, $\mathcal{P}^*$, the* ***Pareto front****, $\mathcal{PF}^*$, is defined as:*

$$\mathcal{PF}^* := \{\mathbf{u} = F(\mathbf{x}^*) \,|\, \mathbf{x}^* \in \mathcal{P}^*\}$$

There are two stages involved in the solution of a multi-objective optimization problem: (i) the optimization of several objective functions; and (ii) the process of deciding the type of "trade-offs" that are appropriate for the design problem in question. The multi-objective optimization techniques are classified based on which solution stage is handled first. For a *posteriori preference technique*, the search for the "trade-offs" is made before making the decision [86]. This approach is adopted when employing the multi-objective genetic algorithm (MOGA) for the solution. For a *priori preference technique*, the decision of the appropriate "trade-off" type is made before searching [86]. This approach is adopted when employing the weighted sum method for the solution. The full Pareto front can be obtained by either method, however, it is necessary to solve the optimization problem more than once with the weighted sum method. On the other hand, the MOGA method can obtain the full Pareto front by solving the optimization problem only one time. In this thesis, MOGA is used to solve the size optimization problems in (3.27-3.30). The weighted sum method is used to verify the solution of the most relevant size optimization problem.

3.4.2.1 Multi-objective genetic algorithm (MOGA)

Genetic algorithms are search algorithms that work based on the mechanics of natural selection from Darwin's theory of evolution [87]. A genetic algorithm first encodes the design variables of the optimization problem into a finite-length binary string. Mapping the real design variable, x_{real} to the binary encoded design variable, x_{encoded}, is obtained by [87]

$$x_{\text{encoded}} = x_l + \frac{x_u - x_l}{2^l - 1} x_{\text{real}} \tag{3.31}$$

where x_u and x_l are the upper and lower bounds of the design variable, respectively, and l is the string length in bits. All binary encoded design variables are combined together to form an n-length string that represents one design. The search process starts from a population of long strings (initial designs) instead of from a single initial design in the design space. Then, the genetic algorithm guides the search for the global optimum through the design space by finding a more fit population using three genetic processes: (i) selection; (ii) crossover; and (iii) mutation [86, 87]. Each process is performed with an operator guided by probabilistic rules. In turn, the genetic algorithm is of a stochastic, not deterministic, nature. The three genetic processes are defined below.

Selection

Selection is the process of selecting the fit population (good designs) to form a mating pool [87]. The selection operator picks and copies the population based on their fitness. The population with high fitness, probabilistically, gets more copies in the mating pool. Thus, highly fit population live and reproduce, while less fit population vanish [87].

Crossover

Crossover is the process of creating new strings by exchanging information among strings of the mating pool that was generated by the selection operator [87]. First, two individual strings (parents) are selected from the mating pool at random. Second, each pair of parents undergoes crossover by swapping some of their characteristics. Finally, new strings (children) are created with distinct characteristics. The chances of producing fit children are supposed to be good since their parents are highly fit strings and they were not screened out by the selection operator. Less fit children could be produced, however, eventually they will be screened out from the population in the next iterator.

Mutation

Mutation is the process of creating new strings by modifying specific characteristics of their original strings [87]. The mutation process accomplishes a local search around randomly

selected individual strings of one generation. This helps in maintaining diversity among the population.

The MOGA method that is implemented for the wet cooling tower size optimization problems aims to find Pareto fronts using the same search approach; by moving from one generation of population to another generation with a more fit population. The optimization algorithm in question is available as part of a third-party optimization library, JEGA [88], which can be accessed through DAKOTA [83] with the keyword `moga`. The standard representation of the design variables with `moga` is real encoded with a precision of six decimal places [83]. The binary representation is applied only if one of the crossover and mutation operators is a binary operator. The latter case is not applied here. Figure 3.8 illustrates the MOGA method flowchart. Table 3.4 presents the DAKOTA input parameters for the MOGA method. There are eight basic steps implemented for the solution as described below [83].

1. **Initialize unique and random designs**
   The algorithm starts with an initial generation of 50 unique designs. The initialization type `unique_random` generates the initial designs at random and it checks their uniqueness [83]. The initial design is rejected if it duplicates any of the rest of the initial designs. The initial designs set is donated by D_i.

2. **Evaluate objective functions and constraints over initial designs**
   The objective functions and constraints are evaluated for each initial design in D_i.

3. **Reproduce designs**
   Reproduction is achieved in four stages. First, the reproduction operator distinguishes the feasible designs and inserts multiple copies of them into a mating pool. Second, the same operator sorts the infeasible designs based on a feasibility metric. The feasibility metric in question computes the constraints violation of each infeasible design as follows [89]

$$\begin{aligned} \mathrm{CV} = \big\{ &[\max(\, T_{wo}\,, 298.80\,)]^2 + [\max(\, -T_{wo}\,, -293.43\,)]^2 \\ &+ [\max(\, v_a\,, 5.00\,)]^2 + [\max(\, -v_a\,, -1.00\,)]^2 \big\}^{1/2} \end{aligned} \tag{3.32}$$

   Finally, the reproduction operator inserts into the mating pool more copies of the infeasible designs with less CV value than copies of the infeasible designs with more CV value [89]. The designs set after performing the reproduction is denoted by D_{ii}

4. **Crossover designs by random shuffle of design variables**
   The crossover operator `shuffle_random` chooses four designs (parents) in the mating

pool to create four new designs (children) [83]. This is achieved by donating one design variable from a parent as a donor for the child. Both the parent and its donated design variable are chosen at random. The probability of a crossover event is determined by the crossover rate, p_c. The designs set after performing the crossover is denoted by D_{iii}.

5. **Mutate children by random variation of one design variable**
   The mutation operator `replace_uniform` introduces some variations in the designs set D_{iii} [83]. First, a design is selected at random for the mutation. Then, a design variable of the selected design is chosen at random. Finally, the chosen design variable is reassigned to a random value within its upper and lower bounds. The probability of a mutation event is determined by the mutation rate, p_m. The designs set after performing the mutation is denoted by D_{iv}.

6. **Evaluate objective functions and constraints over mutated children**
   The objective functions and constraints are evaluated for each design in D_{iv}.

7. **Rank designs $D_{ii} \cup D_{iv}$ based on Pareto Dominance**
   Before ranking, the constraints violation is computed for each infeasible design in D_{iv}. Then, the ranking is done by keeping track of the current worst design in D_{ii}. The infeasible design in D_{ii} with the largest CV value is selected for comparison with the designs in D_{iv}. The former design is rejected and inserted into a database referred to as the graveyard [90] if one of the following two conditions is true: (i) the design being compared with has a less CV value; or (ii) the design being compared with is feasible. On the other hand, the infeasible design in D_{ii} with the largest CV value is not inserted into the graveyard if and only if the design being compared with has a greater CV value. In the latter case, the design from D_{iv} is instead inserted into the graveyard.

   When all designs in D_{ii} are feasible, the Pareto Dominance definition is used to rank each feasible design, using the fitness type `domination_count` in DAKOTA [83]. As defined previously, a feasible design dominates another feasible design if the two objective functions of the former design are less than the two objective functions of the latter design. Before ranking the feasible designs, current worst feasible designs are screened out from $D_{ii} \cup D_{iv}$. Any feasible design in D_{ii} is kept if it is not dominated by a specific number of designs that is defined by the parameter `below_limit` in DAKOTA [83]. The limit in question is set to be five designs. The feasible design in D_{ii} is inserted into the graveyard if it is dominated by more than five feasible designs in D_{iv}. The same rule applies for the feasible design in D_{iv}; it is inserted into the graveyard if it is

dominated by more than five feasible designs in D_{ii}.

The remaining feasible designs in $D_{ii} \cup D_{iv}$ are ranked based on the number of feasible designs that dominate them. The feasible design that is not dominated by any feasible designs is considered the fittest. On the other hand, the feasible design that is dominated by five feasible designs is the least fit. A shrinkage percentage is used to avoid a significant decrease in the population size that might result from the screening process associated with step 7. If the number of the remaining designs is less than the shrinkage percentage, then the best feasible designs in the graveyard are selected to have enough designs for the subsequent generation [83]. This is done by effectively raising the limit of design domination as far as is necessary to satisfy the shrinkage percentage. The final designs set is denoted by D_v.

8. **Apply niche on D_v**
   The nicher `radial` in DAKOTA is a secondary selection operator applied on the designs that belong to the Pareto front of the designs set D_v. The purpose of the nicher is to obtain a uniform distribution along the Pareto front by enforcing a minimum distance between the designs [83]. The minimum distance in question is set as fractions of the non-dominated range for each objective function as follows

$$\frac{\left|W_{\text{fan}}^{(i)} - W_{\text{fan}}^{(i+1)}\right|}{R_1} = 0.0005 \tag{3.33}$$

$$\frac{\left|V_{\text{tower}}^{(i)} - V_{\text{tower}}^{(i+1)}\right|}{R_2} = 0.0005 \tag{3.34}$$

   where the numerator presents the objective function difference between one design in the Pareto front, i, and its subsequent design, $i+1$. R_1 and R_2 are the non-dominated ranges of the objective functions, W_{fan} and V_{tower}, respectively, between the extreme designs located at the Pareto front tips as shown in Figure 3.6. A design that does not satisfy both (3.33) and (3.34) is removed, however, the design is not completely discarded and it is re-inserted along with the designs for the next reproduction operation [83]. The designs set after applying niching is denoted by D_{vi}, which represents one generation of designs.

9. **Test for convergence**
   `metric_tracker` in DAKOTA works by tracking various changes in the Pareto front from the current generation to the prior generation. The converger in question tracks three metrics related to the Pareto fronts of both generations: maximum expansion

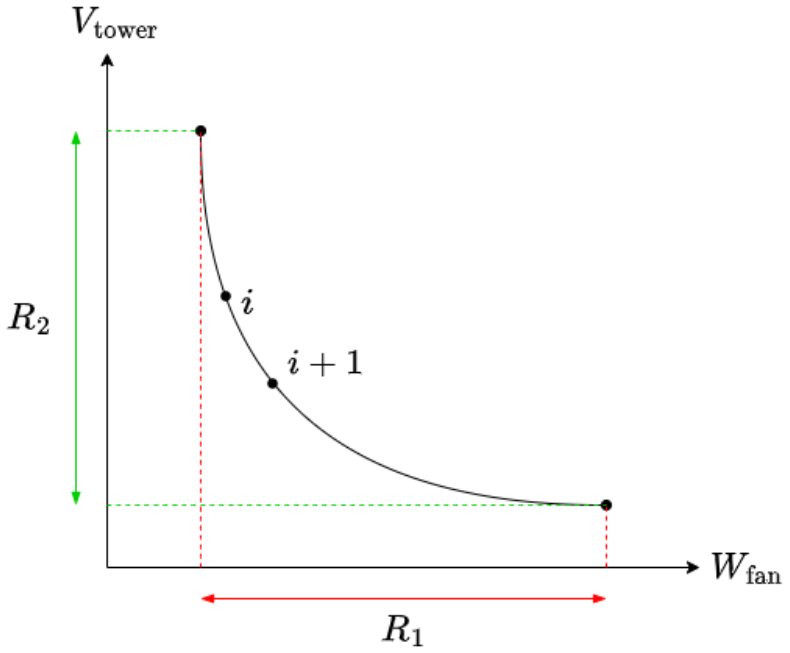

Figure 3.6 – Illustration of the non-dominated ranges of both objective functions used in the radial nicher.

variation, Pareto front density variation, and Pareto front quality variation [83]. The maximum expansion variation, E_m, monitors how the Pareto front expanse is changing between two adjacent generations and it is defined as follows [83]

$$E_m = \max\left(\frac{\left|R_1^{(j)} - R_1^{(j-1)}\right|}{R_1^{(j-1)}}, \frac{\left|R_2^{(j)} - R_2^{(j-1)}\right|}{R_2^{(j-1)}}\right) \tag{3.35}$$

where j is the generation index as shown in Figure 3.7. The Pareto front density variation, $\Delta\rho_{\text{PF}}$, monitors how the density of the Pareto optimal designs is changing between two adjacent generations as shown in Figure 3.7. The Pareto front density for the current generation j, $\rho_{\text{PF}}^{(j)}$, is defined as follows [83]

$$\rho_{\text{PF}}^{(j)} = \frac{N_{\text{PF}}^{(j)}}{R_1^{(j)}\, R_2^{(j)}} \tag{3.36}$$

where $N_{\text{PF}}^{(j)}$ is the number of Pareto optimal designs in the current generation. In turn, $\Delta\rho_{\text{PF}}$ is determined by

$$\Delta\rho_{\text{PF}} = \frac{\rho_{\text{PF}}^{(j)} - \rho_{\text{PF}}^{(j-1)}}{\rho_{\text{PF}}^{(j-1)}} \tag{3.37}$$

Finally, the Pareto front quality variation, G_{PF}, monitors how the goodness of the Pareto front is changing between two adjacent generations [83]. This is done by first

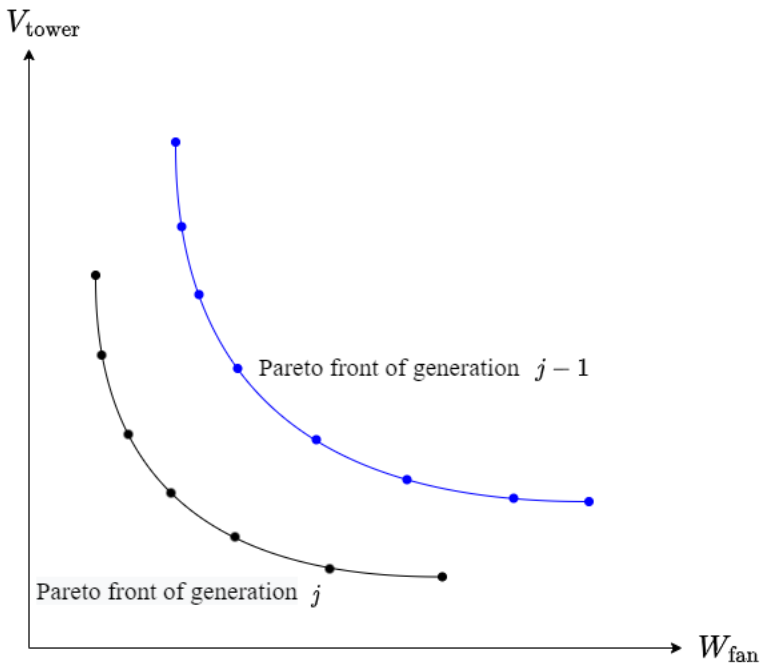

Figure 3.7 – Illustration of changes in the Pareto front between two adjacent generations.

counting the number of designs in the prior generation which are dominated by the designs in the current generation. Then, G_{PF} is computed as the ratio of the number of dominated designs, n_d, to the total number of designs in the prior generation, $n^{(j-1)}$, as follows [83]

$$G_{\text{PF}} = \frac{n_d}{n^{(j-1)}} \tag{3.38}$$

The converger `metric_tracker` records the largest value of E_m, $\Delta\rho_{\text{PF}}$, and G_{PF} at each generation [83]. The algorithm is assumed to converge once the recorded value is below the supplied threshold, i.e., 0.0005, for the supplied number of generations over which the converger should be tracked consecutively, i.e., 100 generations.

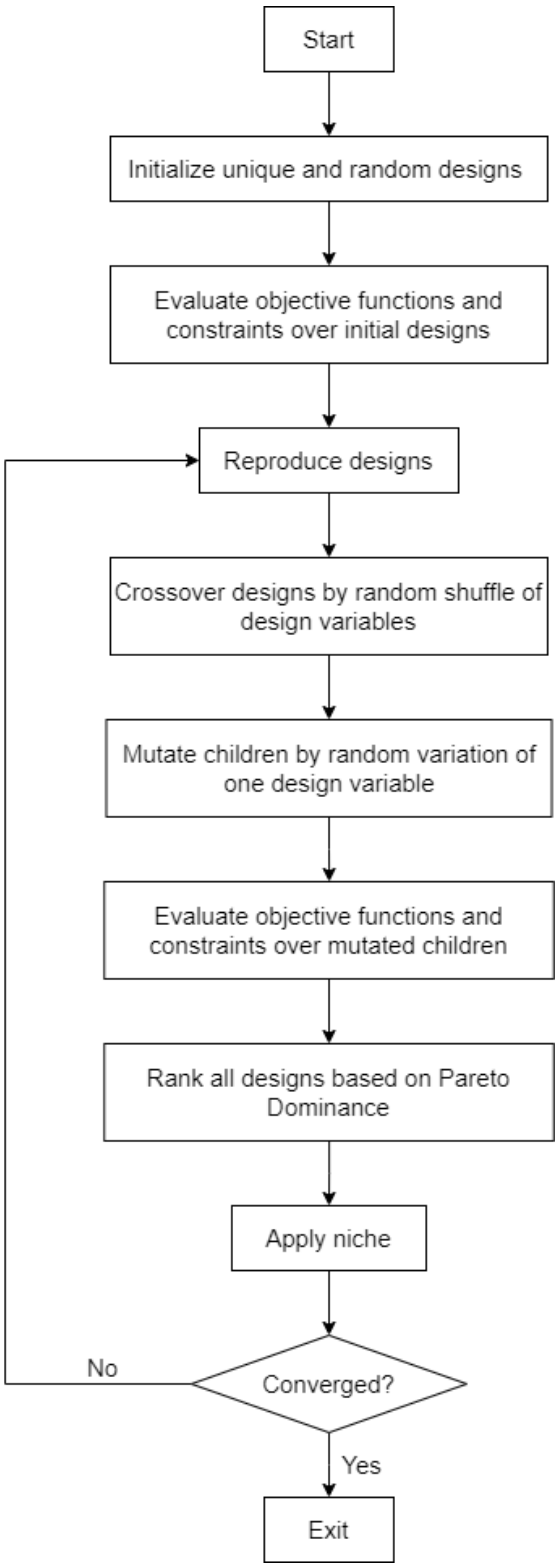

Figure 3.8 – The MOGA Flowchart.

Table 3.4 – DAKOTA input parameters for MOGA.

Parameter	Value
Maximum function evaluations	2500
Number of initial designs	50 designs
Crossover rate	0.7
Number of parents for the crossover	4
Number of children from the crossover	4
Mutation rate	0.2
Pareto Dominance limit	5 designs
Niching percentage	0.05%
Percentage change used for the convergence criterion	0.05%
Number of generations for the convergence criterion	100 generations

3.4.2.2 Weighted sum method

The weighted sum method first transforms the multi-objective optimization problem into a single-objective optimization problem. Each of the two objective functions is multiplied by a weighting factor and the final objective function is the sum of both contributions, i.e., $w_1 W_{\text{fan}} + w_2 V_{\text{tower}}$. The sum of two weights is equal to one and each single set of weights determines one particular Pareto optimal design. Then, the resulting single-objective constrained optimization problem is solved using an appropriate method, e.g., the method of feasible directions (MFD). The Pareto front of the optimization problem (3.28) can be approximated by solving the following single-objective optimization problem at different weight sets, i.e., different numerical values for w_1 and w_2:

$$
\begin{aligned}
&\text{minimize} && w_1 W_{\text{fan}} + w_2 V_{\text{tower}} \\
&\text{w.r.t.:} && m_a \, , H_{\text{fz}} \, , A_{\text{ct}} \\
&\text{subject to:} && 293.43\,\text{K} \leq T_{wo}\,(T_{ai}, T_{wbai}) \leq 298.80\,\text{K} \\
& && 1.0\,\text{m/s} \leq v_a \leq 5.0\,\text{m/s} \\
& && 390.99\,\text{kg/s} \leq m_a \leq 1954.94\,\text{kg/s} \\
& && 0.3\,\text{m} \leq H_{\text{fz}} \leq 3.0\,\text{m} \\
& && 25\,\text{m}^2 \leq A_{\text{ct}} \leq 214\,\text{m}^2
\end{aligned}
\tag{3.39}
$$

Table 3.5 shows the values for the weights and the initial designs at each set, where each set assigns different importance to each objective function.

Table 3.5 – Selected weights and initial designs used to approximate the Pareto front of the optimization problem (3.28) using the weighted sum method.

	w_1	w_2	m_a [kg/s]	H_{fz} [m]	A_{ct} [m^2]
Set 1	0.90	0.10	631.79	0.98	214
Set 2	0.75	0.25	631.79	0.98	193
Set 3	0.50	0.50	631.79	0.98	172
Set 4	0.25	0.75	631.79	0.98	151
Set 5	0.10	0.90	631.79	0.98	132
Set 6	0.0001	0.9999	631.79	0.98	132

3.5 Design problem 3: Size optimization with visible plume constraint

3.5.1 Problem definition

The target of this design problem is to determine the air mass flow rate, m_a, and geometrical dimensions of the wet cooling tower, i.e, the tower frontal area A_{ct} and the fill height H_{fz}, necessary to achieve the best trade-off between the capital and operating costs while meeting all the design constraints for cooling performance, noise generation, fill functioning, and plume visibility. The specifications of the cooling tower in question are given in Table 3.2. A multi-objective constrained optimization problem can be formulated for design problem 3 as follows

$$
\begin{aligned}
&\text{minimize} && W_{\text{fan}}\,, V_{\text{tower}} \\
&\text{w.r.t.:} && m_a\,, H_{\text{fz}}\,, A_{\text{ct}} \\
&\text{subject to:} && 293.43\,\text{K} \leq T_{wo}\left(T_{ai}, T_{wbai}\right) \leq 298.80\,\text{K} \\
& && 1.0\,\text{m/s} \leq v_a \leq 5.0\,\text{m/s} \\
& && h_{\text{vp}}\left(T_{\text{cold}}, T_{\text{cold,wb}}\right) \leq h_{\max} \\
& && 390.99\,\text{kg/s} \leq m_a \leq 1954.94\,\text{kg/s} \\
& && 0.3\,\text{m} \leq H_{\text{fz}} \leq 3.0\,\text{m} \\
& && 25\,\text{m}^2 \leq A_{\text{ct}} \leq 214\,\text{m}^2
\end{aligned}
\tag{3.40}
$$

The visible plume length, h_{vp}, is evaluated at cold ambient condition, whereas the two responses, i.e., W_{fan} and T_{wo}, are evaluated at hot ambient conditions described by T_{ai} and T_{wbai}. The visible plume constraint is obtained when the cooling tower operates during the winter months where there is the highest potential for condensation within the atmospheric

plume. The cold ambient condition described by T_{cold} and $T_{\text{cold,wb}}$ is designated for the coldest days of the year. The maximum allowable length for the visible plume, $h_{\max}$, is set based on local regulations where the cooling tower is located. For research purposes, however, it is interesting to study the effect of selecting T_{cold}, $T_{\text{cold,wb}}$, and $h_{\max}$ on the size optimization of wet cooling towers. The atmospheric plume model used in the analysis assesses the severity of fog formation more accurately at elevations close to the cooling tower. Therefore, T_{cold} and $T_{\text{cold,wb}}$ are selected so that the visible plume formed in this ambient condition is not too long, i.e, $h_{\text{vp}} < 20$ m. The parametric studies given in Appendix D for h_{vp} at various cold ambient conditions show that it is anticipated to have a very long visible plume when $T_{\text{cold}} < 10°\text{C}$ and RH $> 40\%$, i.e., for cold and wet ambient conditions. In this study, $T_{\text{cold,wb}}$ is selected based on RH $= 40\%$.

3.5.2 Solution method

The MOGA method is employed to solve the size optimization problem with visible plume constraint (3.40) using the same DAKOTA input parameters listed in Table 3.4. In this case, constraint violation for the infeasible design is computed as follows

$$\begin{aligned} \text{CV} = \big\{ &[\max(\, T_{wo}\,, 298.80\,)]^2 + [\max(\, -T_{wo}\,, -293.43\,)]^2 \\ &+ [\max(\, v_a\,, 5.00\,)]^2 + [\max(\, -v_a\,, -1.00\,)]^2 \\ &+ [\max(\, h_{\text{vp}}\,, h_{\max}\,)]^2 \big\}^{1/2} \end{aligned} \tag{3.41}$$

Chapter 4

Results and discussion

4.1 Design problem 1: Airflow selection

The optimization problem formulated for airflow selection of a wet cooling tower is solved at three different fill heights: 0.30, 1.83 and 3.00 m. These three values describe three conditions for H_{fz}, i.e., small, medium, and large fill heights, respectively. In the three cases, the MFD method is used in the solution with the same initial feasible design, i.e., $m_a = 977.45\,\text{kg/s}$, i.e., $L/G = 1.0$.

4.1.1 Airflow selection at small fill height

After 10 iterations and approximately 8 minutes on a 2.9 GHz Dual-Core Intel Core i5 computer, the optimization algorithm converged to the final design that provides the desired cooling performance with an air mass flow rate of 938.93 kg/s for $L/G = 1.04$. Figure 4.1 shows the evolution of the objective function, constraint, and design variable during the optimization process. Ultimately, the objective function approached zero indicating that $T_{wo}\,(m_a = 938.93\text{ kg/s}) = T_{\text{desired}}$ at $H_{\text{fz}} = 0.30$ m.

Figure 4.2 shows the distribution of the main thermodynamic properties inside the initial and final designs of the wet cooling tower with small fill height. The initial design provides a slightly excessive cooling, i.e., the water exits the cooling tower at 298.61 K which is less than T_{desired} by 0.19 K. The final design provides the desired cooling performance with the proportion of heat rejected in the rain, fill, and spray zones of 29.70%, 52.89%, and 17.41%, respectively. The fill zone still contributes most of heat rejection, with the temperature profiles showing that the water temperature is reduced by a larger amount in the fill zone than in the other cooling tower zones. The results highlight the essential role played by the fill. Water and air temperatures are similar at the lowest portion of the fill. Below this region, the air temperature is higher than the water temperature, which leads, paradoxically, to cooling the air in the rain zone. The humidity ratio profiles show that the air leaves the

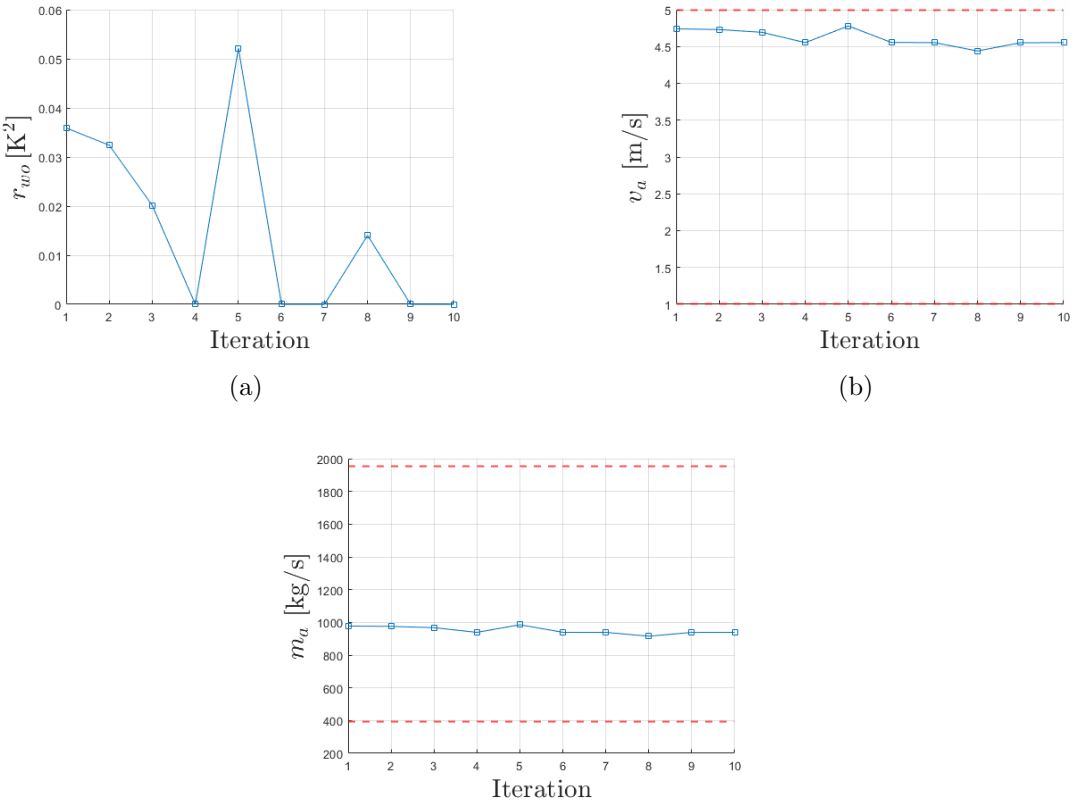

Figure 4.1 – Convergence history to the final design for airflow selection at small fill height.

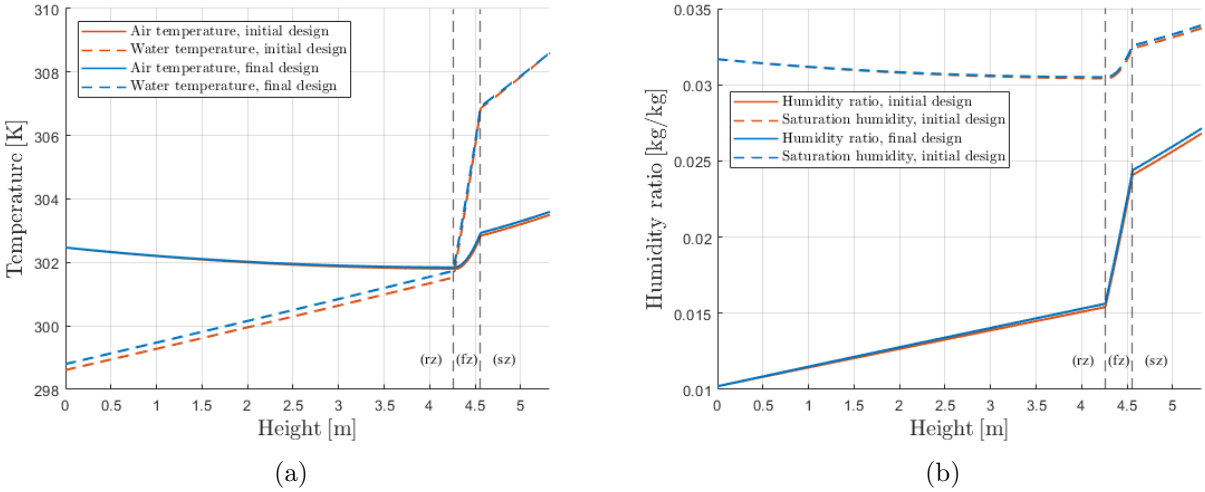

Figure 4.2 – Distribution of temperature and of humidity ratio inside the initial design and final design of the wet cooling tower with small fill height.

cooling tower sub-saturated with vapor in the final design. This is because the small fill height does not allow the air to evaporate more water and hence the air leaves the fill zone with less moisture. The results from solving the air draft equation show that using a small fill height provides a pressure drop of 16.7% of the total static pressure drop through the cooling tower. It is reported that the fan input power at this operating point is equal to 0.72 MW.

4.1.2 Airflow selection at medium fill height

After 22 iterations and approximately 34 minutes on a 2.9 GHz Dual-Core Intel Core i5 computer, the optimization algorithm converged to the final design that provides the desired cooling performance with an air mass flow rate of 518.20 kg/s, i.e., $L/G = 1.89$. Figure 4.3 shows the evolution of the objective function, constraint, and design variable during the optimization process. Ultimately, the objective function approached zero indicating that $T_{wo}\,(m_a = 518.20 \text{ kg/s}) = T_{\text{desired}}$ at $H_{\text{fz}} = 1.83$ m.

Figure 4.4 shows the distribution of the main thermodynamic properties inside the initial and final designs of the wet cooling tower with medium fill height. The initial design provides an excessive cooling performance, i.e., the water exits the cooling tower at 294.58 K which is less than T_{desired} by 4.22 K. The final design provides the desired cooling performance with the proportion of heat rejected in the rain, fill, and spray zones being 21.16%, 74.45%, and 4.38%, respectively. Compared to the cooling tower design with small fill height, increasing H_{fz} by 1.53 m increases heat rejection in the fill by 21.56%. The elongation of the fill does not, however, significantly alter the location at which the air and water temperatures become equal: this point is still located in the lowest portion of the fill. Fill elongation makes the air leaving the fill saturated with water vapor. The air draft equation shows that using a medium fill height contributes in making the fill zone responsible for a substantially larger overall fraction of the static pressure drop, i.e., 45.7%. However, in terms of the fan input power, increasing H_{fz} by 1.53 m reduces W_{fan} by 0.52 MW, which leads to a nontrivial decrease in the operating cost. This is because a less air is required to deliver the desired cooling when the medium fill height is used. The penalty associated with using a cooling tower design with medium fill height is a rise in the capital cost due to purchasing more fill material.

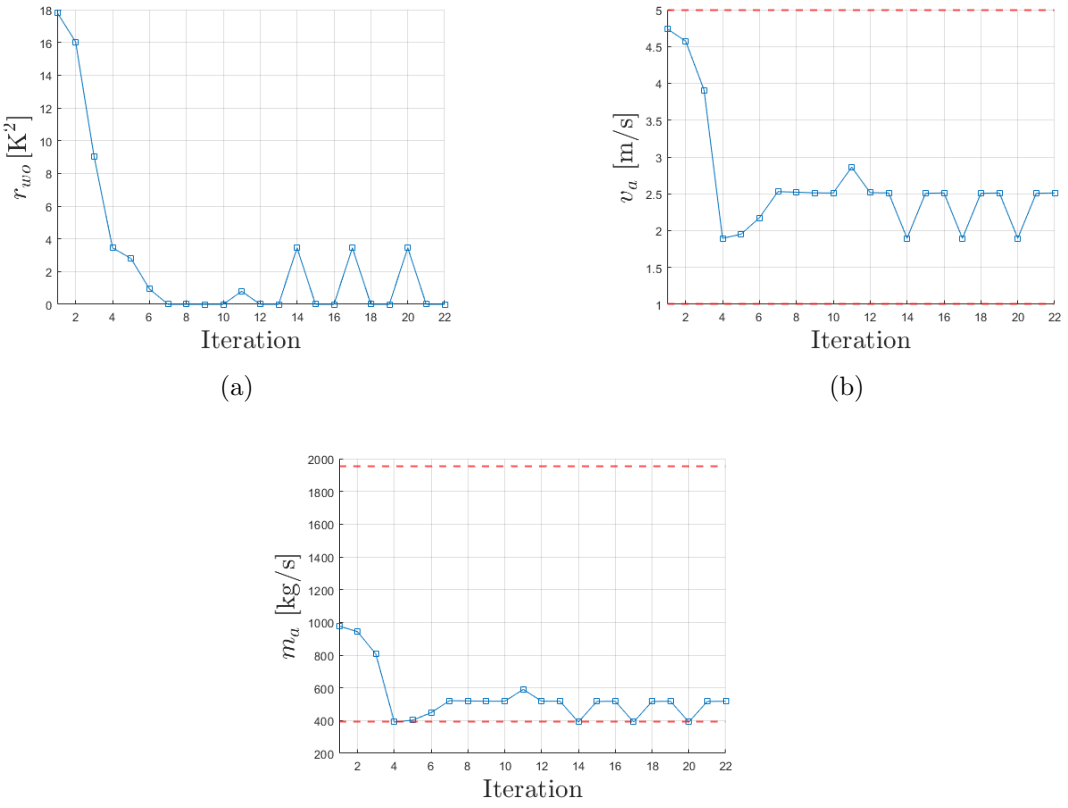

Figure 4.3 – Convergence history to the final design for airflow selection at medium fill height.

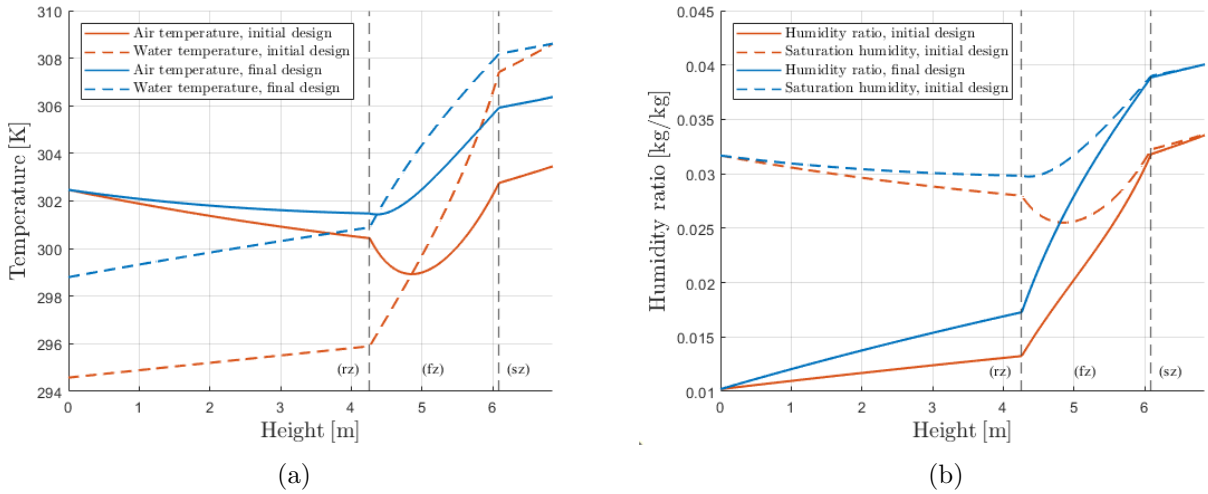

Figure 4.4 – Distribution of temperature and humidity ratio inside the initial design and final design of the wet cooling tower with medium fill height.

4.1.3 Airflow selection at large fill height

After 22 iterations and approximately 20 minutes on a 2.9 GHz Dual-Core Intel Core i5 computer, the optimization algorithm converged to the final design that provides the desired cooling performance with an air mass flow rate of 474.16 kg/s, i.e., $L/G = 2.06$. Figure 4.5 shows the evolution of the objective function, constraint, and design variable during the optimization process. Ultimately, the objective function approached zero indicating that $T_{wo}\,(m_a = 474.16 \text{ kg/s}) = T_{\text{desired}}$ at $H_{\text{fz}} = 3.0$ m.

Figure 4.6 shows the distribution of the main thermodynamic properties inside the initial and final designs of the wet cooling tower with large fill height. The initial design provides excessive cooling, i.e., the water exits the cooling tower at 293.59 K which is less than T_{desired} by 5.21 K. The final design provides the desired cooling with the proportion of heat rejected in the rain, fill, and spray zones being 20.12%, 77.50%, and 2.38%, respectively. Compared to the cooling tower design with medium fill height, increasing H_{fz} by 1.17 m slightly enhanced the heat rejection in the fill by 3.05%. This is attributed to the fact that the fill extension comes after the location where the air becomes saturated with vapor. Beyond the location in question, no further evaporation can occur and the potential for water cooling is substantially reduced. The air draft equation shows that using a large fill height contributes in making the fill zone responsible for a substantially larger overall fraction of the static pressure drop, i.e., 57%. Increasing the fill height from 1.83 m to 3.0 m corresponds to increasing the fan input power by 3 kW. The corresponding impact on operating cost is therefore negligible. The corresponding impact on capital cost may be more substantial, however, because of the larger volume of fill that must now be purchased.

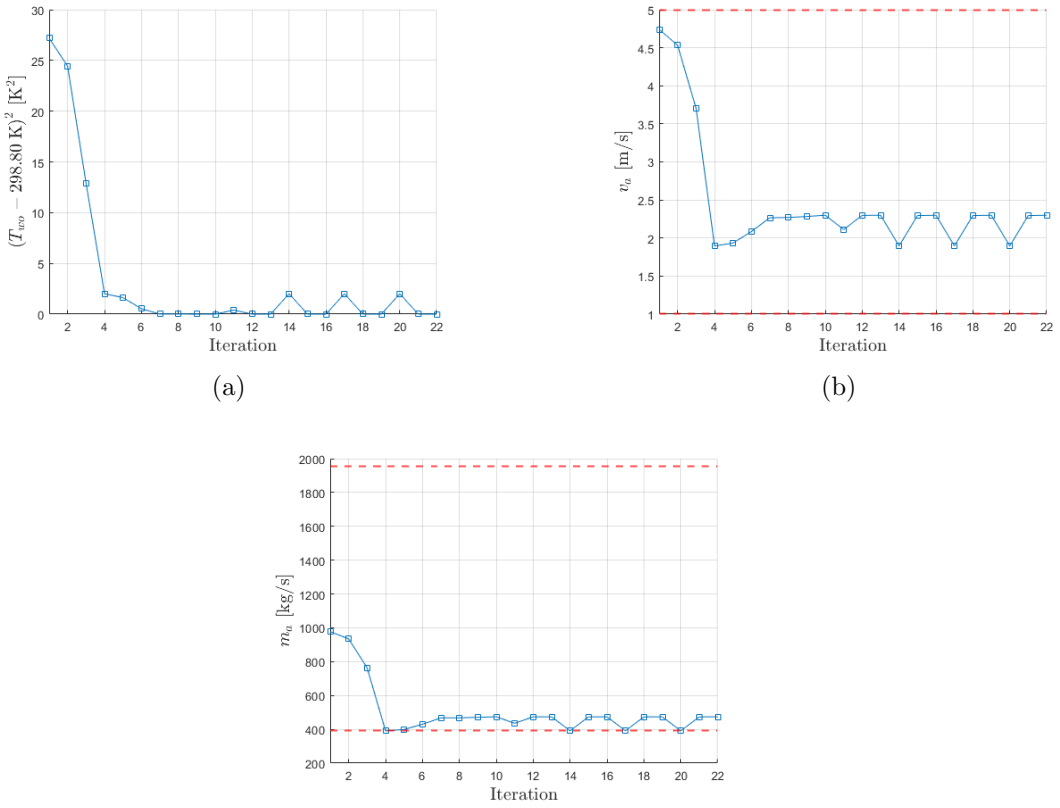

Figure 4.5 – Convergence history to the final design for airflow selection at large fill height.

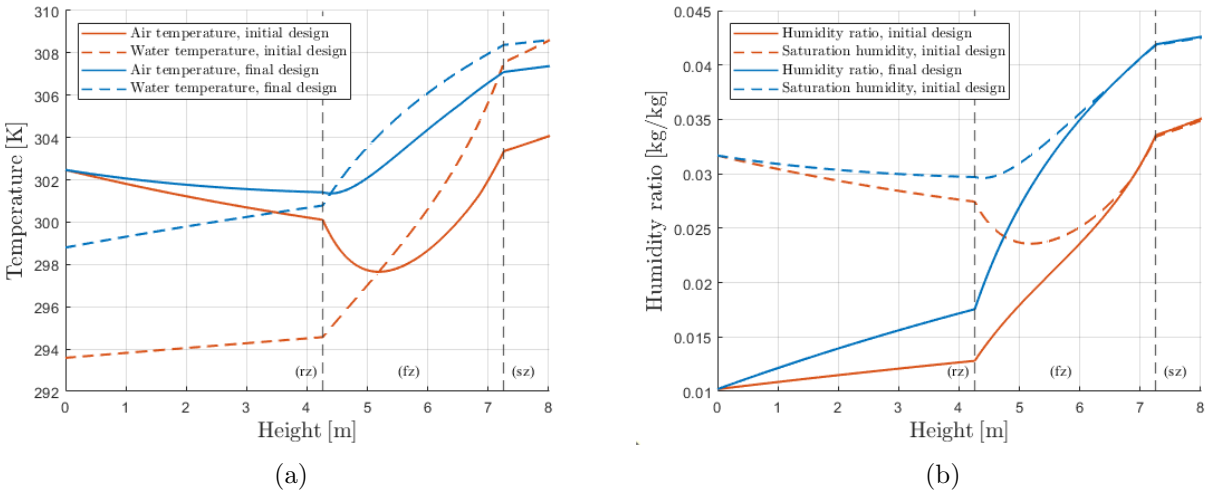

Figure 4.6 – Distribution of temperature and humidity ratio inside the initial design and final design of the wet cooling tower with large fill height.

4.1.4 Globality of the final solution

The use of MFD helps in obtaining the final solution for wet cooling tower fan selection in a reasonable number of iterations. To demonstrate that the final solution is global, we show that this same final solution can be obtained from different initial starting points. Four values within the design domain are specified as Case 1 to Case 4 in Table 4.1. From Case 1 to Case 4, L/G is equivalent to $\{2.5, 2.0, 1.5, 0.5\}$. Figure 4.7 shows the optimal design obtained for the cases in Table 4.1. The same optimal design is obtained every time, which confirms the final solution determined previously (Case 0) is indeed a global optimum. For some initial designs such as in Case 0 and Case 4, the optimization algorithm took several additional iterations, but ultimately they all converged to the same solution.

Table 4.1 – Initial starting points used for checking the globality of the final design with medium fill height.

Design variable	Case 0	Case 1	Case 2	Case 3	Case 4
m_a [kg/s]	977.94	390.99	488.74	651.65	1954.94

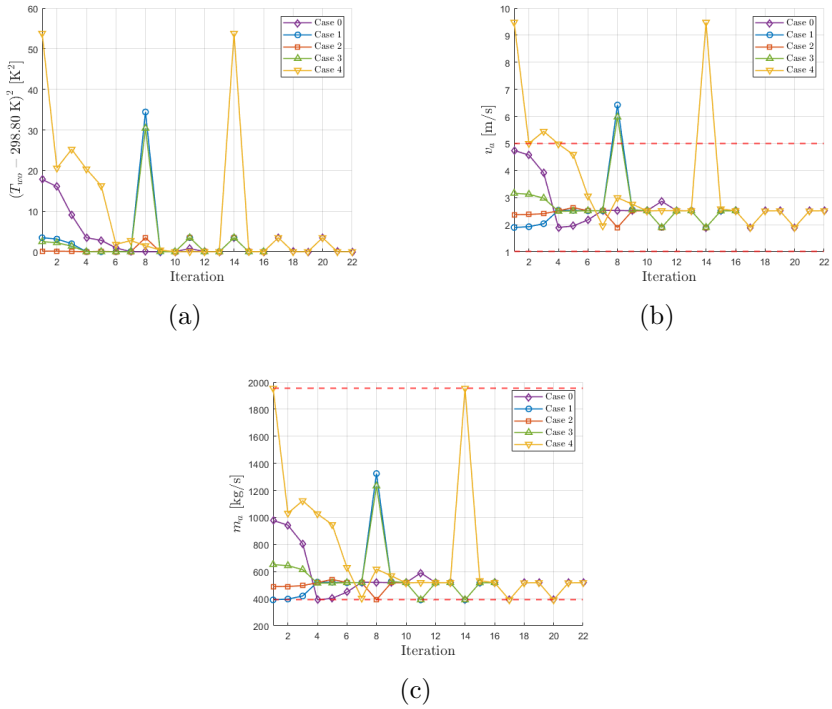

Figure 4.7 – Convergence history to the final design for airflow selection in a wet cooling tower with medium fill height at different initial starting points.

4.1.5 Comparison with field measurements

Table 4.2 presents a comparison between the obtained optimization solution for airflow selection of a wet cooling tower against analogue field measurement for the same tower collected during the performance test reported in [1]. Two hour-long data sets were collected corresponding to two different air inlet temperatures; one of them is $T_{ai} = 302.47\,\mathrm{K}$ given in Table 3.2. Inlet and outlet water temperatures were measured using three and four four-wire resistance-type temperature sensors, respectively. The optimization solution indicates that the outlet water temperature of 298.80 K is achieved by the cooling tower at an air mass flow rate that is more than the measured value by 35.18 kg/s. This difference in m_a corresponds to an error of 6.36%, which reflects the uncertainty of field measurements and the fact that the estimated value of 518.20 kg/s represents an average air mass flow rate in the cooling tower.

Table 4.2 – Comparison of the optimization solution against the field measurements.

Parameter	Optimization solution	Field measurement
T_{wo} [K]	298.80	298.80
m_a [kg/s]	518.20	553.38

4.1.6 Final remarks

A major aspect of wet cooling tower design is estimating the airflow for a desired cooling load in given design operating conditions. Using optimization, airflow estimates were obtained at three fill heights. The results help in understanding the important role of using film fill in the cooling tower. Even when using a small fill height, i.e, 0.30 m, the fill is able to reject more heat from the water than either of the spray or rain zones. Increasing the fill height enhances overall cooling, which leads to smaller airflow requirements. The reduction in the required air mass flow rate reduces the operating cost by decreasing fan power consumption. However, the decrease in question eventually hits a wall of diminishing returns, i.e there is a threshold fill height beyond which decreases of fan power become small. This threshold in question is determined by the location where the air becomes saturated with vapor. Determining where the air becomes saturated can be offered by using the 1D zone-specific thermodynamic model. For a better evaluation of a cooling tower design, the capital and operating costs should be incorporated into the optimization problem.

4.2 Design problem 2: Size optimization

Figure 4.8 shows four Pareto fronts obtained for the four size optimization problems of a wet cooling tower. Each Pareto front offers a number of optimal designs that achieve the best trade-off between minimizing the capital cost and minimizing the operating cost. This variety in the optimal designs helps the user decide on the most appropriate cooling tower design for a given application (and scheme for financing). The four Pareto fronts are different in terms of their breadth. The Pareto front with two design variables has the shortest interval for V_{tower}, i.e., $[1157 - 1642\ \text{m}^3]$. The same Pareto front deviates upward from other Pareto fronts when $V_{\text{tower}} < 1260\ \text{m}^3$ indicating that the optimal designs are restricted by the size of the design space after this point. The Pareto front with three design variables covers a wider range for V_{tower}, i.e., $[776 - 1277\ \text{m}^3]$. Therefore, considering the tower frontal area as a design variable in the size optimization helps in obtaining more optimal designs with lower capital cost. The Pareto front with four design variables covers a wider range for both objectives, i.e, $W_{\text{fan}} \in [0.17 - 0.75\ \text{MW}]$ and $V_{\text{tower}} \in [719 - 2235\ \text{m}^3]$. In other words, considering the rain zone height as a design variable in the size optimization problem helps in obtaining more optimal designs with lower operating cost. The Pareto front with five design variables is similar to the Pareto front with four design variables. This indicates that adding the spray zone height in the design space does not assist in obtaining more optimal designs with either lower capital cost or lower operating cost.

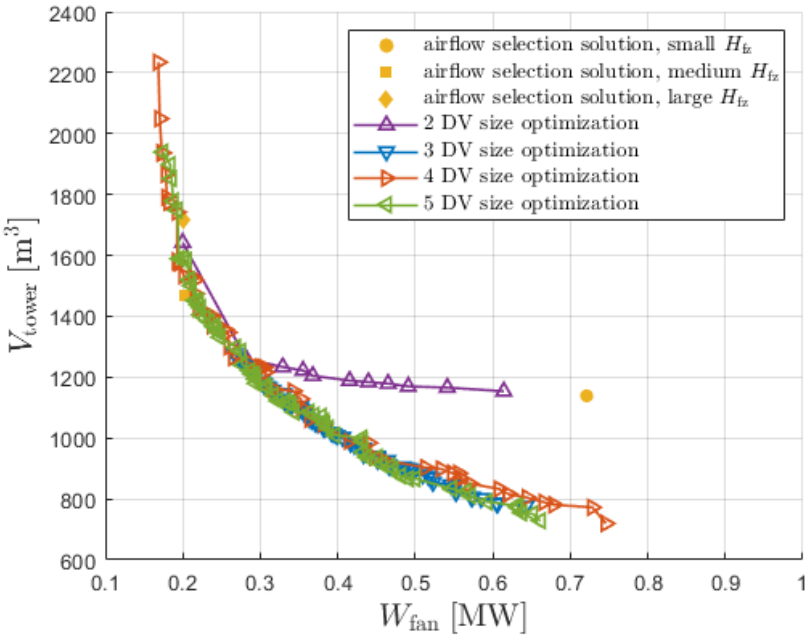

Figure 4.8 – Pareto fronts for the wet cooling tower size optimization problem.

The objective space in Figure 4.8 shows the final designs obtained for design problem 1. The final designs with medium and large fill heights are close to each other and they are adjacent to the Pareto fronts, while the final design with small fill height is located away from the Pareto fronts. The design with small fill height has a total volume of 1139 m^3 and consumes 0.72 MW. This design is sub-optimal according to the criteria used in size optimization. The results show that at approximately the same V_{tower}, there is a design that can deliver the same cooling performance consuming 0.38 MW less in fan input power. From a different perspective, the results show that at approximately the same W_{fan}, there is a design that can deliver the same cooling performance with 366 m^3 less in cooling tower volume. Therefore, the reliance on airflow selection only in wet cooling tower design might lead to a final design with a poor trade-off between minimizing the capital and operating costs.

Figure 4.9 presents an evaluation of constraints for each optimal design obtained based on the size optimization and for each optimal design obtained based on the airflow selection. The cooling performance constraint and the noise constraint are satisfied by all the designs. The evaluation of T_{wo} in Figure 4.9(a) demonstrates that all optimal designs deliver the desired outlet water temperature which corresponds to the upper boundary for T_{wo}. This indicates that the cooling performance constraint is always active during the optimization. On the other hand, the noise generation constraint is not always active since the air velocity can be less than 5 m/s for a design that provides a good trade-off between the design objectives, e.g., a fill whose volume is not too small.

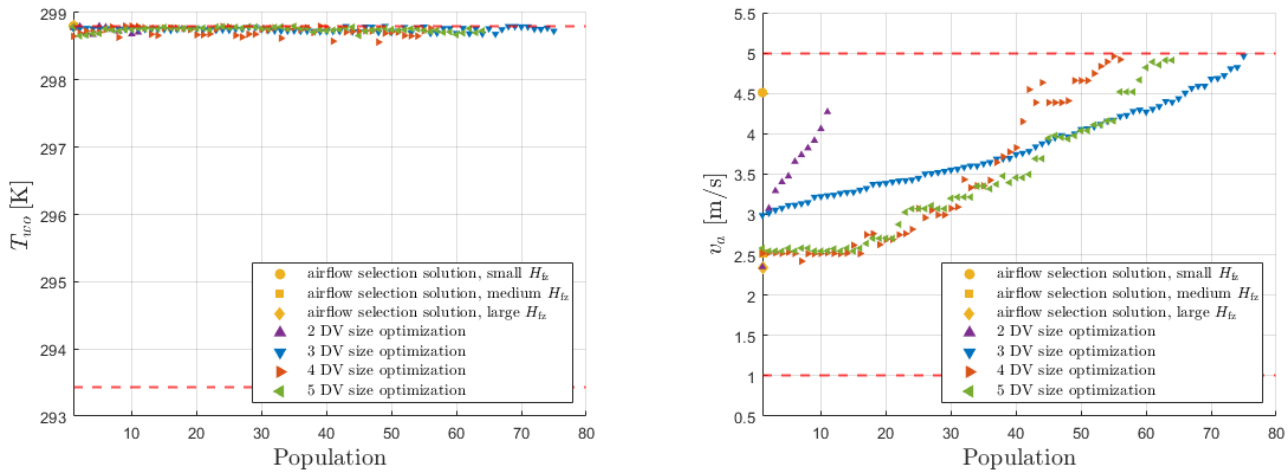

(a) (b)

Figure 4.9 – Scatter distribution of constraints at Pareto fronts for the wet cooling tower size optimization.

Achieving the best trade-off between minimizing the capital cost and minimizing the operating cost occurs through a variety of design variables selections. Figure 4.10 shows a variety of design variable selections in the form of scatter distributions for the populations in each Pareto front. To achieve a design with minimal operating cost, the cooling tower should operate at low airflow for the purpose of reducing the fan input power. As a consequence, the cooling tower should be large in order to satisfy the cooling performance requirement by offering more volume for heat and mass transfer processes. However, any extension of the cooling tower in the vertical direction increases the pressure drop and thus increases the fan input power, which is contrary to the target of minimizing the operating cost. Therefore, increasing the tower height should, as a design principle, be applied cautiously so that the pressure drop rise is not substantial. On the other hand, to build a cooling tower with minimal capital cost, the cooling tower size should be small. As a consequence, the tower must accommodate a high airflow in order to satisfy the cooling performance requirement. Eventually, however, the noise generation constraint may become active because noise increases sharply with air velocity. Therefore, an increase of fan size for purposes of increasing airflow should be undertaken with care so that the air velocity falls within the allowable limit for the noise generation.

For the size optimization with two design variables, there is only one degree of freedom for changing V_{tower} while the rest of the geometrical dimensions are fixed, i.e., $\{A_{\text{ct}}, H_{\text{rz}}, H_{\text{sz}}\} = \{214\ \text{m}^3, 4.26\ \text{m}, 0.76\ \text{m}\}$. The Pareto front with two design variables is shaped by continuously adjusting m_a and H_{fz}. This approach for selecting the design variables is insufficient because small decreases in the cooling tower volume necessitate large increases in the fan input power after the second optimal design. In the limit in question, there is therefore a poor trade-off between minimizing the capital cost and minimizing the operating cost. The optimal design with the minimum operating cost has as its solution $m_a = 484.63\,\text{kg/s}$ and $H_{\text{fz}} = 2.65\,\text{m}$. The air mass flow rate cannot be reduced below 484.63 kg/s because the cooling performance constraint cannot be satisfied, even if the fill height is increased beyond 2.65 m. This is because the air reaches saturation at 2.65 m, which limits the ability of the air to evaporate more water. The optimal design with the minimum capital cost has as its solution $m_a = 880.53\,\text{kg/s}$ and $H_{\text{fz}} = 0.37\,\text{m}$. The fill height cannot be shrunk below 0.37 m because the flow rate of air would then be so large that the noise generation constraint could not be satisfied.

For the size optimization with three design variables, there are two degrees of freedom for changing V_{tower} while the rest of the geometrical dimensions are fixed, i.e., $\{H_{\text{rz}}, H_{\text{sz}}\} = \{4.26\ \text{m}, 0.76\ \text{m}\}$. The Pareto front with three design variables is shaped by continuously adjusting A_{ct}, i.e., from 213 - 132 m^2. The change in the tower frontal area has more influence in reducing V_{tower} from 1277 m^3 to 776 m^3 as shown in Figure 4.8. This fact highlights why

it is essential to include A_{ct} as a design variable in cooling tower size optimization. Figures 4.10(a,b) show that although m_a and H_{fz} are not constant, they vary relatively little along the length of the Pareto front and typically assume one of two values. The optimal design with the minimum operating cost has as its solution $m_a = 612.91\,\text{kg/s}$, $H_{\text{fz}} = 0.98\,\text{m}$, and $A_{\text{ct}} = 213\,\text{m}^2$. The fan input power could be further minimized by respectively decreasing and increasing m_a and H_{fz}, this notwithstanding the rise in the pressure drop through the fill. However, such a cooling tower design is not obtained in this case. The optimal design with the minimum capital cost has as its solution $m_a = 631.79\,\text{kg/s}$, $H_{\text{fz}} = 0.88\,\text{m}$, and $A_{\text{ct}} = 132\,\text{m}^2$. The tower frontal area cannot be reduced below 132 m^2 because of the noise generation constraint. The fill height cannot be shrunk below 0.88 m because this requires that m_a should be more than 631.79 kg/s to satisfy the cooling requirement. As a result, and considering again the noise generation constraint, a large tower frontal area is required, which has the effect of increasing V_{tower} instead of reducing it.

For the size optimization with four design variables, there are three degrees of freedom for changing V_{tower} while keeping the spray zone height fixed, i.e., $H_{\text{sz}} = 0.76$ m. The Pareto front with four design variables is shaped by continuously adjusting H_{rz} for the first 14 designs, i.e., from 7.92 m to 4.34 m, and then it is shaped by adjusting A_{ct}, i.e, from 204 m^2 to 109 m^2. The rain zone is considered the second contributor in heat rejection after the fill zone and it offers a moderate cooling potential per unit height. Therefore, increasing the rain zone height is favored for obtaining an optimal design with less operating cost providing that the rise in pumping cost of water is negligible. The optimal design with the minimum operating cost has as its solution $m_a = 515.34\,\text{kg/s}$, $H_{\text{fz}} = 1.84\,\text{m}$, $A_{\text{ct}} = 212\,\text{m}^2$, and $H_{\text{rz}} = 7.92\,\text{m}$. Compared to an analogous design obtained by the size optimization with three design variables, the rise in H_{rz} and H_{fz} causes m_a to decrease by 22.6%. As a consequence, fan power consumption decreases 0.1 MW. Any further decline in the fan power consumption cannot occur due to the limited cooling potential of the fill zone caused by the air reaching a state of saturation. Thus it is counterproductive to increase H_{fz}. The optimal design with the minimum capital cost has as its solution $m_a = 515.34\,\text{kg/s}$, $H_{\text{fz}} = 1.84\,\text{m}$, $A_{\text{ct}} = 109\,\text{m}^2$, and $H_{\text{rz}} = 4.02\,\text{m}$. Compared to an analogous design obtained by the size optimization with three design variables, the cooling tower size is reduced by $57\,\text{m}^3$ by decreasing the tower frontal area by 23 m^2. Such a reduction is allowed in this case because the airflow is sufficiently low to satisfy the cooling performance constraint given that there is a sufficient fill height, i.e., 1.84 m compared to 0.88 m. Selecting a large fill height in the capital cost-minimizing optimal design is allowed in this case because the rain zone height is reduced to its lowest possible value. Furthermore, the tower frontal area of this design is the smallest possible for satisfying the noise constraint.

For the size optimization with five design variables, there are four degrees of freedom for

changing V_{tower}. Compared to the variation of m_a and H_{fz} in the optimal designs with four design variables, here m_a and H_{fz} appear in the following tandem pairs: $(513.34\,\text{kg/s}, 1.92\,\text{m})$ or $(612.91\,\text{kg/s}, 1.00\,\text{m})$. The spray zone is considered the least contributor in the heat rejection because the air enters the spray zone loaded with moisture which reduces its ability to evaporate more water. The spray zone therefore offers only a very modest cooling potential per unit height. For this reason, the spray zone height in the optimal designs is small compared to its maximum possible value. Most selections of H_{sz} are close to the original value, i.e., 0.76 m. Furthermore, the uniformity of water distribution by the spray nozzles is restricted by the spray zone height, so changing H_{sz} from its original value might lead to a maldistribution of water over the fill. Unless there is a metric capable of describing the uniformity of the water flow distribution, it is likely unwise to include the spray zone height as a design variable.

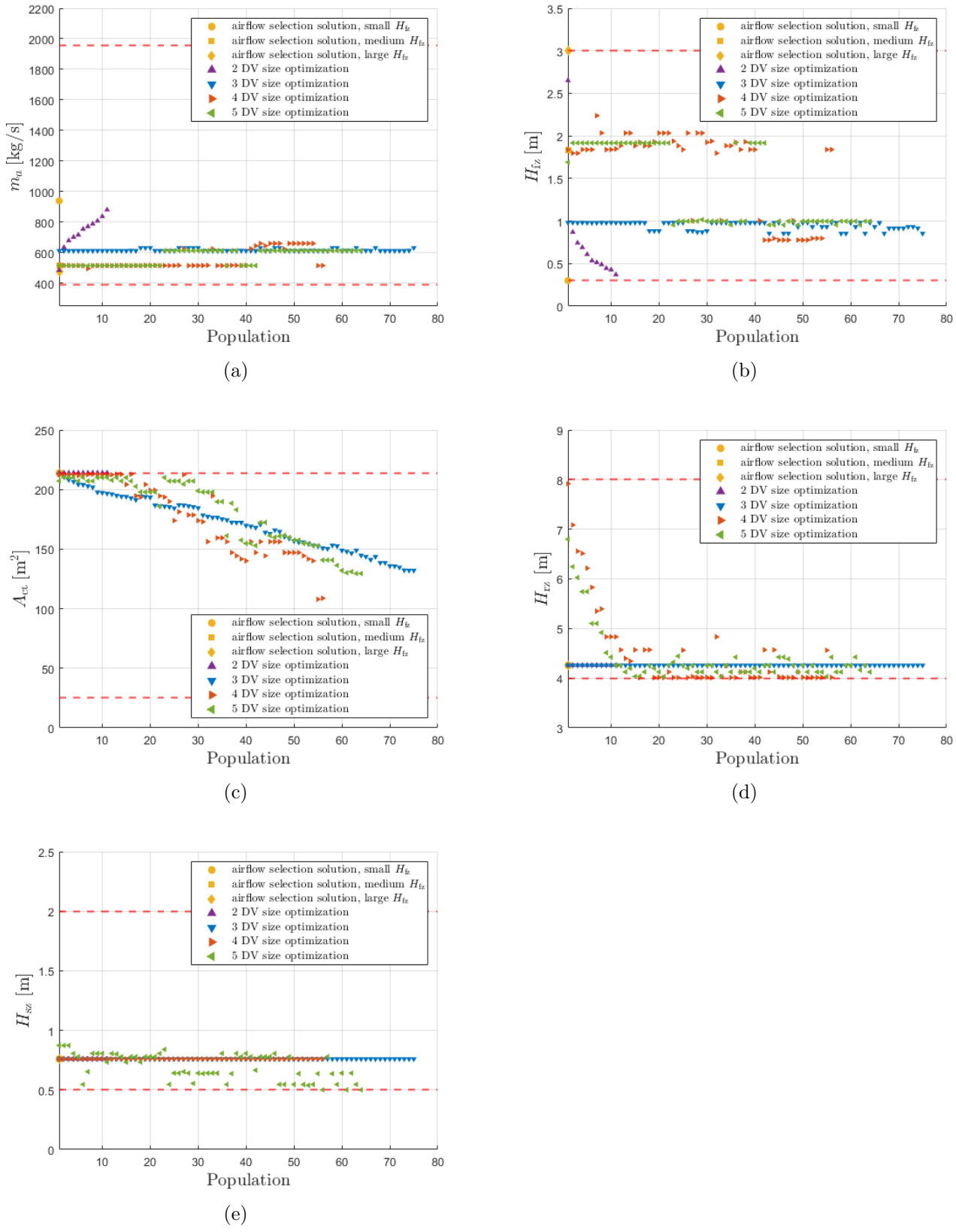

Figure 4.10 – Scatter distribution of design variables at Pareto fronts for the wet cooling tower size optimization.

Three optimal designs named A, B, and C have been selected for a more detailed analysis. Their specifications and performance measures are presented in Tables 4.3 and 4.4. Optimal design A consumes the least fan input power and it has the largest cooling tower volume. It is an ideal design when the priority is to minimize the operating cost. Optimal design C has the lowest cooling tower volume and it consumes the greatest fan input power. It is an ideal design when the priority is to minimize the capital cost. The values of W_{fan} and V_{tower} for optimal design B are in between those for optimal designs A and C. Optimal design B is an ideal design when the priority is to have a balanced trade-off between the capital and operating costs. Optimal designs B and C reject nearly the same amount of heat from water with different proportions of heat rejected by the three wet cooling tower zones. The rain zone of optimal design A has the largest proportion of heat rejected compared to the other two designs because of the extension in H_{rz}. In all three optimal designs, and notwithstanding differences of H_{fz}, more than 60% of heat rejection occurs in the fill zone.

Table 4.3 – Specifications of three selected optimal designs.

Design	m_a [kg/s]	H_{fz} [m]	A_{ct} [m^2]	H_{rz} [m]	H_{sz} [m]	W_{fan} [MW]	V_{tower} [m^3]
A	515.34	1.84	212	7.92	0.76	0.17	2235
B	612.91	0.98	213	4.26	0.76	0.27	1277
C	515.34	1.84	109	4.02	0.76	0.75	719

Table 4.4 – Performance of three selected optimal designs.

Design	Q [MW]	Q_{rz} %	Q_{fz} %	Q_{sz} %	T_{wo} [K]	v_a [m/s]
A	42.33	30.54	65.58	3.89	298.65	2.52
B	41.83	23.18	68.78	8.04	298.78	2.99
C	41.85	24.61	71.22	4.17	298.77	4.92

Figure 4.11 shows the distribution of main thermodynamic properties inside the cooling towers associated with optimal designs A, B, and C. Temperature profiles show that water is cooled to a similar temperature in the three optimal designs. Temperature profiles of air show that air leaves the cooling tower in optimal design B at a lower temperature compared to the other two designs. Water temperature and air temperature are similar in the lower portion of the fill in optimal designs B and C, while the two fluids have a similar temperature in the upper portion of the rain zone of optimal design A. Humidity ratio profiles show the air is saturated with vapor before the fill exit and similarly in the spray zone of the optimal designs

A and C, while the air leaves the cooling tower sub-saturated with a relative humidity of 96% in the optimal design B. This can be attributed to the 47% reduction in H_{fz} for optimal design B relative to the other two designs.

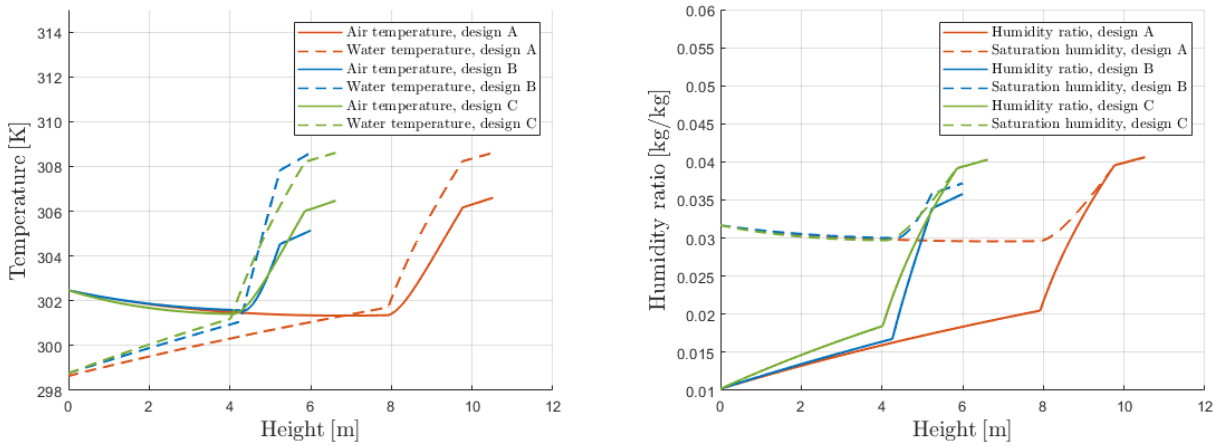

(a) (b)

Figure 4.11 – Distribution of temperature and humidity ratio inside the optimal designs A, B, and C.

4.2.1 Solution verification

Figure 4.12 shows two Pareto fronts for size optimization with three design variables obtained by two different optimization methods, i.e., MOGA and MFD. There is a good agreement between the two Pareto fronts, however, deviations appear for the optimal designs of set 1 and set 6. Table 4.5 reports the design variables selection by MOGA and MFD of all weight sets. Relative to the design variables from MOGA, the largest deviation in the fill height appears for set 1 where the design obtained by MFD has H_{fz} value that is less by 11%. Furthermore, the largest deviation in the air mass flow rate appears for set 1 where the design obtained by MFD has an m_a value that is more by 3%. The largest deviation in the tower frontal area appears for set 6 where the design obtained by MFD has an A_{ct} value that is less by 3%.

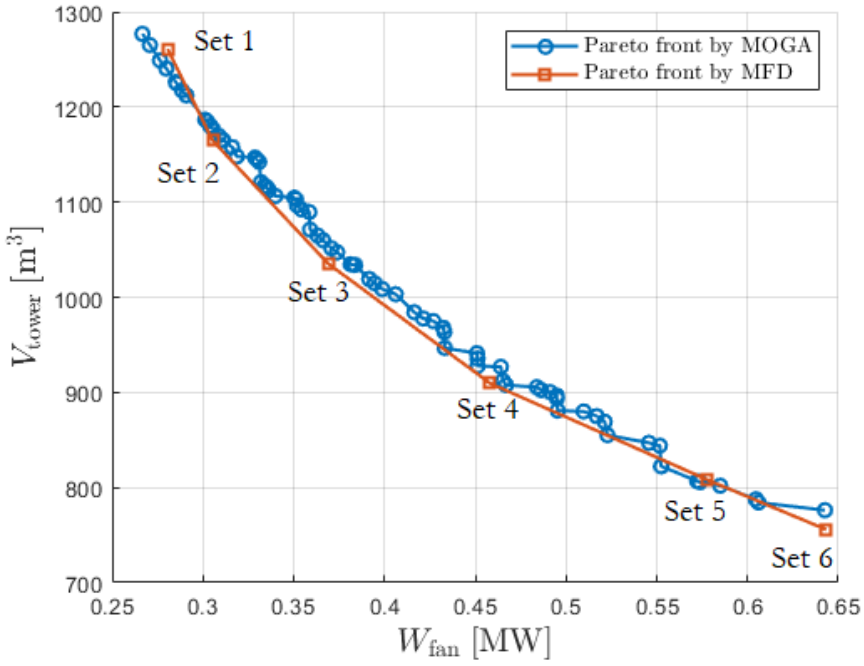

Figure 4.12 – Pareto fronts for wet cooling tower size optimization with three design variables obtained by MOGA and MFD.

Table 4.5 – Comparison of the optimization solutions obtained by MOGA and MFD.

	MFD solution	**MOGA solution**
Set 1	{633.17 kg/s, 0.87 m, 214 m^2}	{612.91 kg/s, 0.98 m, 208 m^2}
Set 2	{610.23 kg/s, 0.97 m, 194 m^2}	{612.91 kg/s, 0.98 m, 194 m^2}
Set 3	{606.76 kg/s, 0.97 m, 173 m^2}	{612.91 kg/s, 0.98 m, 174 m^2}
Set 4	{604.13 kg/s, 0.97 m, 152 m^2}	{614.02 kg/s, 0.93 m, 150 m^2}
Set 5	{623.43 kg/s, 0.86 m, 137 m^2}	{612.91 kg/s, 0.92 m, 136 m^2}
Set 6	{616.39 kg/s, 0.89 m, 128 m^2}	{631.79 kg/s, 0.85 m, 132 m^2}

4.2.2 Final remarks

The size of a wet cooling tower is optimized to obtained the best trade-off between minimizing the capital cost and minimizing the operating cost while satisfying all design constraints. The three main design variables in wet cooling tower size optimization are air mass flow rate, fill height, and tower frontal area. Adding the rain zone height as the forth design variable helps in finding more optimum designs especially those with less fan power consumption. Finally, adding the spray zone height as a design variable does not offer any meaningful design benefit. By solving multi-objective constrained optimization problem with the three main design variables, a range of optimum designs of the wet cooling tower is obtained for the decision-maker to select the most appropriate design for any given application. The cooling tower design with a low airflow is more suitable for applications requiring low operating cost. The cooling tower design with a small frontal area is more suitable for applications requiring low capital cost. The fill height selection is based on satisfying the cooling performance constraint.

4.3 Design problem 3: Size optimization with visible plume constraint

In design problem 3, there are two cases to be investigated (a) the effect of selecting the maximum allowable length for the visible plume, $h_{\max}$, and (b) the effect of selecting cold ambient temperature, T_{cold}.

4.3.1 Effect of selecting the maximum allowable length for the visible plume

The optimization problem formulated in (3.40) is solved at four different values for $h_{\max}$; 8, 12, 16, and 20 m. The plume visibility is evaluated at $T_{\text{cold}} = 12.5°\text{C}$ and $T_{\text{cold,wb}} = 6.0°\text{C}$. Figure 4.13 shows five Pareto fronts for the size optimization of the wet cooling tower obtained in five situations; when visible plume length is unconstrained, and when visible plume length is constrained at the four prescribed values for $h_{\max}$. When the plume visibility constraint is applied in the optimization, the Pareto front is positioned further away from the origin. This indicates that with keeping the same cooling tower volume, more fan input power is required to maintain a shorter visible plume. On the other hand, with keeping the same fan input power, a larger cooling tower design is required, again to maintain a shorter visible plume. Figure 4.14 shows the constraints evaluation in the Pareto optimal designs. The plume visibility constraint is typically active at $h_{\max} = 8$ m, but this is not always the case at the other $h_{\max}$ values. As expected, using a lower maximum allowable length for the visible plume imposes more limitations in obtaining the optimal designs.

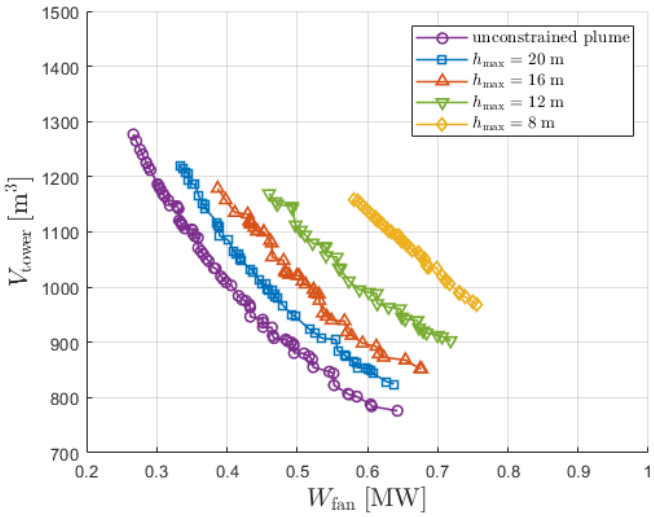

Figure 4.13 – Pareto fronts for wet cooling tower size optimization with visible plume constraint evaluated at $T_{\text{cold}} = 12.5°\text{C}$ and $T_{\text{cold,wb}} = 6.0°\text{C}$ and various $h_{\max}$.

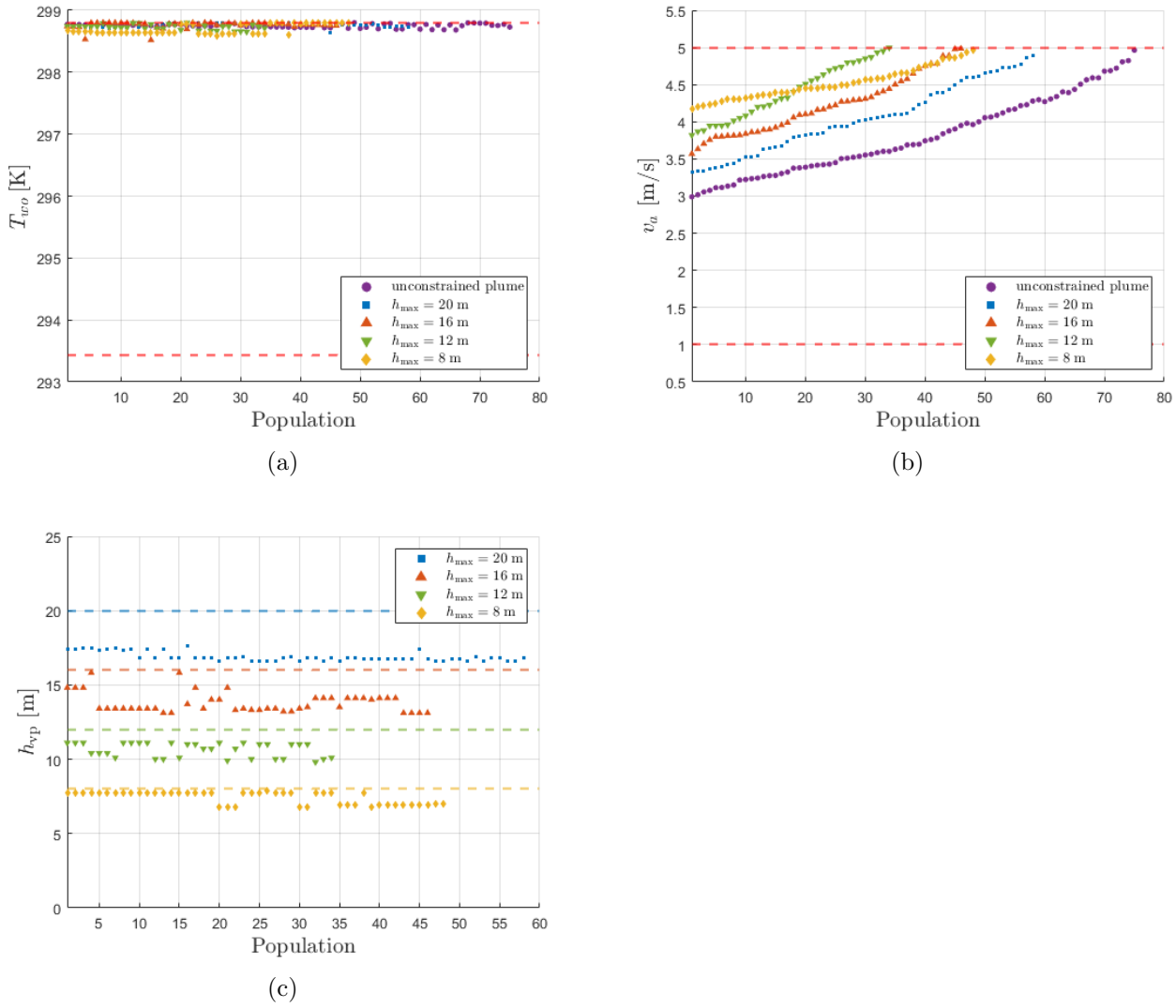

Figure 4.14 – Scatter distribution of constraints at Pareto fronts for wet cooling tower size optimization with visible plume abatement at various $h_{\max}$.

Figure 4.15 shows distributions of the design variables on the Pareto fronts. Although the plume visibility constraint is not always active for each $h_{\max}$, the design variables selection changes as $h_{\max}$ decreases. When the visible plume length is unconstrained, the fill height is the largest, i.e., 0.85 m. When the plume visibility constraint is applied, the fill height is reduced. The visible plume length is driven by the moisture content in the discharged air from the cooling tower. When the fill height decreases, it reduces the ability of the fill to evaporate water and therefore the air exists the cooling tower at a lower saturation ratio. At such conditions, the plume visibility is minimized. More airflow is needed to substitute the loss of cooling performance caused by reducing the fill height. As a result, more fan input power is needed to accommodate the larger airflow so that the cooling tower is able to

meet the cooling performance constraint. The increase of airflow requires a corresponding increase of tower frontal area so that the noise generation constraint is not violated.

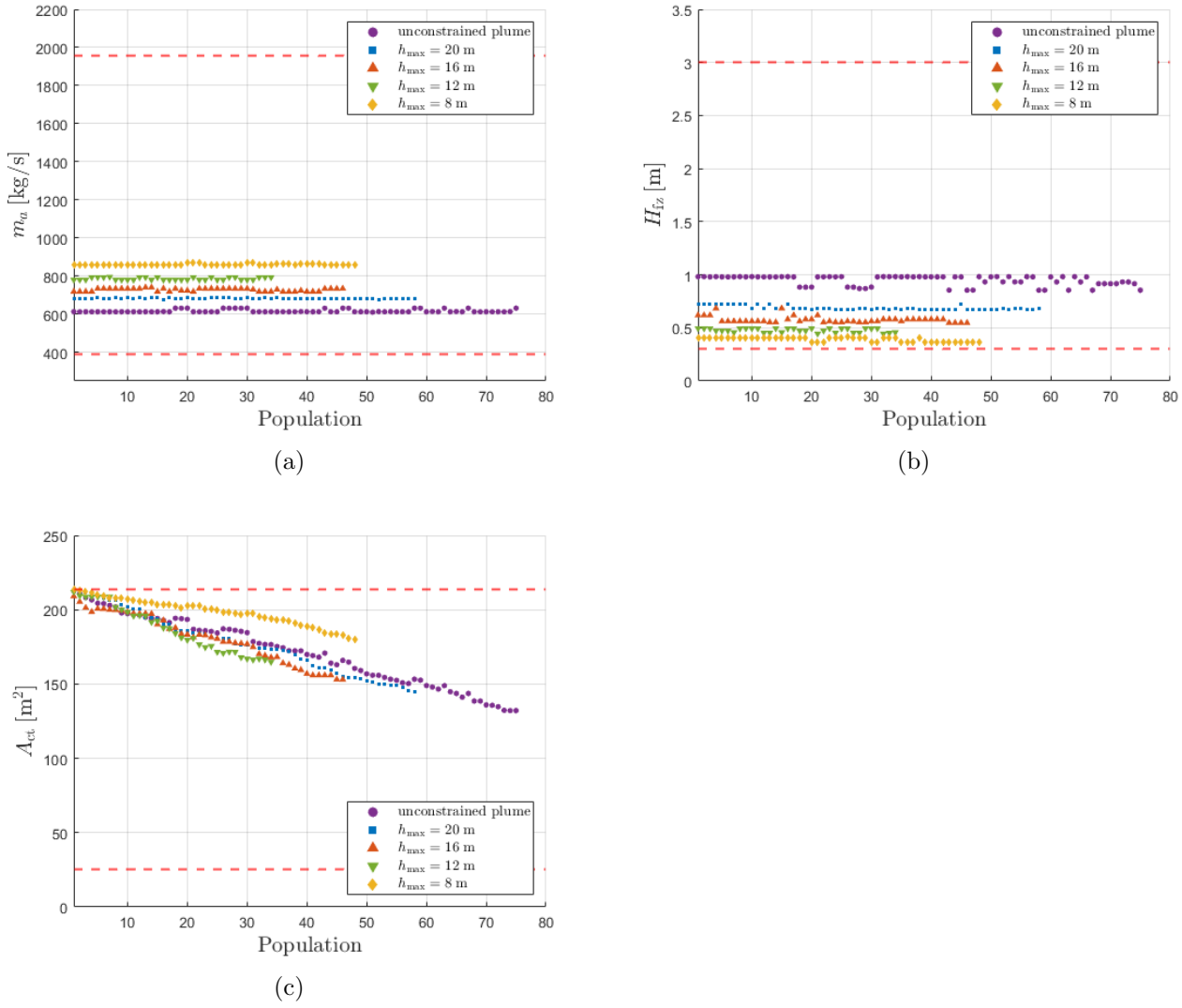

Figure 4.15 – Scatter distribution of design variables at Pareto fronts for wet cooling tower size optimization with visible plume abatement at various $h_{\max}$.

Table 4.6 presents a comparison between the plume source conditions at four optimal designs that have the same size, i.e., $V_{\text{tower}} = 988$ m^3. Figure 4.16 shows the vertical variation of plume excess temperature and relative humidity for the selected optimal designs. The temperature distributions show that the plume cools faster with the design 'd' compared to the other designs. Not coincidentally, the visible plume length (of 7 m) is less for design 'd' than for any of the other designs e.g. h_{vp} is only 17 m for design 'a'. This improvement in terms of reducing the visible plume length is a consequence of (i) raising the air mass flow rate from 681.73 kg/s to 861.28 kg/s; (ii) reducing the fill height from 0.69 m to 0.36 m;

and (iii) increasing the tower frontal area from 173 m^2 to 184 m^2. These changes in the cooling tower design manifest as changes in the plume source conditions. For instance, the volume flux and the momentum flux at the plume source are increased by 24.6% and 46.3%, respectively, due to the rise of air velocity at the plume source. The sensible heat flux and the total moisture flux at the plume source are decreased by much smaller proportions, i.e. by 0.8% and 1.5%, respectively. The amount of ambient air entrained with the plume near the source increases due to the rise in the volume flux and the momentum flux. This helps in accelerating plume dilution by mixing greater volumes of (relatively) dry ambient air into the plume core. As a consequence, the plume humidity rapidly decreases thus reducing the visible plume length by 10 m. The only cost for reducing h_{vp} is an increase in the fan power consumption from 0.47 MW to 0.73 MW, however, this might be offset by the corresponding decrease of fill height, i.e. from 0.69 m to 0.36 m.

Table 4.6 – Plume source conditions for the optimal designs with $V_{\mathrm{tower}} = 988\ \mathrm{m}^3$ at constant cold and dry ambient conditions of $T_{\mathrm{cold}} = 12.5°\mathrm{C}$ and $T_{\mathrm{cold,wb}} = 6.0°\mathrm{C}$.

Optimal design	**Volume flux** [m^3/s]	**Momentum flux** [m^4/s^2]	**Total sensible heat flux** [m^3 K/s]	**Total moisture flux** [$m^3\ kg_w/kg_a\ s$]
a {681.73 kg/s, 0.69 m, 173 m^2}	713.71	1295.94	11400.94	18.21
b {734.19 kg/s, 0.55 m, 177 m^2}	765.09	1454.28	11404.02	18.11
c {793.86 kg/s, 0.45 m, 181 m^2}	823.40	1651.28	11373.11	18.01
d {861.28 kg/s, 0.36 m, 184 m^2}	889.22	1895.85	11314.80	17.94

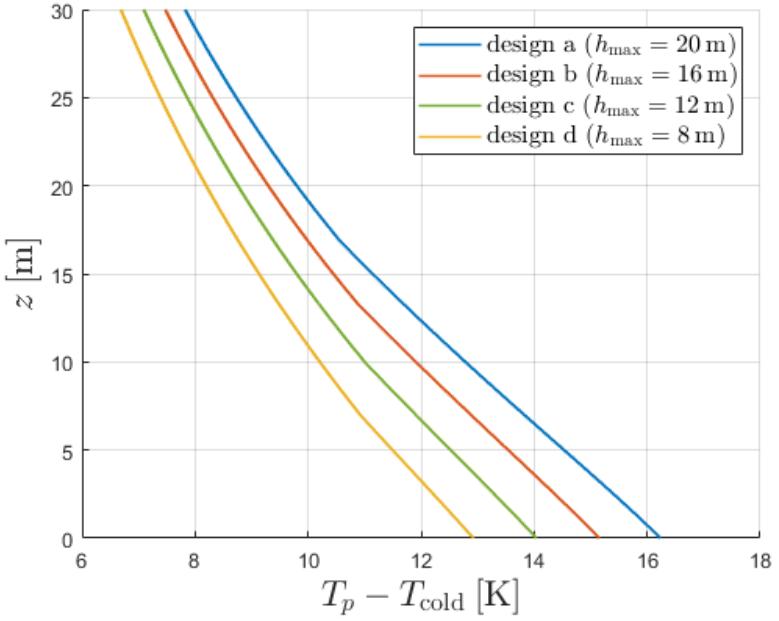

(a)

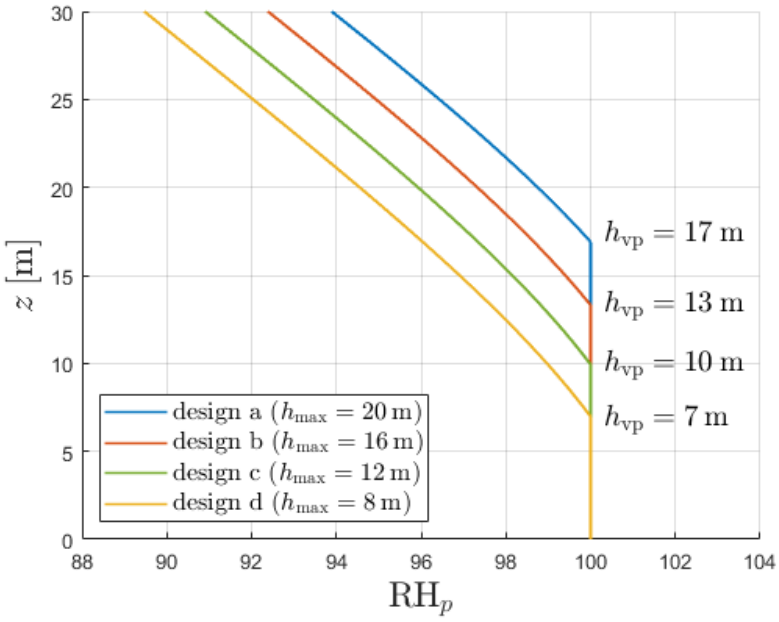

(b)

Figure 4.16 – Variation of (a) plume excess temperature and (b) plume relative humidity with height above the cooling tower evaluated for the optimal designs given in Table 4.6.

4.3.2 Effect of cold ambient temperature

The optimization problem formulated in (3.40) is solved at three different combinations for $(T_{\text{cold}}, T_{\text{cold,wb}})$; (15.0°C, 7.9°C), (12.5°C, 6.0°C), and (10.0°C, 4.0°C) while $h_{\max}$ is fixed at 16 m. The relative humidity at the three cold and dry ambient conditions is fixed at 40%. Figure 4.17 shows four Pareto fronts for the size optimization of the wet cooling tower obtained in four situations; when the visible plume length is unconstrained, and when the visible plume length is constrained at three different cold ambient temperatures. At $T_{\text{cold}} = 15.0$°C, the Pareto front is positioned a small distance away from the Pareto front corresponding to an unconstrained plume, however, there are common designs between the two fronts. This indicates that the use of a high T_{cold} combined with a high $h_{\max}$ for the plume visibility constraint makes it less stringent in the size optimization of the wet cooling tower. On the other hand, the plume visibility constraint is more stringent as T_{cold} decreases. The fan power consumption increases substantially when T_{cold} decreases in order to satisfy the plume visibility constraint. Overall, the operating cost must increase if it is essential to maintain a short visible plume in a lower ambient temperature.

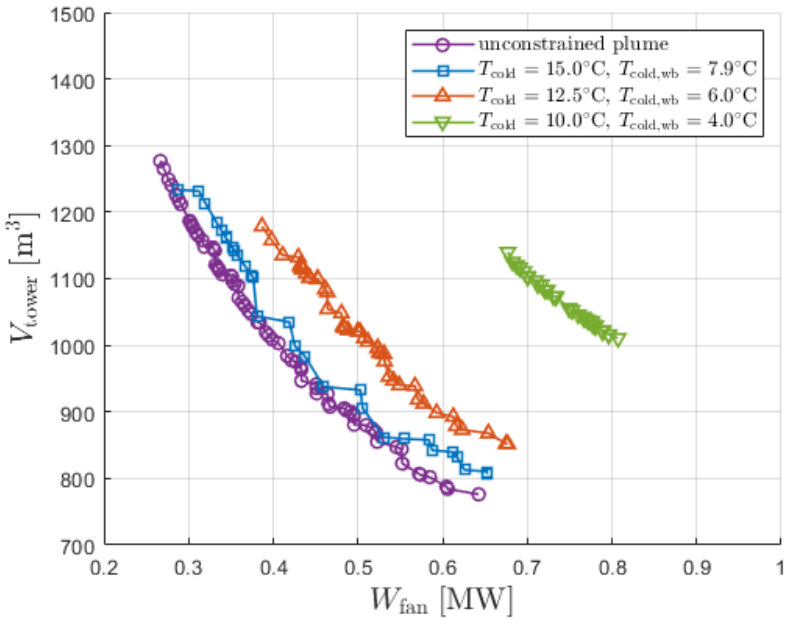

Figure 4.17 – Pareto fronts for wet cooling tower size optimization with visible plume abatement evaluated at various cold and dry ambient conditions with $h_{\text{vp}} \leq 16$ m.

Figures 4.18 and 4.19 show the evaluation of the constraints and the design variables in the Pareto optimal designs, respectively. At $T_{\text{cold}} = 15.0°\text{C}$, a visible plume length is anticipated in the range 8.0 - 10.2 m in the majority of Pareto optimal designs. This indicates that the plume visibility constraint is inactive. This is a reason for the similarity of some optimal designs with other designs obtained with an unconstrained plume in terms of the air mass flow rate and fill height. At $T_{\text{cold}} = 12.5°\text{C}$, the plume visibility constraint is active for two optimal designs and the visible plume length varies between 13.4 - 14.8 m for the rest of the optimal designs. Although the plume visibility constraint is typically inactive, the selection of m_a and H_{fz} has changed. More airflow and less fill height are favored as T_{cold} decreases from 15.0°C to 12.5°C. At $T_{\text{cold}} = 10.0°\text{C}$, the variability in h_{vp} is the smallest between the optimal designs indicating that the plume visibility constraint,though still inactive, causes more limitation in obtaining the optimal designs. In this case, the selection of H_{fz} has reached the low boundary of the design domain for all optimal designs. This indicates that no feasible design is expected if T_{cold} is reduced much below 10.0°C since it would be impossible to satisfy the plume visibility constraint.

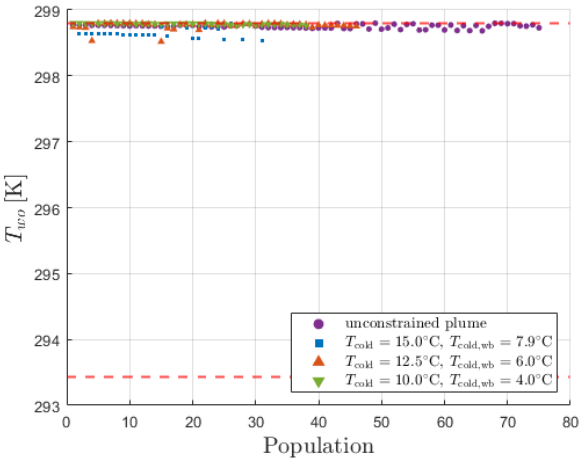

(a)

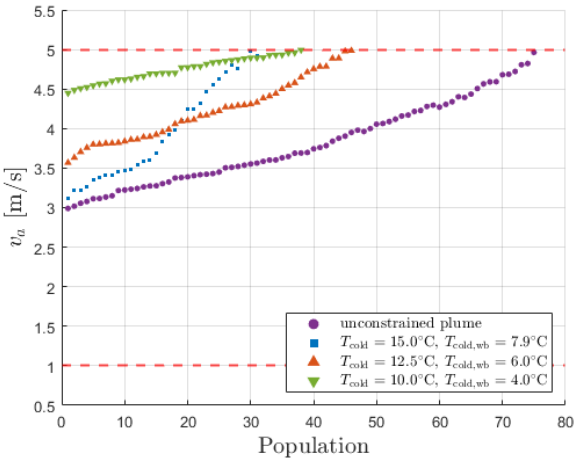

(b)

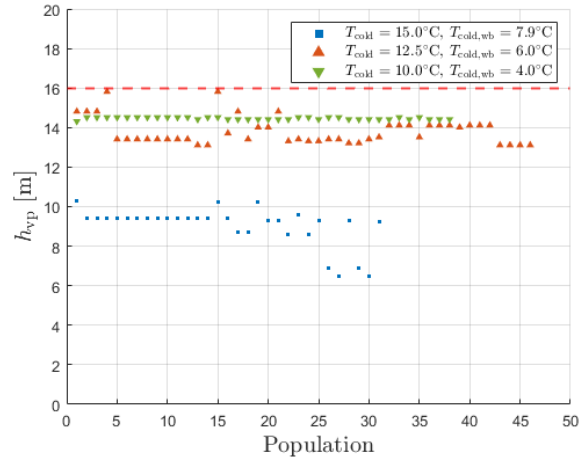

(c)

Figure 4.18 – Scatter distribution of design variables at Pareto fronts for wet cooling tower size optimization with visible plume abatement at various cold and dry ambient conditions.

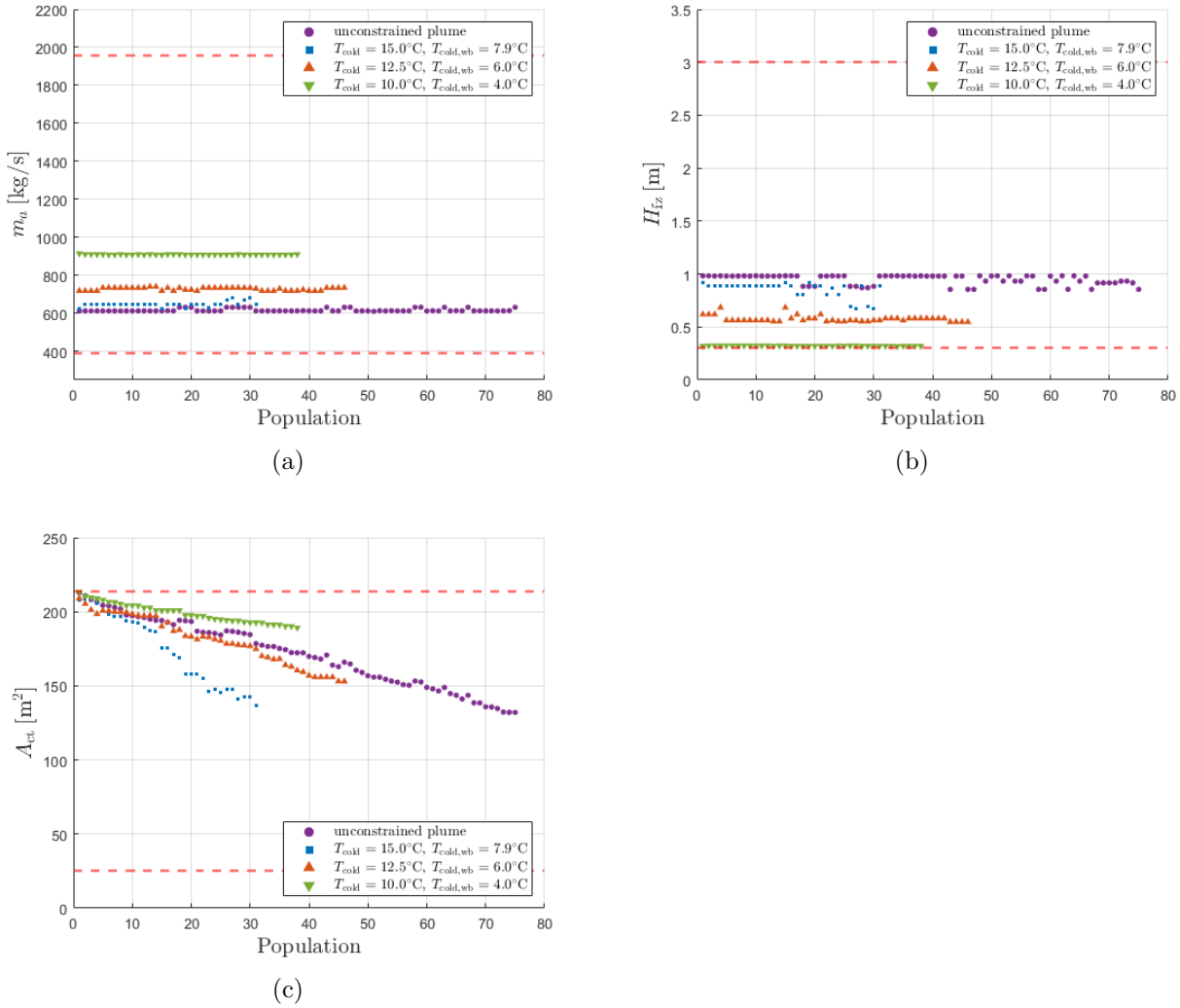

Figure 4.19 – Scatter distribution of design variables at Pareto fronts for wet cooling tower size optimization with visible plume abatement at various cold and dry ambient conditions.

Table 4.7 presents a comparison between the plume source conditions at three optimal designs that have the same size in terms of the cooling tower volume, i.e., 1102 m^3. Figure 4.20 shows the vertical variation of plume excess temperature and humidity for the selected optimal designs. Although the ambient temperature decreases from designs 'e' to 'f' to 'g', the plume cools at nearly the same rate with the three designs as shown by the temperature distributions. The volume of ambient air entrained with the plume near the source increases from the optimal designs 'e' to 'g' due to the rise in the volume flux and the momentum flux at the plume source. Therefore, it is expected that the visible plume length should decrease. Paradoxically, however, Figure 4.20(b) reveals the opposite behavior. This is attributed to the rise in the total sensible heat flux at the plume source due to the decrease of T_{cold}. For example, when comparing designs 'e' and 'g', the total sensible heat flux at the plume source increases with design 'g' by 31.57% as a result of the ambient temperature drop from 15°C to 10°C. Therefore, the visible plume length rises from 9 m with design 'e' to 15 m with design 'g'. The growth in the total sensible heat flux at the plume source enhances the condensation of moisture held by the plume thus extending the visible plume length. As a consequence, the amount of latent energy released due to condensation increases as well, which in turn leads to warm the plume. The effect associated with the ambient temperature drop is counterbalanced with the rise of plume temperature caused by the condensation. Therefore, the plume excess temperature remains similar with the three designs.

Table 4.7 – The plume source conditions for three optimal designs with V_{tower} = 1102 m^3 at three different combinations for $(T_{\text{cold}}, T_{\text{cold,wb}})$: e (15.0°C, 7.9°C), f (12.5°C, 6.0°C), and g (10.0°C, 4.0°C).

Optimal design	**Volume flux** [m^3/s]	**Momentum flux** [m^4/s^2]	**Total sensible heat flux** [m^3 K/s]	**Total moisture flux** [m^3 kg_w/kg_a s]
e {646.95 kg/s, 0.88 m, 187 m^2}	680.92	1094.53	10004.97	18.25
f {734.19 kg/s, 0.55 m, 181 m^2}	765.05	1421.72	11394.13	18.09
g {910.73 kg/s, 0.32 m, 189 m^2}	935.72	2038.29	13163.63	18.21

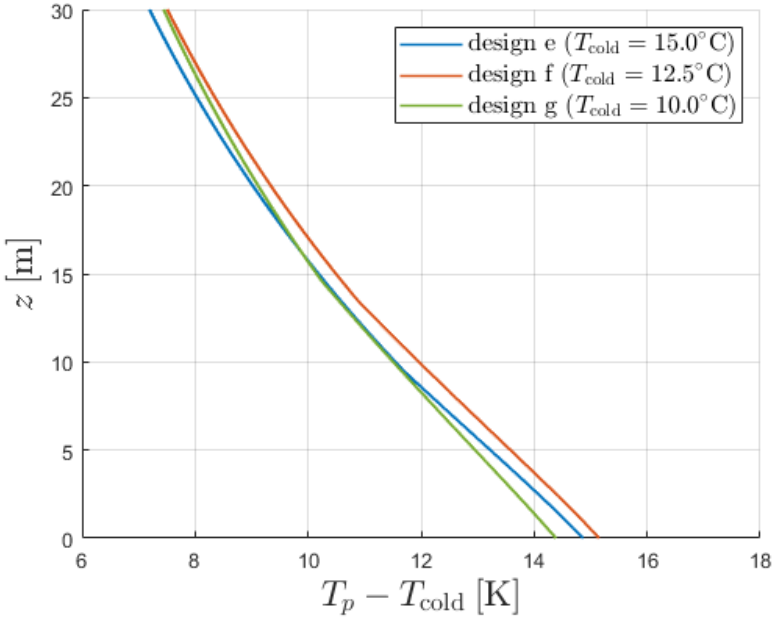

(a)

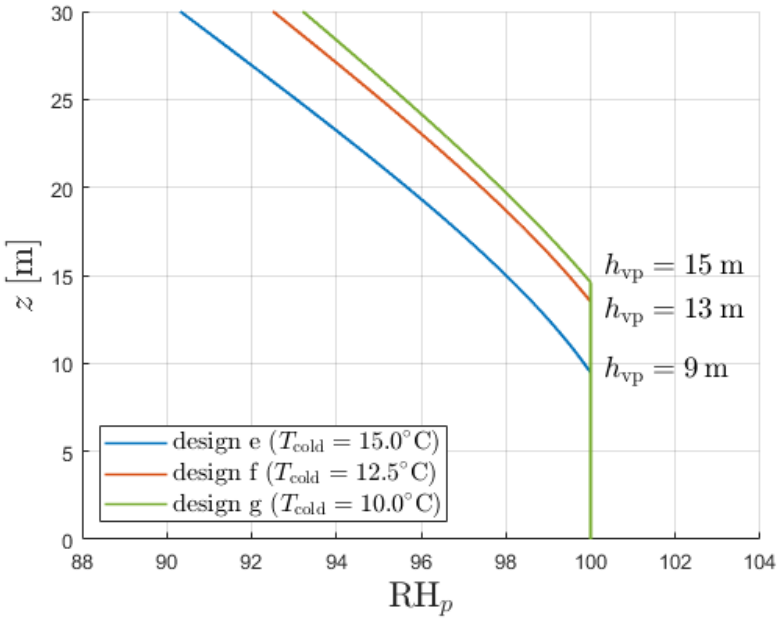

(b)

Figure 4.20 – Variation of (a) plume excess temperature and (b) plume relative humidity with height above the cooling tower evaluated for the optimal designs given in Table 4.7.

4.3.3 Final remarks

There are applications that necessitate having tolerable dimensions for the visible plume during the winter months of the year as a part of the design requirements for a wet cooling tower. Previous results emphasize that the wet cooling tower design that provides a adequate entrainment of ambient air into the plume core leads to a reduction in visible plume length. Cooling the hot water at a high airflow, less fill height, and moderate tower frontal area are the main requirements for a wet cooling tower with less severe fog formation. The associated cost of this design is represented in more fan power consumption for providing the requisite airflow. However, the suggested design becomes insufficient in reducing the severity of fog formation as the cold ambient temperature drops below 10.0°C. In such ambient conditions, the effect of a high condensation rate overcomes the effect of high plume entrainment. As a result, a long visible plume is formed at these cold ambient conditions with the optimized wet cooling tower design. Stated differently, one may have limited options if trying to avoid or minimize visible plume formation in environments including a cold ambient. When there is no option but to eliminate the visible plume (e.g. because of the proximity of the cooling tower to critical infrastructure), a hybrid design that additionally incorporates dry cooling may be necessary.

Chapter 5

Conclusions and future work

5.1 Conclusions

The design of effective, economic, and environment-friendly cooling towers is paramount for industrial applications. In this regard, a numerical optimization framework has been developed in this thesis to obtain optimized cooling tower designs. The optimization framework has three main features: (i) a state-of-the-art wet cooling tower model; (ii) a plume visibility constraint; and (iii) single-objective and multi-objective optimization capabilities. The latter two features are unique within the cooling tower design literature. Three design problems related to a mechanical induced-draft counter-flow wet cooling tower have been solved using the optimization framework.

The developed optimization framework consists of two components that are coupled: a cooling tower analysis package and an optimization package. The former is composed of three solvers built-in within the cooling tower simulation package (CoolIT). Starting with the wet cooling solver, a one-dimensional zone-specific thermodynamic model is solved to evaluate the main properties for the water and air inside the cooling tower. The air draft solver evaluates the pressure drop through each component of the cooling tower in order to find the total pressure drop and thus estimate the fan input power. The plume solver carries out the integration of the turbulent plume equations which evaluate the plume properties with respect to height above the cooling tower. The outcomes from the three solvers comprehensively describe the performance and environmental impact of the cooling tower. The optimization package DAKOTA offers a collection of standard algorithms to solve single objective or multi-objective optimization problems. The optimization algorithm works in conjunction with the analytical models.

The first design problem is the standard problem solved in cooling tower design. It estimates the airflow required for delivering a desired cooling performance at the design operating conditions. This is achieved through solving a single-objective constrained op-

timization problem using the method of feasible directions (MFD). The results show that increasing the fill height leads to smaller airflow requirements which decreases fan power consumption. Thus, the corresponding impact from increasing the fill height is reducing the operating cost, however, the capital cost increases because of the larger volume of fill that must now be purchased. The results reveal that there is a threshold fill height beyond which fan power savings become small. This threshold is determined by the location where the air becomes saturated with vapor. The latter can be determined from the vertical distribution of air humidity ratio obtained by solving the one-dimensional zone specific thermodynamic model.

The best trade-offs between capital and operating costs are studied in detail by simultaneously optimizing the airflow and geometrical dimensions of the cooling tower for a desired cooling performance as in the second design problem. The results show that the main design variables in wet cooling tower size optimization are air mass flow rate, fill height, and tower frontal area. By solving a multi-objective constrained optimization problem with respect to the three main design variables, a range of optimum designs of the wet cooling tower is obtained for the decision-maker to select the most appropriate design for a particular application. For applications requiring low capital cost, the design with a small tower frontal area is more suitable. The air mass flow rate and fill height of this design are selected such that the cooling performance constraint is satisfied provided that the air mass flow rate is not too large for violating the noise generation constraint at small tower frontal areas. For applications requiring low operating cost, the design with a low airflow and large tower frontal area is more suitable. The fill height of this design is selected such that the cooling performance constraint is satisfied. In numerical comparisons, the results show that the design with the lowest capital cost delivers the desired cooling performance at given design operating conditions with 3.1% more air mass flow rate, 13.0% less fill height, and 37.9% less tower frontal area with respect to the design with the lowest operating cost. As a result, the former design has 39.2% less cooling tower volume on account of a 141.0% increase in fan power consumption. On the other hand, the design with the lowest operating cost delivers the desired cooling performance at the same design operating conditions with 3.0% less air mass flow rate, 14.9% more fill height, and 61.0% more tower frontal area with respect to the design with the lowest capital cost. As a result, the former design consumes 58.5% less fan power on account of a 64.5% increase in cooling tower volume. Whether operating or capital cost minimization is more important is specific to the details, (technical, economic and otherwise) of a particular project.

The third design problem aims to study the best trade-offs between capital and operating costs by optimizing the airflow, fill height, and cooling tower frontal area for desired cooling performance at a hot ambient condition as well as limited visible plume length at a cold

ambient condition. The results show that a short visible plume is obtained with the design that provides an adequate entrainment of ambient air into the plume core. At cold and dry ambient conditions of 12.5°C and 40% relative humidity, the cooling performance requirements are met and the visible plume length is reduced by one order of magnitude with 26% more air mass flow rate, 48% less fill height, and 6% more tower frontal area with respect to an optimal cooling tower design with the same volume. However, the suggested design becomes insufficient in reducing the visible plume length as the cold ambient temperature drops below 10.0°C at the same relative humidity. In such ambient conditions, the effect of a high condensation rate overcomes the effect of high plume entrainment.

5.2 Recommendations for future work

If visible plume abatement is critical in such instances, alternative designs must be considered. Veldhuizen and Ledbetter [8] presented three approaches to eliminate cooling tower visible plumes by: (i) superheating the plume and thereby increasing its dew point; (ii) elevating the plume; and (iii) using air cleaning methods, e.g., impingement of water droplets of the plume on cold surfaces. Li and Flynn [91] presented a comprehensive review of alternatives for visible plume abatement using different configurations of hybrid cooling towers. For a series path wet/dry (SPWD) cooling tower, Li and Flynn [91] summarized different methods for superheating the exhaust air from the wet-cooling section, e.g., using heat pumps [17, 92] or solar collectors [93]. For a parallel path wet/dry (PPWD) cooling tower, Li and Flynn [91] discussed the methods for enhancing the mixing of both the dry and wet air-streams in the plenum chamber, e.g., using a static delta-shaped vortex generator [94] or a stirring device consisting of a number of circularly spaced guide vanes [95]. Li and Flynn [91] discussed another alternative for visible plume abatement by using a cooling tower with a condensing module, i.e., using thermosyphons with porous media [96] or an air-to-air heat exchanger [97].

This thesis has focused only on the design optimization of wet cooling towers. The same holistic optimization approach can be applied to hybrid cooling towers design. The design problem can be formulated in a multi-objective constraint optimization problem as for the wet cooling tower design, however, the total heat transfer surface area of the fin-and-tube heat exchanger serves as a third objective function to minimize. The latter conflicts with minimizing the total wet cooling volume or with minimizing the fan input power. As already described, hybrid cooling towers are used to abate the visible plume. They have a further advantage in that they conserve water relative to wet cooling towers and so are ideal in arid environments. When visible plume abatement is the main motivation for using the hybrid cooling tower, the visible plume length is constrained. When water conservation is the main

motivation for using the hybrid cooling tower, the makeup water flow rate is constrained instead of imposing a constraint on fog formation. Geometrical parameters describing a fin-and-tube heat exchanger are considered as new design variables besides the air mass flow rates across the heat exchanger and the wet cooling section, fill height, and tower frontal area. The new optimization problem can be solved using the optimization framework, however, two additional solvers are required for solving: (i) the energy balance that characterizes the dry cooling; and (ii) the mass and energy balances that characterizes the mixing of dry and wet streams in the plenum chamber.

Another possible avenue of research in cooling towers design optimization is through a multi-fidelity optimization framework. A CFD model can be used to increase the accuracy of cooling tower performance analysis where the multi-dimensional CFD model can predict any fluid flow and temperature non-uniformities within the cooling tower. In the case of hybrid cooling towers, the CFD model can predict more accurately the mixing of wet and dry air streams in the plenum chamber. A drawback of using a CFD model is that it requires more computational time compared to the analytical one-dimensional model. To resolve this issue, a multi-fidelity optimization framework should be used. In this case, the one-dimensional model is used in the initial stages of the optimization, then the model switches to the multi-dimensional CFD model. In turn, the optimization results will be based on a high-fidelity surrogate model that corrects any inaccuracies in the one-dimensional model. The surrogate-based optimization strategy is accessed through the meta-algorithm capabilities provided by DAKOTA [83].

Bibliography

[1] A. Zargar, A. Kodkani, A. Peris, E. Clare, J. Cook, P. Karupothula, B. Vickers, M. R. Flynn, and M. Secanell. Numerical analysis of a counter-flow wet cooling tower and its plume. *International Journal of Thermofluids*, 14:100–139, 2022.

[2] M. Seneviratne. In *A Practical Approach to Water Conservation for Commercial and Industrial Facilities*, pages 83–116. Elsevier, Oxford, 2006.

[3] B. Davidson and R. W. Bradshaw . Thermal pollution of water systems. *Environmental Science & Technology*, 1(8):618–630, 1967.

[4] G. B. Hill, E. J. Pring, P. D. Osborn, and W. Stanford. *Cooling Towers: Principles and Practice.* Butterworth-Heinemann, 1990.

[5] N. P. Cheremisinoff and P. N. Cheremisinoff. *Cooling Towers: Selection, Design and Practice.* Ann Arbor Science Publishers, 1981.

[6] J. C. Hensley. *Cooling Tower Fundamentals.* SPX Cooling Technologies, Inc., 2009.

[7] T. Havey. California's coastal power plants: alternative cooling system analysis. Technical report, Tetra Tech, Inc.

[8] H. Veldhuizen and J. Ledbetter. Cooling tower fog: control and abatement. *Journal of the Air Pollution Control Association*, 21(1):21–24, 1971.

[9] S. M. Walser, D. G. Gerstner, B. Brenner, C. Höller, B. Liebl, and C. E. W. Herr. Assessing the environmental health relevance of cooling towers – a systematic review of legionellosis outbreaks. *International Journal of Hygiene and Environmental Health*, 217(2):145–154, 2014.

[10] *2017 ASHRAE Handbook - Fundamentals (SI Edition).* American Society of Heating, Refrigerating and Air-Conditioning Engineers Inc., 2017.

[11] D. G. Kröger. *Air-Cooled Heat Exchangers and Cooling Towers - Thermal-Flow Performance Evaluation and Design*, volume 1. PennWell, 2004.

[12] K. W. Li and A. P. Priddy. *Power Plant System Design*. Wiley, 1985.

[13] D. Baker. *Cooling Tower Performance*. Chemical Publishing Co., 1984.

[14] F. Merkel. Verdunstungskühlung. *V. D. I. Forschungsarbeiten*, (275), 1925.

[15] H. B. Nottage. Merkel's cooling diagram as a performance correlation for air-water evaporative cooling systems. *ASHVE Transactions*, 47:429–448, 1941.

[16] J. C. Kloppers. *A critical evaluation and refinement of the performance prediction of wet-cooling towers*. PhD thesis, University of Stellenbosch, Stellenbosch, Western Cape, 2003.

[17] S. K. Tyagi, S. Wang, and Z. Ma. Prediction, potential and control of plume from wet cooling tower of commercial buildings in hong kong: a case study. *International Journal of Energy Research*, 31(8):778–795, 2007.

[18] J. S. Arora. *Introduction to Optimum Design*. Academic Press, 2016.

[19] J. Nocedal and S. J. Wright. *Numerical Optimization*. Springer, New York, 2006.

[20] P. J. Erens. *VDI Heat Atlas*. Springer Berlin Heidelberg, 2010.

[21] *Water cooling towers, part 2: methods for performance testing*. British Standards 4485, 1988.

[22] *CTI code tower, standard specifications, acceptance test code for water-cooling towers*, volume 1. Cooling Tower Institute.

[23] H. Jaber and R.L. Webb. Design of cooling towers by the effectiveness-NTU method. *Journal of Heat Transfer*, 111(4):837–843, 1989.

[24] A.K.M Mohiuddin and K. Kant. Knowledge base for the systematic design of wet cooling towers. part I: selection and tower characteristics. *International Journal of Refrigeration*, 19(1):43–51, 1996.

[25] A.K.M Mohiuddin and K. Kant. Knowledge base for the systematic design of wet cooling towers. part II: fill and other design parameters. *International Journal of Refrigeration*, 19(1):52–60, 1996.

[26] J.W. Sutherland. Analysis of mechanical-draught counterflow air/water cooling towers. *Journal of Heat Transfer*, 105(3):576–583, 1983.

[27] R. L. Webb, R. K. Shah, E. C. Subbarao, and R. A. Mashelkar. *Heat Transfer Equipment Design*. Hemisphere Publishing Co., 1988.

[28] J.C. Kloppers and D.G. Kröger. The lewis factor and its influence on the performance prediction of wet-cooling towers. *International Journal of Thermal Sciences*, 44(9): 879–884, 2005.

[29] M. Poppe and H. Rogener. *Berechnung von Ruckkiihlwerken*. Springer Berlin Heidelberg, 1991.

[30] J. C. Kloppers and D. G. Kröger. A critical investigation into the heat and mass transfer analysis of crossflow wet-cooling towers. *Numerical Heat Transfer, Part A: Applications*, 46(8):785–806, 2004.

[31] J. C. Kloppers and D. G. Kröger. A critical investigation into the heat and mass transfer analysis of counterflow wet-cooling towers. *International Journal of Heat and Mass Transfer*, 48(3):765–777, 2005.

[32] A. Klimanek and R.A. Białecki. Solution of heat and mass transfer in counterflow wet-cooling tower fills. *International Communications in Heat and Mass Transfer*, 36 (6):547 – 553, 2009.

[33] A. K. Majumdar, A. K. Singhal, and D. B. Spalding. Numerical modeling of wet cooling towers — part 1: mathematical and physical models. *Journal of Heat Transfer*, 105 (4):728–735, 1983.

[34] A. K. Majumdar, A. K. Singhal, H. E. Reilly, and J. A. Bartz. Numerical modeling of wet cooling towers — part 2: Application to natural and mechanical draft towers. *Journal of Heat Transfer*, 105(4):736–743, 1983.

[35] M. N. A. Hawlader and B. M. Liu. Numerical study of the thermal–hydraulic performance of evaporative natural draft cooling towers. *Applied Thermal Engineering*, 22 (1):41–59, 2002.

[36] A. Klimanek, R. A. Białecki, and Z. Ostrowski. CFD two-scale model of a wet natural draft cooling tower. *Numerical Heat Transfer, Part A: Applications*, 57(2):119–137, 2010.

[37] A. Klimanek. Numerical modelling of natural draft wet-cooling towers. *Archives of Computational Methods in Engineering*, 20(1):61–109, 2013.

[38] A. Klimanek, M. Cedzich, and R. Białecki. 3D CFD modeling of natural draft wet-cooling tower with flue gas injection. *Applied Thermal Engineering*, 91:824–833, 2015.

[39] ANSYS Fluent. Fluent 5.0 user's guide. *ANSYS FLUENT Inc.*, 1999.

[40] R. Al-Waked and M. Behnia. The effect of windbreak walls on the thermal performance of natural draft dry cooling towers. *Heat Transfer Engineering*, 26(8):50–62, 2005.

[41] R. Al-Waked and M. Behnia. CFD simulation of wet cooling towers. *Applied Thermal Engineering*, 26(4):382–395, 2006.

[42] R. Al-Waked and M. Behnia. Enhancing performance of wet cooling towers. *Energy Conversion and Management*, 48(10):2638–2648, 2007.

[43] N. Williamson, S. Armfield, and M. Behnia. Numerical simulation of flow in a natural draft wet cooling tower - the effect of radial thermofluid fields. *Applied Thermal Engineering*, 28(2-3):178 – 189, 2008.

[44] N. Williamson, M. Behnia, and S. Armfield. Comparison of a 2D axisymmetric CFD model of a natural draft wet cooling tower and a 1D model. *International Journal of Heat and Mass Transfer*, 51(9):2227–2236, 2008.

[45] B. R. Morton. Buoyant plumes in a moist atmosphere. *Journal of Fluid Mechanics*, 2 (2):127–144, 1957.

[46] G. T. Csanady. Bent-over vapor plumes. *Journal of Applied Meteorology*, 10(1):36–42, 1971.

[47] T. M. L. Wigley and P. R. Slawson. A comparison of wet and dry bent-over plumes. *Journal of Applied Meteorology*, 11(2):335–340, 1972.

[48] G. A. Briggs. A plume rise model compared with observations. *Journal of the Air Pollution Control Association*, 15(9):433–438, 1965.

[49] G. A. Briggs. Plume rise and buoyancy effects. *Atmospheric Science and Power Production*, 850:327–366, 1984.

[50] R. A. Carhart, A. J. Policastro, and S. Ziemer. Evaluation of mathematical models for natural-draft cooling-tower plume dispersion. *Atmospheric Environment*, 16(1):67–83, 1982.

[51] M. Schatzmann and A. J. Policastro. An advanced integral model for cooling tower plume dispersion. *Atmospheric Environment*, 18(4):663–674, 1984.

[52] R. A. Carhart and A. J. Policastro. A second-generation model for cooling tower plume rise and dispersion — I single sources. *Atmospheric Environment. Part A. General Topics*, 25(8):1559–1576, 1991.

[53] U. Janicke and L. Janicke. A three-dimensional plume rise model for dry and wet plumes. *Atmospheric Environment*, 35(5):877–890, 2001.

[54] S. Li, A. Moradi, B. Vickers, and M. R. Flynn. Cooling tower plume abatement using a coaxial plume structure. *International Journal of Heat and Mass Transfer*, 120: 178–193, 2018.

[55] M. M. Castro, T. W. Song, and J. M. Pinto. Minimization of operational costs in cooling water systems. *Chemical Engineering Research and Design*, 78(2):192–201, 2000.

[56] G. F. Cortinovis, J. L. Paiva, T. W. Song, and J. M. Pinto. A systemic approach for optimal cooling tower operation. *Energy Conversion and Management*, 50(9):2200–2209, 2009.

[57] J. M. Ponce-Ortega, M. Serna-González, and A. Jiménez-Gutiérrez. Optimization model for re-circulating cooling water systems. *Computers Chemical Engineering*, 34 (2):177–195, 2010.

[58] G. Jin, W. Cai, L. Lu, E. L. Lee, and A. Chiang. A simplified modeling of mechanical cooling tower for control and optimization of HVAC systems. *Energy Conversion and Management*, 48(2):355–365, 2007.

[59] H. Sayyaadi and M. Nejatolahi. Multi-objective optimization of a cooling tower assisted vapor compression refrigeration system. *International Journal of Refrigeration*, 34(1): 243–256, 2011.

[60] W. Cui, S. Zhou, and X. Liu. Optimization of design and operation parameters for hybrid ground-source heat pump assisted with cooling tower. *Energy and Buildings*, 99:253–262, 2015.

[61] W. Bornman, J. Dirker, D. C. Arndt, and J. P. Meyer. Operational energy minimisation for forced draft, direct-contact bulk air cooling tower through a combination of forward and first-principle modelling, coupled with an optimisation platform. *Energy*, 114:995–1006, 2016.

[62] Z. Zou, Z. Guan, and H. Gurgenci. Optimization design of solar enhanced natural draft dry cooling tower. *Energy Conversion and Management*, 76:945–955, 2013.

[63] O. K. Sadaghiyani, S. Khalilaria, and I. Mirzaee. Energic, exergic, exergo-economic investigation and optimization of auxiliary cooling system (ACS) equipped with compression refrigerating system (CRS). *Case Studies in Thermal Engineering*, 10:517–531, 2017.

[64] K. Singh and R. Das. A feedback model to predict parameters for controlling the performance of a mechanical draft cooling tower. *Applied Thermal Engineering*, 105: 519–530, 2016.

[65] K. Singh and R. Das. An improved constrained inverse optimization method for mechanical draft cooling towers. *Applied Thermal Engineering*, 114:573–582, 2017.

[66] M. S. Söylemez. On the optimum performance of forced draft counter flow cooling towers. *Energy Conversion and Management*, 45(15-16):2335–2341, 2004.

[67] K. Singh and R. Das. An experimental and multi-objective optimization study of a forced draft cooling tower with different fills. *Energy Conversion and Management*, 111:417–430, 2016.

[68] R. K. Singla, K. Singh, and R. Das. Tower characteristics correlation and parameter retrieval in wet-cooling tower with expanded wire mesh packing. *Applied Thermal Engineering*, 96:240–249, 2016.

[69] N. Williamson, M. Behnia, and S. W. Armfield. Thermal optimization of a natural draft wet cooling tower. *International Journal of Energy Research*, 32(14):1349–1361, 2008.

[70] M. S. Söylemez. On the optimum sizing of cooling towers. *Energy Conversion and Management*, 42(7):783–789, 2001.

[71] J. C. Kloppers and D. G. Kröger. Cost optimization of cooling tower geometry. *Engineering Optimization*, 36(5):575–584, 2004.

[72] A. Ataei, M. H. Panjeshahi, and M. Gharaie. A new algorithm for optimum design of mechanical draft wet cooling towers. *Journal of Applied Sciences*, 9(3):561–566, 2009.

[73] M. Serna-González, J. M. Ponce-Ortega, and A. Jiménez-Gutiérrez. MINLP optimization of mechanical draft counter flow wet-cooling towers. *Chemical Engineering Research and Design*, 88(5-6):614–625, 2010.

[74] R. V. Rao and V. K. Patel. Optimization of mechanical draft counter flow wet-cooling tower using artificial bee colony algorithm. *Energy Conversion and Management*, 52 (7):2611–2622, 2011.

[75] R. V. Rao and K. C. More. Optimal design and analysis of mechanical draft cooling tower using improved Jaya algorithm. *International Journal of Refrigeration*, 82:312–324, 2017.

[76] E. Rubio-Castro, M. Serna-González, J. M. Ponce-Ortega, and M. A. Morales-Cabrera. Optimization of mechanical draft counter flow wet-cooling towers using a rigorous model. *Applied Thermal Engineering*, 31(16):3615–3628, 2011.

[77] A. Kodkani. Numerical analysis of a hybrid cooling tower and its plume. Master's thesis, University of Alberta, Edmonton, Alberta, 2021.

[78] F. H. Y. Wu and R. C. Y. Koh. *Mathematical model for multiple cooling tower plumes.* Environmental Research Laboratory, Office of Research and Development, 1978.

[79] J. Kierzenka and L. F. Shampine. A BVP solver based on residual control and the Maltab PSE. *ACM Transactions on Mathematical Software*, 27(3):299–316, 2001.

[80] A Hindmarsh. ODEPACK, a collection of ODE system solvers. *IMACS Transactions on Scientific Computing*, 1:55–64, 1992.

[81] J. R. Singham. *Heat Exchanger Design Handbook.* Hemisphere Publishing Co., 1983.

[82] M. E. Schaffer. *A Practical Guide to Noise and Vibration Control for HVAC Systems.* American Society of Heating, Refrigerating, and Air-Conditioning Engineers, Inc., 2005.

[83] M. Eldred, D. M. Vigil, K. R. Dalbey, W. J. Bohnhoff, B. M. Adams, L. P. Swiler, S. Lefantzi, P. D. Hough, and J. P. Eddy. *DAKOTA: a multilevel parallel object-oriented framework for design optimization, parameter estimation, uncertainty quantification, and sensitivity analysis.* Sandia National Laboratories, Albuquerque, New Mexico, 2006.

[84] M. S. Gallart. Development of a design tool for aerodynamic shape optimization of airfoils. Master's thesis, University of Victoria, Victoria, British Columbia, 2004.

[85] G. N. Vanderplaats. *Numerical Optimization Techniques for Engineering Design: With Applications.* McGraw-Hill series in mechanical engineering. McGraw-Hill, 1984.

[86] C. A. Coello Coello, G. B. Lamont, and D. A. Van Veldhuizen. *Evolutionary Algorithms for Solving Multi-objective Problems.* Genetic and evolutionary computation series Series. Springer Science+Business Media, LLC, 2007.

[87] D. E. Goldberg. *Genetic Algorithms in Search, Optimization, and Machine Learning*. Addison-Wesley, 1989.

[88] J. Eddy. JEGA v 2.3. [Computer Software] `https://doi.org/10.11578/dc.20200930.2`, 3 2009.

[89] J. Eddy and K. Lewis. Effective generation of pareto sets using genetic programming. Pittsburgh, PA, 2001. ASME.

[90] J. Eddy, K. Hacker, and K. Lewis. Solving computationally expensive optimization problems using hybrid methods in parallel computing environments. American Institute of Aeronautics and Astronautics Inc., 2000.

[91] S. Li and M. R. Flynn. Cooling tower plume abatement and plume modeling: a review. *Environmental Fluid Mechanics*, 21(3):521 – 559, 2021.

[92] J. Wang, S. Wang, X. Xu, and F. Xiao. Evaluation of alternative arrangements of a heat pump system for plume abatement in a large-scale chiller plant in a subtropical region. *Energy and Buildings*, 41(6):596–606, 2009.

[93] S. W. Wang, S. K. Tyagi, A. Sharma, and S. C. Kaushik. Application of solar collectors to control the visible plume from wet cooling towers of a commercial building in hong kong: A case study. *Applied Thermal Engineering*, 27(8):1394–1404, 2007.

[94] H. Ruscheweyh. A mixing system for gas flow. *Journal of Wind Engineering and Industrial Aerodynamics*, 16(2):189–199, 1984.

[95] J. S. Moon. Vortex—cooling tower having an air mixer, 2017. KR Patent 101724128(B1).

[96] M. H. B. Mantelli. Development of porous media thermosyphon technology for vapor recovering in cross-current cooling towers. *Applied Thermal Engineering*, 108:398–413, 2016.

[97] B. J. Hubbard, E. F. Mockry, and O. L. Kinney JR. Air-to-air atmospheric exchanger for condensing cooling tower efuent, 2003. US Patent 6,663,694.

[98] General Electric. *Heat Transfer and Fluid Flow Data Book*. General Electric Co., Corporate Research Division, New York, 1982.

[99] United Kingdom Committee on the Properties of Steam. *U.K. Steam Tables in SI Units, 1970*. Edward Arnold Ltd., London, 1970.

[100] A. M. Godridge. *British Coal Utilisation Research Association Monthly*, volume 18. 1954.

[101] V. M. Faires and C. M. Simmang. *Thermodynamics*. Macmillan Publishing Co. Inc., 1978.

[102] H. J. Lowe and D. G. Christie. Heat transfer and pressure drop data on cooling tower packings and model studies of the resistance of natural draft towers to airflow. In *Proceedings of the International Heat Transfer Conference*, pages 933–950, 1961.

[103] D. M. Bell, B. M. Johnson, and E. V. Werry. *Cooling Tower Performance Prediction and Improvement*. 1990 Electric Power Research Institute, Inc., 1990.

[104] E. de Villiers and D. G. Kröger. Analysis of heat, mass, and momentum transfer in the rain zone of counterflow cooling towers. *Journal of Engineering for Gas Turbines and Power*, 121(4):751–755, 1999.

[105] F. Bosnjakovic and P. L. Blackshear. *Technical Thermodynamics*. Holt, Reinhart and Winston, 1965.

Appendix A

Thermophysical properties

A.1 Thermophysical properties of dry air

The equations presented below are valid for dry air at standard atmospheric pressure, i.e., $p = 101325$ Pa, and a temperature, T, between 220 K - 380 K.

Dynamic viscosity (μ)

$$\mu = 2.287973 \times 10^{-6} + 6.259793 \times 10^{-8}\, T - 3.131956 \times 10^{-11}\, T^2 + 8.15038 \times 10^{-15}\, T^3 \quad \text{(A.1)}$$

where μ is measured in kg/(m.s) [98].

Thermal conductivity (k)

$$k = 4.937787 \times 10^{-4} + 1.018087 \times 10^{-4}\, T - 4.627937 \times 10^{-8}\, T^2 + 1.250603 \times 10^{-11}\, T^3 \quad \text{(A.2)}$$

where k is measured in W/(m.K) [98].

Specific heat (c_p)

$$c_p = 1.045356 \times 10^{3} - 3.161783 \times 10^{-1}\, T + 7.083814 \times 10^{-4}\, T^2 - 2.705209 \times 10^{-7}\, T^3 \quad \text{(A.3)}$$

where c_p is measured in J/(kg.K) [98].

Density (ρ)

$$\rho = \frac{p}{287.08\, T} \quad \text{(A.4)}$$

where ρ is measured in kg/m^3 [98].

A.2 Thermophysical properties of saturated water vapor

The equations presented below are valid for saturated vapor at standard atmospheric pressure, i.e., $p = 101325$ Pa, and a temperature, T, between 273.15 - 380 K.

Dynamic viscosity (μ)

$$\mu = 2.562435 \times 10^{-6} + 1.816683 \times 10^{-8}\, T - 2.579066 \times 10^{-11}\, T^2 - 1.067299 \times 10^{-15}\, T^3 \quad \text{(A.5)}$$

where μ is measured in kg/(m.s) [98].

Thermal conductivity (k)

$$k = 1.3046 \times 10^{-2} - 3.756191 \times 10^{-5}\, T - 2.217964 \times 10^{-7}\, T^2 - 1.11156 \times 10^{-10}\, T^3 \quad \text{(A.6)}$$

where k is measured in W/(m.K) [98].

Specific heat (c_p)

$$c_p = 1.3605 \times 10^3 + 2.31334\, T - 2.46784 \times 10^{-10}\, T^5 - 5.91332 \times 10^{-13}\, T^6 \quad \text{(A.7)}$$

where c_p is measured in J/(kg.K) [98].

Density (ρ)

$$\rho = -4.06232 + 0.10277044\, T - 9.76300 \times 10^{-4}\, T^2 + 4.47520 \times 10^{-6}\, T^3 - 1.00459 \times 10^{-8}\, T^4 + 8.91548 \times 10^{-12}\, T^5 \quad \text{(A.8)}$$

where ρ is measured in kg/m^3 [99].

A.3 Thermophysical properties of moist air

The equations presented below are valid for most air at a dry-bulb temperature, T, between 273.15 K - 380 K.

Vapor pressure (p_v)

$$\ln p_v = \frac{A_1}{T} + A_2 + A_3\, T + A_4\, T^2 + A_5\, T^3 + A_6\, \ln T \tag{A.9}$$

where

p_v is measured in Pa,
$A_1 = -5.8002206 \times 10^3$,
$A_2 = 1.3914993$,
$A_3 = -4.8640239 \times 10^{-2}$,
$A_4 = 4.1764768 \times 10^{-5}$,
$A_5 = -1.445209 \times 10^{-8}$, and
$A_6 = 6.5459673$ [10].

Saturation humidity ratio (ω_s)

$$\omega_s = 0.621945\, \frac{p_v}{p - p_v} \tag{A.10}$$

$$p = 101325\, \left(1 - 2.25577 \times 10^5\, Z\right)^{5.2559} \tag{A.11}$$

where

p_v is the vapor pressure measured in Pa, given by (A.9),
p is the barometric pressure measured in Pa, and
Z is the attitude measured in m [10].

Humidity ratio (ω)

$$w = \frac{w_s\, (2501 - 2.381\, T_{\text{wb}}) - (T - T_{\text{wb}})}{2501 + 1.805\, T - 4.186\, T_{\text{wb}}} \tag{A.12}$$

where T_{wb} is the wet-bulb temperature and both T_{wb} and T are measured in K [10].

Dynamic viscosity (μ)

$$\mu = \frac{X_a \mu_a M_a^{1/2} + X_v \mu_v M_v^{1/2}}{X_a M_a^{1/2} + X_v M_v^{1/2}} \qquad \text{where} \qquad X_a = \frac{1}{1.608\, \omega + 1}\,, \qquad X_v = \frac{\omega}{\omega + 1.608} \tag{A.13}$$

where $M_a = 28.970\,\text{kg/mol}$, $M_v = 18.016\,\text{kg/mol}$, μ_a and μ_v are, respectively, the dynamic viscosities of the dry air calculated using (A.1) and the saturated vapor calculated using (A.5) [100].

Thermal conductivity (k)

$$k = \frac{X_a k_a M_a^{1/3} + X_v k_v M_v^{1/3}}{X_a M_a^{1/3} + X_v M_v^{1/3}} \qquad \text{where} \qquad X_a = \frac{1}{1.608\,\omega + 1}\,, \qquad X_v = \frac{\omega}{\omega + 1.608} \tag{A.14}$$

where $M_a = 28.970\,\text{kg/mol}$, $M_v = 18.016\,\text{kg/mol}$, μ_a and μ_v are, respectively, the thermal conductivities of the dry air calculated using (A.2) and the saturated vapor calculated using (A.6) [11].

Specific heat (c_p)

$$c_p = \frac{c_{pa} + \omega\, c_{pv}}{\omega + 1} \tag{A.15}$$

where c_{pa} and c_{pv} are the specific heats of, respectively, the dry air calculated using (A.3) and the saturated vapor calculated using (A.7) [101].

Density (ρ)

$$\rho = \frac{1 + \omega}{v} \qquad \text{where} \qquad v = \frac{0.287042 \times 10^{-3}\,(T + 273.15)(1 + 1.607858\,\omega)}{p} \tag{A.16}$$

where

ρ is measured in kg/m^3,

v is the specific volume of moist air measured in m^3/kg, and

T is the dry-bulb temperature measured in K [10].

A.4 Thermophysical properties of water

The equations presented below are valid for water at a temperature, T, between 273.15 K - 380 K.

Specific heat (c_p)

$$c_p = 8.15599 \times 10^3 - 28.0627\, T + 5.11283 \times 10^{-2}\, T^2 - 2.17582 \times 10^{-13}\, T^6 \tag{A.17}$$

where c_p is measured in J/(kg.K) [11].

Density (ρ)

$$\rho_w = \left(1.49343 \times 10^{-3} - 3.7164 \times 10^{-6}\, T + 7.09782 \times 10^{-9}\, T^2 - 1.90321 \times 10^{-20}\, T^6\right)^{-1} \tag{A.18}$$

where ρ is measured in kg/m^3 [11].

Latent heat of evaporation (r_o)

$$r = 3.4831814 \times 10^6 - 5.8627703 \times 10^3\, T + 12.139568\, T^2 - 1.40290431 \times 10^{-2}\, T^3 \tag{A.19}$$

where r is measured in J/K [11].

Surface tension (σ)

$$\sigma = 5.148103 \times 10^{-2} + 3.998714 \times 10^{-4}\, T - 1.4721869 \times 10^{-6}\, T^2 + 1.21405335 \times 10^{-9}\, T^3 \tag{A.20}$$

where σ is measured in N/m [99].

Appendix B

Merkel number and Lewis factor correlations

Merkel number calculation

The Merkel number for the spray zone is calculated using the the correlation reported by Kröger [11] that, in turn, is based on the data given by Lowe and Christie [102].

$$\mathrm{Me}_{\mathrm{sz}} = 0.2 H_{\mathrm{sz}} \left(\frac{G_a}{G_w} \right)^{0.5} \tag{B.1}$$

where H_{sz} is the spray zone height, and G_a and G_w are the mass velocities of the air and water, respectively.

The Merkel number for the fill zone is calculated using the correlation by Bell et al. [103].

$$\mathrm{Me}_{\mathrm{fz}} = C_1 \, H_{\mathrm{fz}}^{C_2} \, G_w^{C_3} \, G_a^{C_4} \tag{B.2}$$

where H_{fz} is the fill zone height, the constants C_1 through C_4 are the fitting parameters associated with a specific fill design.

The Merkel number for the rain zone is calculated using the correlation by reported de

Villiers and Kröger [104].

$$
\begin{aligned}
\mathrm{Me}_{\mathrm{rz}} = \frac{3.6\, p_{ai}\, D\, H_{\mathrm{rz}}\, \mathrm{Sc}^{0.33}}{R_v\, T_{ai}\, \rho_w\, \bar{v}_{\mathrm{rz}}\, \bar{d}_d^{\,2}} \left[\ln\left(\frac{\omega_s + 0.622}{\omega + 0.622}\right)\frac{1}{\omega_s - \omega}\right] \\
\Big(4.68851\, a_\rho\, \rho_a - 187128.7\, a_\mu\, \mu_{av} - 2.29322 + 22.411 \\
\times \left[0.350396\ (a_v\, \bar{v}_{\mathrm{rz}})^{1.38046} + 0.09\right] \\
\times \left[1.60934\ (a_L\, H_{\mathrm{rz}})^{-1.12083} + 0.66\right] \\
\times \left[34.6765\ (a_L\, \bar{d}_d)^{0.732448} + 0.45\right] \\
\times \exp\Big\{7.7389 \exp(-0.399827\, a_L\, H_{\mathrm{rz}}) \\
\times \ln\left[0.087498 \exp(0.05323\, a_L \frac{W_{\mathrm{ct}}}{2}) + 0.85\right]\Big\}\Big)
\end{aligned}
\tag{B.3}
$$

where $\bar{d}_d$ is the average droplet diameter, which we assume, consistent with Kloppers [16], to be 3.5 mm, T_{ai} and p_{ai} are respectively the temperature and pressure of the inlet air, μ_{av} is the dynamic viscosity of moist air calculated using (A.13), H_{rz} is the rain zone height, and W_{ct} is the cooling tower width. The coefficients, 'a', are obtained from the water density, ρ_w, water surface tension, σ_w, and gravitational acceleration, g, i.e., $a_\mu = 3.06 \times 10^{-6}\,(\rho_w^4 g^9/\sigma_w)^{1/4}$, $a_\rho = 998/\rho_w$, $a_v = 73.298\,(g^5\sigma_w^3/\rho_w^3)^{1/4}$ and $a_L = 6.122\,(g\sigma_w/\rho_w)^{1/4}$. Furthermore, $\bar{v}_{\mathrm{rz}}$ is the average air velocity in the rain zone, D is the diffusion coefficient, and Sc is the Schmidt number. These latter variables are calculated using

$$
\bar{v}_{\mathrm{rz}} = \frac{m_a}{\rho_{av} A_{\mathrm{ct}}} \tag{B.4}
$$

$$
\mathrm{D} = 0.04357\, T_{ai}^{1.5} \frac{(1/M_a + 1/M_v)^{0.5}}{p_{ai}[V_a^{0.333} + V_v^{0.333}]^2} \tag{B.5}
$$

$$
\mathrm{Sc} = \frac{\mu_{av}}{\rho_{av} D} \tag{B.6}
$$

where $M_a = 28.970$ kg/mol, $M_v = 18.016$ kg/mol, $V_a = 29.9$ m^3/mol, $V_v = 18.8$ m^3/mol, $R_v = 461.52$ J/(kg.K), ρ_{av} is the inlet air density, which is calculated using (A.16), and A_{ct} is the cross-sectional area of cooling tower. Equation B.3 is only valid for cases where:

$$
\begin{aligned}
0\ ^\circ\mathrm{C} &\leq T_{ai} \leq 40^\circ\mathrm{C}, \\
10\ ^\circ\mathrm{C} &\leq T_w \leq 40^\circ\mathrm{C}, \\
1\ \mathrm{m/s} &\leq \bar{v}_{\mathrm{rz}} \leq 5\ \mathrm{m/s}, \\
4\ \mathrm{m} &\leq H_{\mathrm{rz}} \leq 8\ \mathrm{m} \\
2\ \mathrm{m} &\leq W_{\mathrm{ct}} \leq 20\ \mathrm{m}.
\end{aligned}
$$

Lewis factor calculation

The heat transfer coefficient, α, and the mass transfer coefficient, β, are linked by the Lewis factor, $\mathrm{Le_f}$, which is defined as

$$\mathrm{Le_f} \equiv \frac{\mathrm{St}}{\mathrm{St}_m} = \frac{\alpha}{\beta(c_{pa} + \omega\, c_{pv})} \tag{B.7}$$

Here, St and St_m are, respectively, the heat and mass transfer Stanton numbers. Bosnjakovic and Blackshear [105] developed an empirical relation for the Lewis factor for air-vapor system where

$$\mathrm{Le_f} = 0.866^{2/3} \frac{\left(\frac{\omega_s + 0.622}{\omega + 0.622} - 1\right)}{\ln\left(\frac{\omega_s + 0.622}{\omega + 0.622}\right)} \tag{B.8}$$

Appendix C

Pressure loss coefficient correlations

The pressure loss coefficient for the spray zone is calculated using the correlation reported by Kröger [11] that, in turn, is based on the data given by Lowe and Christie [102].

$$K_{\mathrm{sz}} = H_{\mathrm{sz}} \left[0.4 \left(\frac{G_w}{G_a} \right) + 1 \right] \tag{C.1}$$

where H_{sz} is the spray zone height, and G_a and G_w are the mass velocities of air and water, respectively.

The pressure loss coefficient for the rain zone is calculated using the correlation by reported de Villiers and Kröger [104].

$$\begin{aligned} K_{\mathrm{rz}} = \frac{3\, a_v\, \overline{v}_w\, H_{\mathrm{rz}}}{2\, \bar{d}_d} \Big[& 0.219164 + 8278.7 a_\mu\, \mu_{av} - 0.30487 a_\rho\, \rho_{av} \\ & + 0.954153 \left\{ 0.328467 \exp(135.7638\, a_L\, \bar{d}_d) + 0.47 \right\} \\ & \times \left\{ 26.28482\ (a_L\, H_{\mathrm{rz}})^{-2.95729} + 0.56 \right\} \\ & \times \exp\{ \ln(\, 0.204814 \exp(0.133036\, a_L\, W_{\mathrm{ct}}) + 0.21) \\ & \times (3.9186 \exp(-0.3\, a_L\, H_{\mathrm{rz}})) \\ & \times (0.31095 \ln(a_L\, \bar{d}_d) + 2.63745) \} \\ & \times \left\{ 2.177546\ (a_v\, \bar{v}_{\mathrm{rz}})^{-1.46541} + 0.21 \right\} \Big] \end{aligned} \tag{C.2}$$

where $\bar{d}_d$ is the average droplet diameter, which we assume, consistent with Kloppers [16], to be 3.5 mm, μ_{av} is the dynamic viscosity of moist air calculated using (A.13), H_{rz} is the rain zone height, and W_{ct} is the cooling tower width. The coefficients, 'a', are obtained from the water density, ρ_w, water surface tension, σ_w, and gravitational acceleration, g, i.e., $a_\mu = 3.06 \times 10^{-6}\, (\rho_w^4 g^9 / \sigma_w)^{1/4}$, $a_\rho = 998/\rho_w$, $a_v = 73.298\, (g^5 \sigma_w^3 / \rho_w^3)^{1/4}$ and $a_L = 6.122\, (g \sigma_w / \rho_w)^{1/4}$. Furthermore, $\bar{v}_{\mathrm{rz}}$ and $\overline{v}_w$ are the average velocities of air and water, respectively, in the rain

rain zone. These latter variables are calculated using

$$\bar{v}_{\mathrm{rz}} = \frac{m_a}{\rho_{av} A_{\mathrm{ct}}} \tag{C.3}$$

$$\bar{v}_w = \frac{m_w}{\rho_w A_{\mathrm{ct}}} \tag{C.4}$$

where ρ_{av} and ρ_w are the densities of moist air and water entering the rain zone and these densities are calculated using (A.16) and (A.18), respectively. A_{ct} is the cross-sectional area of cooling tower. Equation C.2 is only valid for cases where:

$$\begin{aligned}
0\ ℃ &\leq T_{ai} \leq 40℃,\\
10\ ℃ &\leq T_w \leq 40℃,\\
1\ \mathrm{m/s} &\leq \bar{v}_{\mathrm{rz}} \leq 5\ \mathrm{m/s},\\
0.0075\ \mathrm{m/s} &\leq \bar{v}_w \leq 0.003\ \mathrm{m/s},\\
4\ \mathrm{m} &\leq H_{\mathrm{rz}} \leq 8\ \mathrm{m}\\
2\ \mathrm{m} &\leq W_{\mathrm{ct}} \leq 20\ \mathrm{m}.
\end{aligned}$$

Appendix D

Parametric study for visible plume length

As mentioned in section 3.5.1, we are interested in studying the effect of selecting the cold ambient conditions, T_{cold} and $T_{\text{cold,wb}}$, used for evaluating the visible plume length, h_{vp}. The latter is a constraint in the design problem 3. The current appendix extends this analysis by showing, in greater detail, the impact of varying T_{cold} and $T_{\text{cold,wb}}$ upon h_{vp}. To this end, we show in Figures D.1-D.4 the variation of h_{vp} with two design variables, m_a and H_{fz}, at different cold ambient conditions. h_{vp} is more sensitive to m_a and H_{fz} compared to A_{ct}. The cooling tower specifications are given in Table 3.2. Figures D.1-D.4 show that it is anticipated to have a long visible plume, i.e., $h_{\text{vp}} > 20\,\text{m}$, when $T_{\text{cold}} = 7.5°\text{C}$. The plume visibility is more severe at two wet cold ambient conditions, i.e., $T_{\text{cold}} = 10.0°\text{C}\,\text{RH} = 80\%$. Therefore, and from optimization point of view, feasible designs of the wet cooling tower are found when h_{vp} is evaluated at $T_{\text{cold}} = \{15.0°\text{C}, 12.5°\text{C}, 10.0°\text{C}\}$. Although some feasible designs are found at RH = 80% for $T_{\text{cold}} = \{15.0°\text{C}, 12.5°\text{C}\}$, dry and cold ambient conditions are selected in this study, i.e., RH is fixed at 40%.

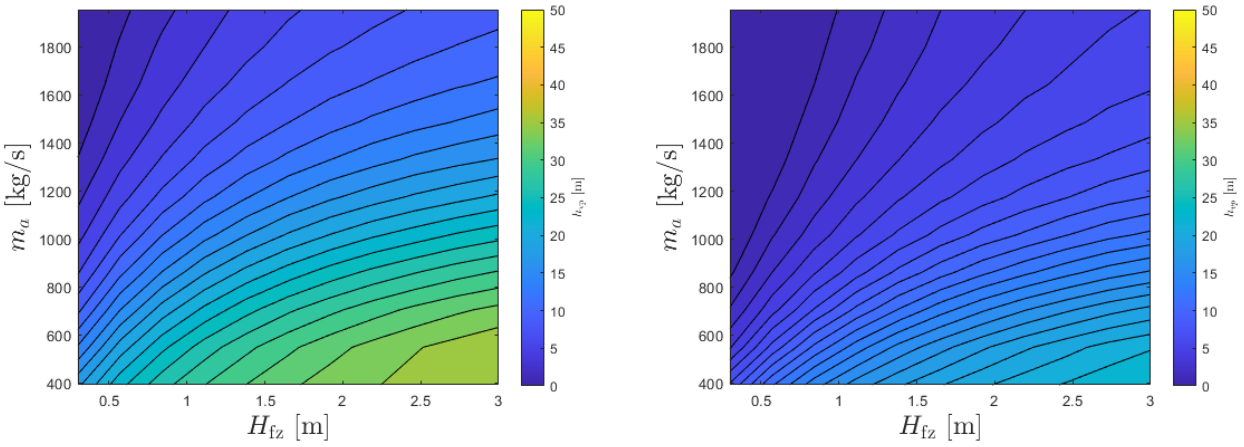

Figure D.1 – Sensitivity of visible plume length with respect to fill height and air mass flow rate at (a) $T_{\mathrm{cold}} = 15.0°\mathrm{C}$, $T_{\mathrm{cold,wb}} = 10.4°\mathrm{C}$ corresponding to RH = 80% (b) $T_{\mathrm{cold}} = 15.0°\mathrm{C}$, $T_{\mathrm{cold,wb}} = 7.9°\mathrm{C}$ corresponding to RH = 40%.

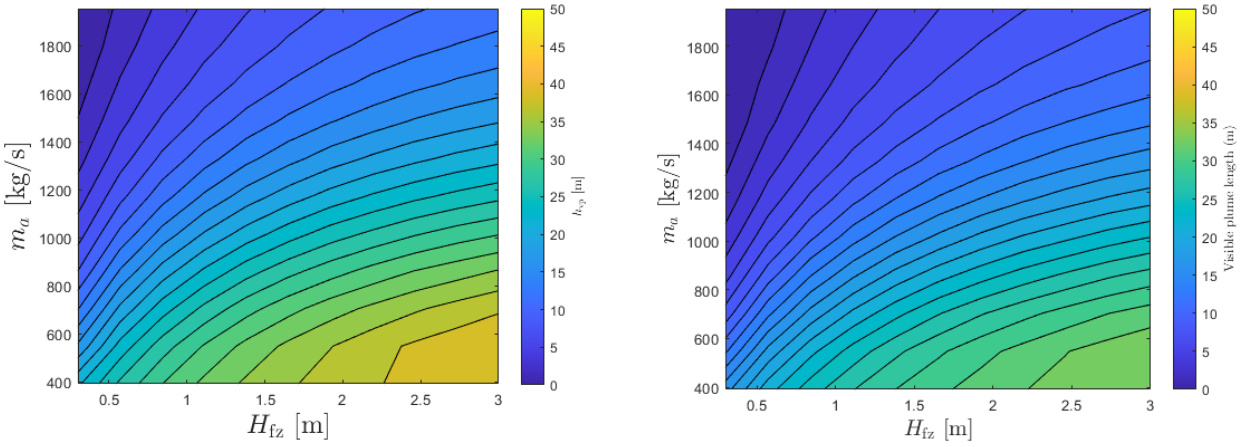

Figure D.2 – Sensitivity of visible plume length with respect to fill height and air mass flow rate at (a) $T_{\mathrm{cold}} = 12.5°\mathrm{C}$, $T_{\mathrm{cold,wb}} = 9.2°\mathrm{C}$ corresponding to RH = 80% (b) $T_{\mathrm{cold}} = 12.5°\mathrm{C}$, $T_{\mathrm{cold,wb}} = 6.0°\mathrm{C}$ corresponding to RH = 40%.

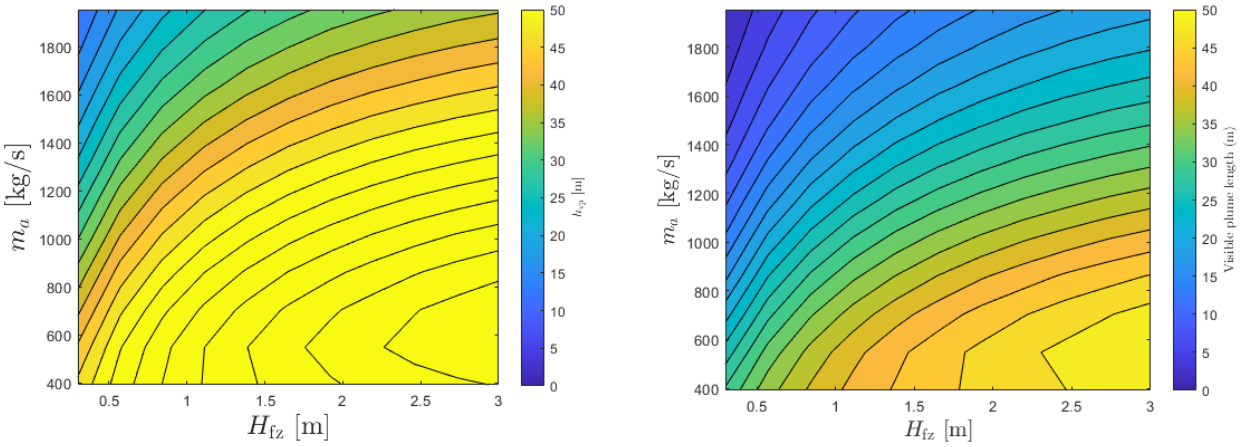

(a) (b)

Figure D.3 – Sensitivity of visible plume length with respect to fill height and air mass flow rate at (a) $T_{cold} = 10.0°C$, $T_{cold,wb} = 6.5°C$ corresponding to RH = 80% (b) $T_{cold} = 10.0°C$, $T_{cold,wb} = 2.1°C$ corresponding to RH = 40%.

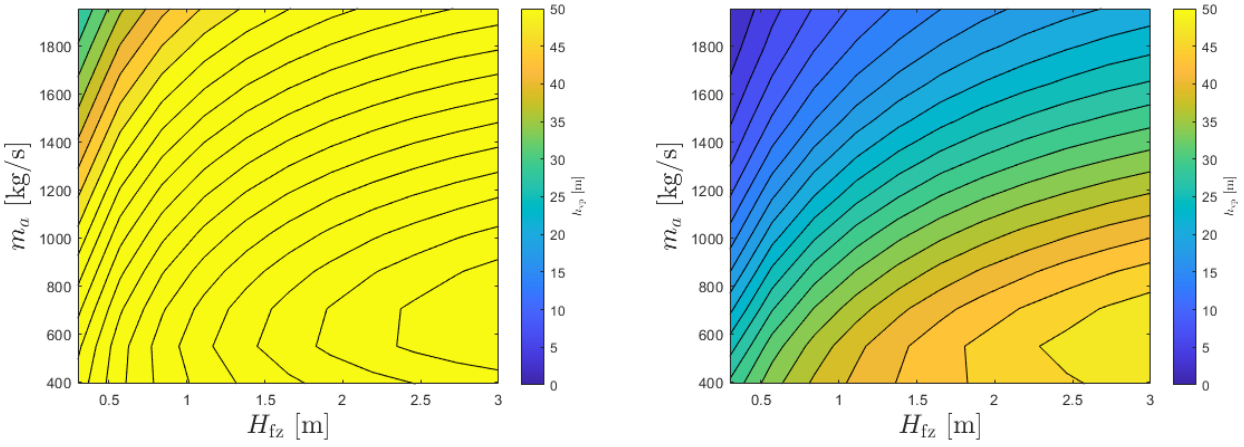

(a) (b)

Figure D.4 – Sensitivity of visible plume length with respect to fill height and air mass flow rate at (a) $T_{cold} = 7.5°C$, $T_{cold,wb} = 4.4°C$ corresponding to RH = 80% (b) $T_{cold} = 7.5°C$, $T_{cold,wb} = 0.5°C$ corresponding to RH = 40%.